INVESTIGATING THE TENSILE BEHAVIOUR OF UNSATURATED SOILS USING THE BRAZILIAN DISC TEST

TIAGO ALEXANDRE VALENTIM GASPAR

A dissertation submitted in partial fulfilment of the requirements for the degree of

MASTER OF ENGINEERING (GEOTECHNICAL ENGINEERING)

in the

FACULTY OF ENGINEERING, BUILT-ENVIRONMENT AND INFORMATION TECHNOLOGY

University of Pretoria

FEBRUARY 2017

ABSTRACT

Title:	Investigating the tensile behaviour of unsaturated soils using the Brazilian Disc Test
Author:	Tiago Gaspar
Supervisor:	Professor S.W. Jacobsz
Department:	Civil Engineering
University:	University of Pretoria
Degree:	Master of Engineering (Geotechnical Engineering)

In geotechnical practice, soils are generally assumed to have negligible tensile strength. However, in the context of unsaturated soils, this strength can be significant and important to consider. In contrast to the two-phase soil matrix considered in classical saturated soil mechanics, the presence of a third air phase in unsaturated soils brings about the manifestation of surface tension and matric suction. These phenomena provide unsaturated soils with a certain degree of tensile strength, which in turn affects the overall shear strength behaviour of the soil mass.

This dissertation investigates the behaviour of three different unsaturated soils tested using the Brazilian Disc Test (BDT). The soils considered were two types of tailings from South African mines, i.e. gold and iron tailings, and one natural silty, clayey soil from Centurion, south of Pretoria. The tensile strength of 120 samples was determined using displacement controlled Brazilian Disc Tests with sample deformation recorded using Digital Image Correlation (DIC). Through the use of 30° curved loading strips, the BDT was found to consistently result in centrally located crack initiation by reducing compressive stress concentrations close to the points of load application. This modification of the loading conditions prevented the premature 'crushing' failures observed by previous authors.

It was found that while the testing procedure was suitable for all soils considered, the increased ductility at high moisture contents resulted in a more complex material response upon loading. For these ductile samples, it was found that simply adopting the maximum achieved load as being indicative of the mobilisation of tensile strength is inadequate and can result in a gross overestimation of the tensile strength of these soils.

The tensile strengths measured for each soil type, across a range of moisture contents, was subsequently compared to the Soil Water Retention Curves (SWRC) of each material. This comparison allowed for correlations between matric suction and tensile strength to be determined. For both gold and iron tailings, an increase in tensile strength was observed with an increase in suction. The contribution of matric suction to tensile strength was however found to diminish in the pendular regime.

In contrast, the tensile strength of the Centurion soil increased with a reduction in saturation, achieved a peak value and decreased in the pendular regime. This trend was attributed to the dependency of both surface tension and matric suction on the contact area between particles, which in turn is affected by particle shape.

DECLARATION

I, the undersigned hereby declare that:

I understand what plagiarism is and I am aware of the University's policy in this regard;

The work contained in this project report is my own original work;

I did not refer to work of current or previous students, lecture notes, handbooks or any other study material without proper referencing;

I have not allowed anyone to copy any part of my project report;

I have not previously in its entirety or in part submitted this project report at any university for a degree.

_____

Tiago Alexandre Valentim Gaspar

10096401

02 February 2017

ACKNOWLEDGEMENTS

First and foremost, I would like to express my tremendous gratitude and appreciation to my supervisor, Professor S.W. Jacobsz. Without his expertise and enthusiasm, this dissertation would not have been possible. From everything I have learnt under his supervision, the phrase "…it would be interesting to see …" will forever be ingrained in my memory as a prelude to countless more hours (or days) of laboratory work.

I am immensely grateful to Professor G. Heymann whose enthusiasm and passion for geotechnical engineering is second to none. The door to Prof. Heymann's office was always open whenever I needed some guidance or advice on my research.

My thanks to Prof. E. Kearsley for always taking the time to advise me on various aspects of my dissertation. Her experience in the field of materials testing proved to be a tremendous help in providing me with a starting point for my research on the Brazilian Disc Test.

I would like to thank Mr Jurie van Staden for his help throughout my laboratory work, and managing to remain calm as I made a complete mess of his laboratory.

To the postgraduate group of 2015 and 2016, I would like to thank you all for helping maintain my sanity throughout the completion of this dissertation. I believe our frequent coffee breaks played an enormous role in keeping me motivated. Specifically, I wish to express my appreciation to Sophia Smit and Rick Vandoorne for proofreading parts of this dissertation.

I am immensely grateful to my father for manufacturing a substantial portion of the customised equipment used for my laboratory testing. His willingness to sacrifice his time to assist me is greatly appreciated.

Last but certainly not least I would like to thank my mother. Without her financial support, I would never have had the opportunity to undertake postgraduate studies, to begin with. Furthermore, this achievement would not have been possible without her moral support and patience throughout the duration of this dissertation.

TABLE OF CONTENTS

LIST OF TABLES

PAGE

LIST OF FIGURES

PAGE

NOMENCLATURE

Symbol	Description	Units
u_a	pore-air pressure, air pressure	kPa
u_v	partial vapour pressure	kPa
u_w	pore-water pressure, water pressure	kPa
θ	volumetric water content	%
θ_r	residual volumetric water content	%
θ_s	saturated volumetric water content	%
ψ	suction pressure	kPa
ψ_m	matric suction	kPa
ψ_o	osmotic suction	kPa
ψ_t	total suction	kPa
S_r	degree of saturation	%
w	gravimetric water content	%
T_s	surface tension	N/m
BDT	Brazilian Disc Test	
SWRC	Soil-water retention curve	
HAE	High Air-Entry	
AEV	Air-Entry Value	

1 INTRODUCTION

For several decades, the practice of geotechnical engineering has been based almost entirely on the principles of classical saturated soil mechanics. It has however been established that approximately 33% of the earth's surface is classified as arid or semi-arid (Dregne, 1976; ICE, 2011). In light of this fact it can be stated that the inherent assumptions of classical saturated soil mechanics may be inappropriate for many geotechnical problems. This study aims to investigate the tensile behaviour of three unsaturated soils when subjected to the Brazilian Disc Test.

1.1 BACKGROUND

The basic assumption of classical soil mechanics is that the soil under consideration is a two-phase continuum consisting of solid soil particles and a fluid (either air or water, but not both). In arid regions, such as South Africa, low-lying water tables are prominent. For this reason, the soils encountered in practice usually exist in an unsaturated/partially saturated state, i.e. a three-phase system consisting of solid particles, water and air. In such a situation, the assumptions related to classical soil mechanics become invalid and as such, the soils should be classified, analysed and modelled according to their unsaturated soil properties.

Although engineers have long been aware of the unsaturated state of these soils, reluctance to adopt unsaturated soil mechanics in practice can primarily be attributed to the difficulties and costs associated with determining their properties (Fredlund, 2000; Lu & Likos, 2004). Despite the conservatism associated with analysing all soils as being fully saturated, there are instances where the true behaviour of the soil may be of importance. Examples of these circumstances include, but are not limited to:

- certain problem soils such as:
    - collapsible soils;
    - dispersive soils;
    - dolomitic soils (where the soil arching over a cavity is often in a partially saturated state);
- slope stability designs and
- bearing capacity problems of shallow foundations.

Furthermore, the stability of short-term structures such as temporary excavations and cut slopes could be analysed using unsaturated soil mechanics. Analyses which fully capture the behaviour of unsaturated soils could provide contractors with additional flexibility during construction and, as a result, lead to substantial monetary savings.

A key characteristic of unsaturated soils is related to the presence of tensile strength. Whereas saturated soils are generally assumed to have none (in the absence of cementation or particle interlock), partially saturated soils do possess a certain degree of tensile strength. The existence of two phenomena known as surface tension and matric suction brought about by the presence of the third air phase, result in the development of inter-particle forces of attraction. Tensile strength between soil particles of an unsaturated soil increases the effect of particle interlock, which in turn increases the overall shear strength of the soil mass. Due to its profound effect, the focus of this dissertation is to investigate the tensile behaviour of unsaturated soils across a range of moisture contents.

1.2 STUDY OBJECTIVES

The primary focus of this study was to investigate the tensile behaviour of three different unsaturated soils across a range of moisture contents. The behaviour was investigated with reference to strain development, the magnitude of tensile strength, as well as the relationship between tensile strength and matric suction. To perform this investigation, the Brazilian Disc Test (BDT) method, an indirect testing procedure commonly used to test brittle materials such as concrete and rock was modified such that it could be applied to measure the tensile strength of unsaturated soils repeatably. The aim of this study can be subdivided into the following objectives.

- Modify the Brazilian Disc Test (BDT) procedure so that it could be repeatably and reliably used to measure the tensile strength of *unsaturated* soil discs.
- Evaluate the applicability of the BDT to different soil types across a range of moisture contents.
- For each soil type, investigate:
    - the materials' response to loading (i.e. brittleness or ductility);
    - the variation in tensile strength over a range of moisture contents and
    - the effect of matric suction on tensile strength.
- For the relationships stated in the preceding objective, identify similarities and differences between each soil type.

1.3 SCOPE OF STUDY

The scope of this dissertation is limited to the following aspects:

- Three material types were considered, namely gold tailings (coarse grained silt), iron tailings (fine grained silt) and a natural transported, clayey soil horizon overlying dolomitic bedrock;
- The controlled parameter of the samples tested was the gravimetric moisture content, i.e. no attempt was made to target specific unit weights;
- A constant sized disc (50 mm in diameter and 25 mm in thickness) was used for all BTDs performed (effect of samples size on test results was not investigated).

1.4 METHODOLOGY

The methodology followed for this dissertation is described below.

- A literature review was conducted on the basic concepts of unsaturated soils as well as common testing procedures employed to determine their parameters. Furthermore, research specific to the Brazilian Disc Test applied across a range of disciplines (soil mechanics, rock mechanics and concrete technology) was performed. The insight obtained regarding the application of the BDT from varying disciplines allowed for the most applicable experimental setup to be developed for testing unsaturated soils.
- A framework for the experimental work conducted is outlined as follows:
    - materials were chosen to bear some practical relevance to engineering problems encountered in practice and to cover a range of particle size distributions;
    - testing was performed to determine the Soil Water Retention Curves (SWRCs) for all materials considered. This allowed for qualitative correlations to be drawn between the tensile strength and matric suction with a variation in moisture content;
    - moisture contents were selected to, as far as possible, cover the three saturation regimes of each soil type (capillary, funicular and pendular regimes);
    - the tensile strength of each material across the range of moisture contents considered was determined through the use of the BDT.
- Results of the above-mentioned experimental work were analysed with particular emphasis on the characteristics and relationships outlined in Section 1.2

1.5 ORGANISATION OF REPORT

The layout of this dissertation is as follows:

- Chapter 1 provides an introduction to this dissertation.
- Chapter 2 presents a literature review beginning with a discussion on the various characteristics of unsaturated soils. The relevance of this particular field is then emphasised with particular reference to three practical engineering problems. Finally, a section is included highlighting some common laboratory tests performed on unsaturated soils and is concluded with a discussion on tensile testing procedures.
- Chapter 3 describes the experimental procedure that was carried out;
- Chapter 4 presents an analysis of the results obtained from the experimental work, as well as a general discussion of trends and relationships that were observed;
- Chapter 5 highlights the conclusions reached in this study and provides recommendations for further research;
- A list of references pertaining to this study;
- Appendix A contains the dimensions, masses, densities, gravimetric moisture contents and the degree of saturation of every sample tested;
- Appendix B contains a conference publication which served as a preliminary study to this dissertation.

2 LITERATURE REVIEW

Based on past and current research, this chapter provides discussions of the various facets contributing to the tensile strength of unsaturated soils. The literature review begins by introducing a collection of definitions and concepts which are important to understanding the fundamental mechanisms associated with unsaturated soils. Once a basic understanding of the field is established, focus is turned to the various applications of unsaturated soil mechanics and, in particular, the presence and importance of tensile strength. The chapter outlines some of the conventional testing procedures for unsaturated soils and concludes with a discussion of the test around which this dissertation is based, namely the Brazilian Disc Test.

2.1 INTRODUCTION TO UNSATURATED SOILS

In the early development of soil mechanics, when concepts and principles were being established to outline a relatively new science, much of the research took place in wetter regions where the annual precipitation exceeds evaporation. In such regions, the water table is positioned close to the ground surface and, as a result, the assumption of soil being completely saturated is generally acceptable. In the past few decades however, as geotechnical engineering practice has advanced, it has become increasingly known that this assumption is often not valid as 37% of the earth's surface is classified as arid or semi-arid (Warren, 1994).

Taking cognisance of this fact as well as the knowledge that the behaviour of unsaturated soils differs substantially from their saturated counterpart, it becomes evident that it is vital to gain a comprehensive understanding of these soils.

In an effort to understand the behaviour of unsaturated soils it is beneficial to begin by discussing its most fundamental property, namely the presence of a third phase. In contrast to what has been well established in saturated soil mechanics, unsaturated soils are primarily characterised by the simultaneous presence of water and air in the soil matrix. Unsaturated soils are thus generally referred to as being a three-phase system. However, as will be described in this section, the air-water interface (contractile skin) plays a key role in the behaviour of unsaturated soils and as a result, the argument for it being considered as a fourth separate phase when considering stress analyses is warranted (Fredlund & Rahardjo, 1993).

The presence of the air-water interface brings about two phenomena which are largely responsible for the increased strength of unsaturated soils, namely surface tension and matric suction, both of which are discussed in the following section.

2.1.1 Surface tension

At an elementary level, surface tension is often thought of as an 'elastic skin' (Sophocleous, 2010) on the surface of the liquid which gives it the ability to support the weight of a denser material, e.g. floating a needle on a water surface. To understand how this property manifests itself, one needs to investigate it at a molecular level. Consider Figure 2-1 which illustrates a volume of water in direct contact with the air. A comprehensive explanation of this property as provided by Sophocleous (2010) is summarised in the following paragraph.

In Figure 2-1, a molecule in the body of the water (Molecule A) will experience both attractive and repulsive forces of equal magnitude in all directions. This interaction between neighbouring molecules has the effect of reducing their potential energy. Moving upwards towards the interface, water molecules begin interacting with the molecules of the gas directly above it. Since the molecules in this region (e.g. Molecule B) have fewer neighbouring molecules above it, they will experience a net downward force of attraction towards the body of the fluid. Furthermore, a consequence of having fewer neighbouring molecules is that their potential energy will be reduced by a smaller amount. Work therefore needs to be done to counteract this downward pull. As a result, molecules at or near the surface of the liquid will possess a positive potential energy which is termed *surface tension* with units of potential energy per unit area (J/m^2) or equivalently, force per unit length (N/m).

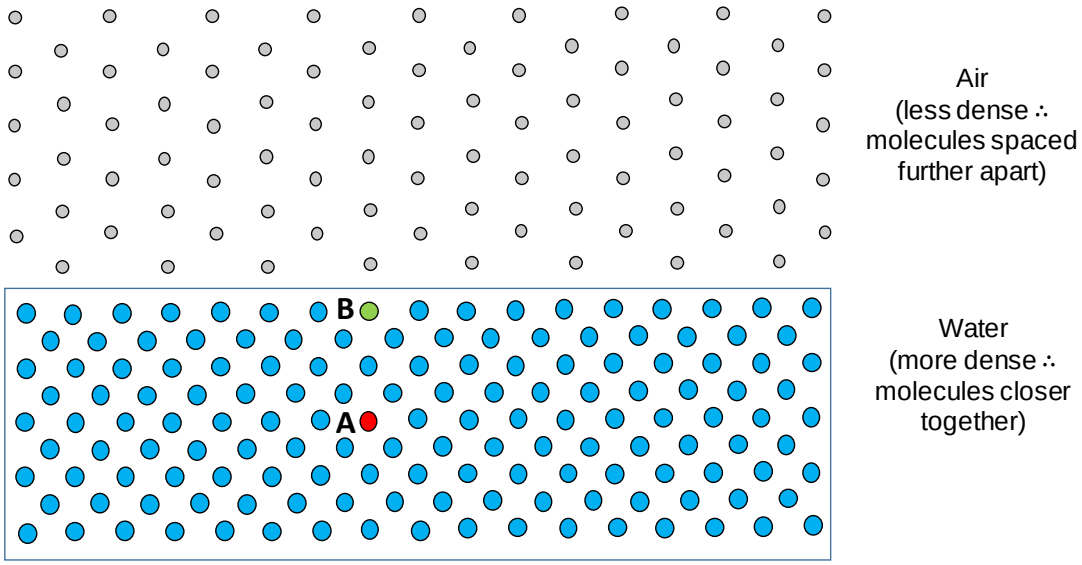

Figure 2-1: Interaction between liquid and gaseous phases

The presence of surface tension and the accompanying change in geometry of the air-water interface occurs as a result of the existing pressure difference across the contractile skin. The curvature that develops within the meniscus will always orientate itself concave towards the region of higher pressure. This is due to the fact that the less dense medium will tend to expand (Lu & Likos, 2004). Therefore, similar to the manner in which an inflated balloon will display a concave curvature towards the higher pressure inside the balloon, the air-water interface in unsaturated soils will develop a curvature that is concave towards the gaseous phase. Relative to the air pressure, generally assumed to be atmospheric ($u_a = 0$), the pore water pressure must then be negative ($u_w < 0$) (Fredlund & Rahardjo, 1993). By considering mechanical equilibrium of the air-water interface, a relationship provided in Equation 2.1 between surface tension, pressure difference and radius of curvature can be established. Figure 2-2 illustrates, in two-dimensional space, the forces and pressures acting on the air-water interface. The values of u and $(u + \Delta u)$ represent the pressures acting on either side of the meniscus, R denotes its radius of curvature and T_s represents the surface tension.

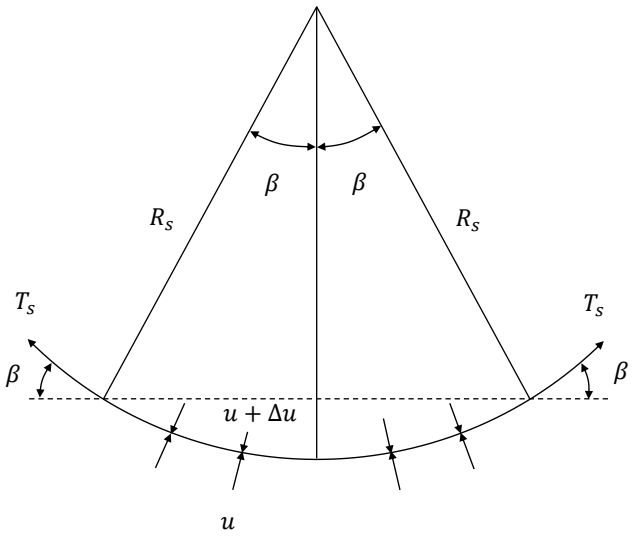

Figure 2-2: Forces acting on the air-water interface (Fredlund & Rahardjo, 1993)

Considering vertical force equilibrium along the interface:

$\Sigma F_Y = 0$:

$$2T_s sin\beta + \big(u - (u + \Delta u)\big)2Rsin\beta = 0$$

$$\Delta u = \frac{T_s}{R} \quad 2.1$$

Equation 2.1 can then be extended to the Young-Laplace equation (Sophocleous, 2010) to describe the pressure difference across an interface in three dimensions. This relationship is provided in Equation 2.2.

$$\Delta u = T_s\left(\frac{1}{R1} + \frac{1}{R2}\right) \quad 2.2$$

Where:

R_1 and R_2 are the radii of curvature along two orthogonal directions.

As previously established, the pressures acting across the air-water interface in unsaturated soils are the atmospheric air pressure (u_a) and the soil-water pressure (u_w). If it is assumed that $R_1 = R_2 = R$, Equation 2.2 can be simplified to the form presented in Equation 2.3.

$$(\mathrm{u_a} - \mathrm{u_w}) = \frac{2T_s}{R} \quad 2.3$$

This difference in pressure across the interface ($u_a - u_w$) is termed matric suction. A characteristic which becomes evident when considering Equation 2.3 is that the value of matric suction and the radius of curvature of the meniscus are inversely related. Therefore, for high values of matric suction, the radius of curvature will reduce. At the other extreme if the matric suction was reduced to zero, it would result in there being no curvature of the air-water interface and thus the radius of curvature would tend to infinity. The presence of matric suction and surface tension in unsaturated soils is vital since it is the combination of these two components which provide unsaturated soils with tensile strength (Kim & Hwang, 2003). Matric suction however is only one component of total soil suction, which is a concept described in the following section.

2.1.2 Soil suction

The original development of the concept of soil suction (or soil-water potential) took place in the 1900s and was primarily concentrated in the field of agricultural sciences to describe soil-water-plant relationships (D. G. Fredlund & Rahardjo, 1993). The purpose of this concept in agriculture is to define the *availability* of water rather than the *presence* of it. For example, if a sandy soil and a clayey soil at the same volumetric water content are compared, a plant would be able to access more water in the sandy material than it would in the clayey one. This is attributed to the different energy states of the two soils (Radcliffe & Šimůnek, 2010). From an engineering perspective, however, it is crucial that the concept is understood to properly describe the mechanical and physiochemical behaviour of unsaturated soils. Soil suction can be defined as the thermodynamic potential of soil-water, relative to the potential of free-water. Free-water is water that is free of solutes, has no external forces acting on it (other than gravity), and no interactions with other phases that might result in curvature of the air-water interface (Lu & Likos, 2004). Equation 2.4 illustrates how soil suction can be represented mathematically as the algebraic sum of *matric* and *osmotic* suction. It should be noted that both components of total suction decrease the thermodynamic potential of soil-water relative to the state of free-water (Lu & Likos, 2004; Radcliffe & Šimůnek, 2010).

$$\psi_T = \psi_m + \psi_o \qquad 2.4$$

Where:

ψ_T = Total suction (kPa)

ψ_m = Matric suction (kPa)

ψ_o = Osmotic suction (kPa)

Matric suction

Matric suction is the component of total suction which incorporates the effects of both capillarity and short-range adsorption (Lu & Likos, 2004; Radcliffe & Šimůnek, 2010). To illustrate the concept of capillarity, soil pores can be interpreted as capillary tubes partially submerged in a container of water, as illustrated in Figure 2-3. The height to which water rises in a capillary tube, as well as the shape of the meniscus, is dependent on the interaction of

cohesive intermolecular forces within the water and the adhesive forces between the water and glass (solid) surfaces (Tiab & Donaldson, 2004). The adhesive forces which cause water to attach itself to the circumference of the tube, as well as the intermolecular cohesion of water will cause water to rise within the tube (Sophocleous, 2010).

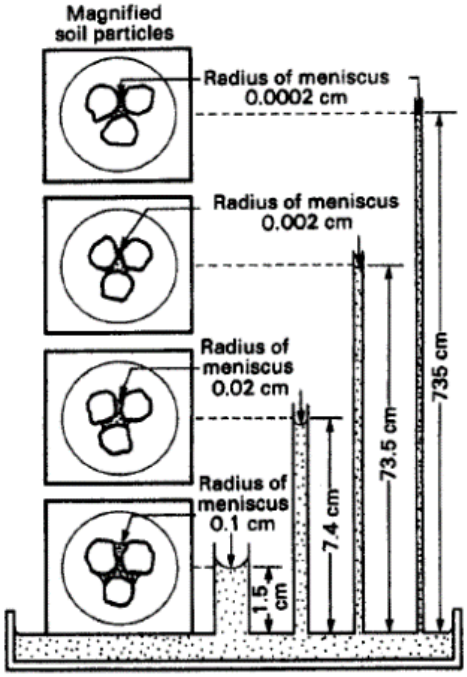

Figure 2-3: Capillary tubes illustrating the effect of capillarity within soil profiles (Fredlund & Rahardjo, 1993)

Within a soil profile, it often happens that a finite portion of soil above the water table will become saturated. This region is called the capillary fringe which, as the name implies, occurs as a result of capillarity. For a fine grained material with narrower pore spaces or capillaries, the extent of capillary rise will be greater than in a coarser material (see Figure 2-3).

Short-range adsorption between soil-water and soil solids is the second component of matric suction. This component occurs as a result of the electrical and van der Waals force fields present around the vicinity of the soil-water interface. Since the strength of these fields decreases substantially with distance away from the soil particle surface, the effect of adsorption is most applicable for soils at low moisture contents. In this state, soil-water is present only as thin films covering the individual soil particles (Lu & Likos, 2004).

Osmotic suction

Osmotic suction accounts for the effects of dissolved ions in soil-water. Since water is attracted to dissolved solutes, soil-water tends to move from a position of low ion concentration to an area of high ion concentration (Radcliffe & Šimůnek, 2010). This property can be illustrated by considering two sections of a container separated by a semi-impermeable membrane which allows only pure water to pass through it as shown in Figure 2-4.

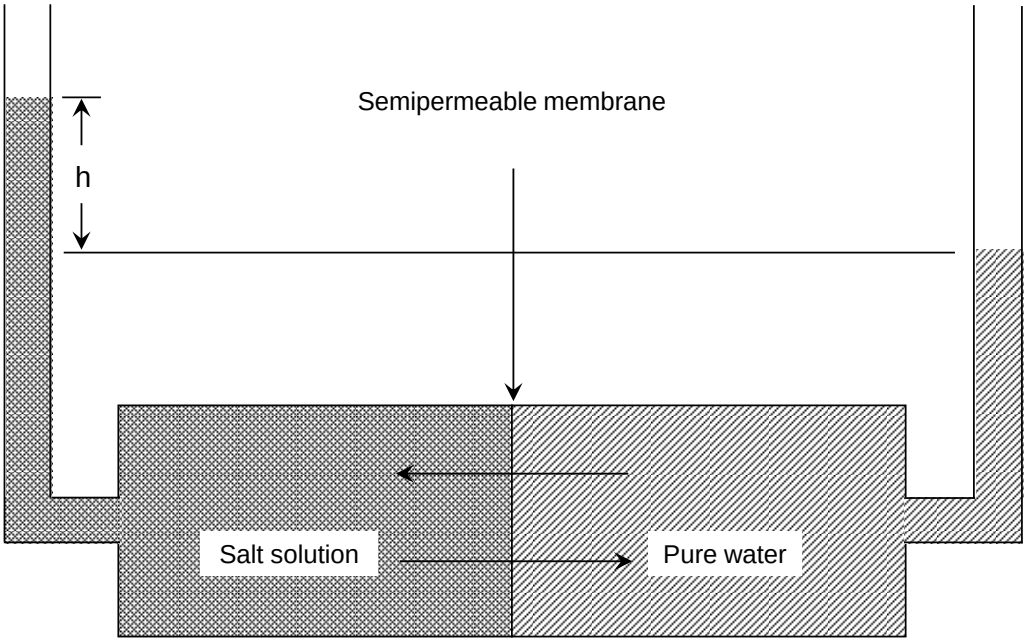

Figure 2-4: Graphical description of osmotic suction (adapted from Radcliffe & Šimůnek, 2010)

If the left side of the container contains solutes and the right side of the container consists of pure water, the attraction of water to dissolved ions will result in a flow of water moving towards the salt solution. This will result in a pressure increase in the left portion of the container which is termed *osmotic pressure*. The applicability of osmotic suction is particularly relevant when considering volume changes within clayey profiles. Under such conditions, phenomena such as osmotic consolidation or osmotically induced consolidation can occur. Details of these mechanisms have been discussed by Barbour & Fredlund (1989).

2.1.3 The Soil Water Retention Curve (SWRC)

Arguably the most powerful/versatile tool in describing the behaviour of unsaturated soils is the Soil Water Retention Curve (SWRC), which illustrates the relationship between moisture content (either gravimetric or volumetric) and soil suction. The relationship between soil suction and moisture content has also been referred to as the Soil Water Characteristic Curve (SWCC). However, since the relationship is strongly dependent on the initial state of the soil, it cannot be considered as a 'characteristic' (Toll, 2012). For this reason, the term Soil Water Retention Curve (SWRC) is used for the remainder of this dissertation. The first published SWRCs were the result of research conducted by a soil physicist by the name of Edgar Buckingham in 1907 (Narasimhan, 2005). Since then, SWRCs have been invaluable to research conducted across several disciplines including soil physics, agronomy and agriculture (Fredlund, 2000). From an engineering perspective, the information provided in an SWRC allows soil parameters such as unsaturated hydraulic conductivity and shear strength to be derived (Yang *et al*., 2004).

The negative pore pressure in unsaturated soils can be considered as existing in separate regimes or stages, all of which are illustrated in Figure 2-5. Terms used by various authors to describe the different regimes are included in Figure 2-5. For the remainder of this dissertation, those proposed by Lu & Likos (2004) are adopted. The capillary regime is a term used to describe the portion of soil above the phreatic surface which is kept saturated due to the presence of a negative pore water pressure (commonly referred to as the capillary fringe). In the capillary regime, the only point where soil-water comes into contact with the air-phase is at the boundary of the soil mass. This has an important implication on the inter-particle force of attraction since the contribution of surface tension is only present at the boundaries of the soil mass. In its body, however, only negative pore-water pressure contributes to tensile strength.

Within capillary regime, the water content of the soil will remain relatively constant (close to the saturated water content) with an increase in suction. Suction will continue to increase until the air-entry pressure of the soil is reached. At this point, air begins being sucked into the macropores of the soil structure. The soil then begins to desaturate and transition into the funicular regime.

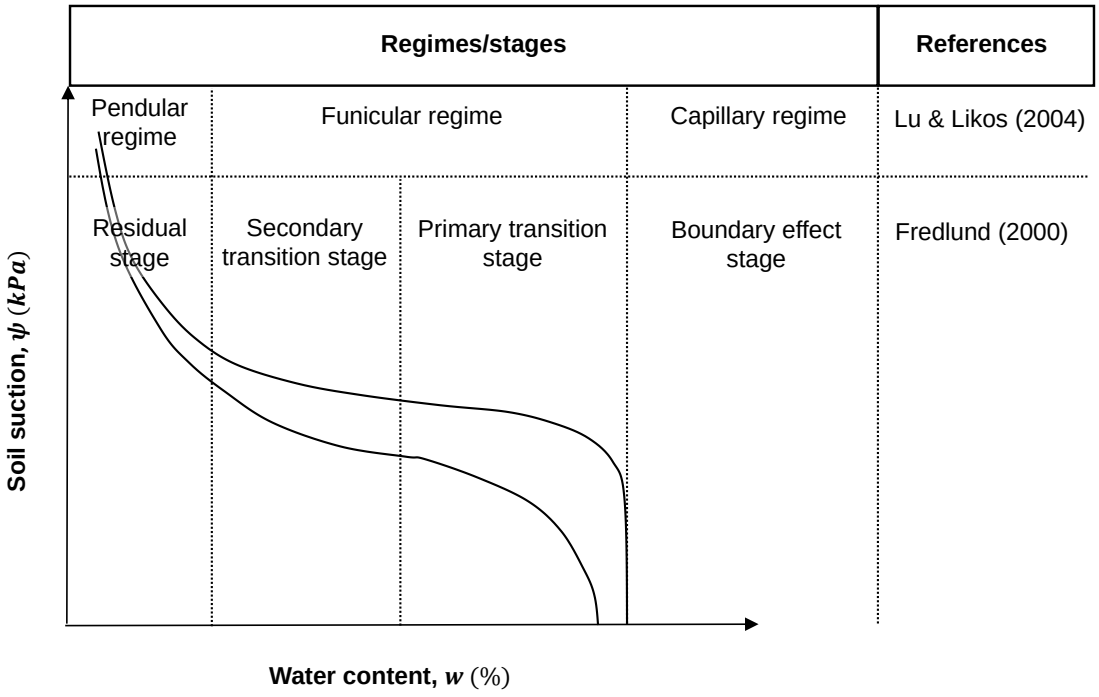

Figure 2-5: Different regimes/stages of negative pore water pressure

The state of pore water in the funicular regime consists of both liquid bridges and pores filled with water. As a result, both short-range adsorption and capillarity contribute to suction in this region (capillarity being the dominant mechanism). A quality of this section of the SWRC is that it reflects the pore size distribution of the soil. For a soil with a narrow pore size distribution (i.e. a uniformly graded soil), the gradient of the funicular regime will be gradual. In contrast, a steeper slope in this region would be indicative of a wide pore size distribution (a well graded soil) (Lu & Likos, 2004). These correlations between the gradient of the SWRC in the funicular regime and the pore size distribution of the soil will be inverted if the curve is plotted with suction as the independent variable.

At high values of suction, the moisture content of the soil reaches a point where it again remains constant. This region is termed the pendular regime and the moisture content with which it is associated is the residual moisture content. In this region, the water phase is discontinuous and exists only as thin layers surrounding individual soil particles (Kim & Hwang, 2003). The dominant mechanism of suction in the pendular regime is the short-range adsorption effects between the discontinuous water phase and the surfaces of soil solids (Lu *et al.*, 2009). It should be noted that the effects of osmotic suction remain constant across the entire range of moisture contents, unless the concentration of dissolved solutes is changed (Lu & Likos, 2004).

Another distinctive feature of the SWRC is the hysteretic behaviour it exhibits upon wetting and drying (shown in Figure 2-6). A soil sample starting from a saturated state that is dried out

will follow the *Primary Drying Curve*. In contrast, an initially oven dried soil that is inundated with water will follow the *Primary Wetting Curve*. These bounding curves establish an envelope of possible states within which a soil can exist (Toll, 2012). A soil starting from a saturated state that is dried to a moisture content of *w* will experience a higher value of suction than one which was brought to the same moisture content through wetting processes (e.g. infiltration or capillary rise).

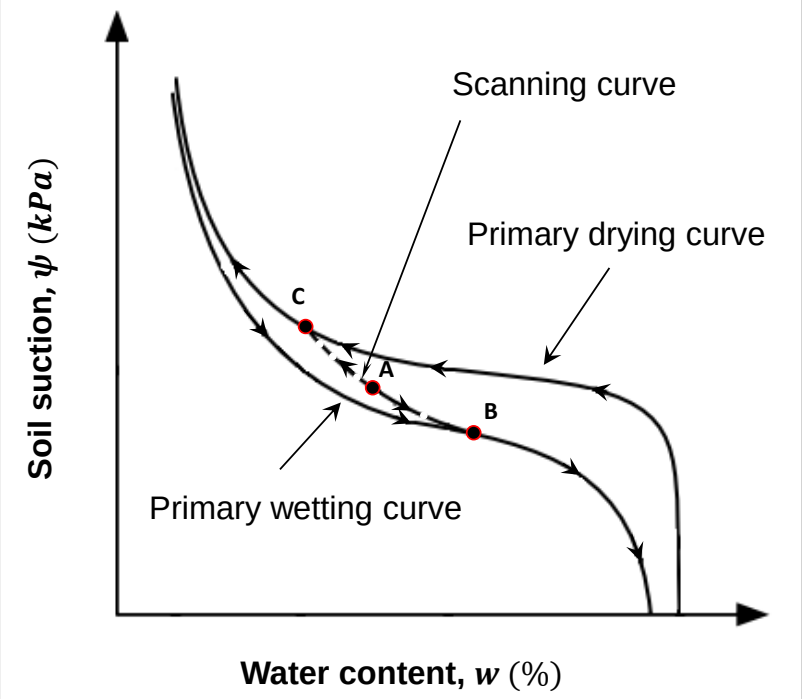

Figure 2-6: SWRC hysteresis (adapted from Lu & Likos, 2004)

Various authors (Lu & Likos 2004; Pham *et al.*, 2005) have attributed this hysteretic behaviour to several mechanisms which include:

- the 'ink-bottle' effect (related to pore geometry);
- entrapped air bubbles that occur during the wetting process;
- the alteration of pore fabric during swelling (wetting) and shrinking (drying) and
- wetting and drying contact angle hysteresis.

In addition to the four mechanisms mentioned above, Lu & Likos (2004) have stated that 'capillary condensation', a unique wetting process at low moisture contents could also be a contributing factor to SWRC hysteresis. Another feature indicated in Figure 2-6 is a so-called scanning curve. If an undisturbed soil sample is tested, it will have an initial in-situ moisture

content and suction value which lies somewhere between the bounding wetting and drying curves (Point A). If a sample, initially at Point A is then inundated with water, it will follow a scanning curve until it reaches the bounding wetting curve at Point B. Similarly, if the same sample were to be dried out from its initial state, a scanning curve approaching the bounding drying curve would be followed, eventually meeting it at Point C.

There are therefore infinitely many scanning curves contained within the two bounding curves which may be followed for small wetting and drying cycles (Lu & Likos, 2004). It can thus be stated that the initial state of the sample is of utmost importance if quantitative relationships between matric suction and moisture content are required.

2.1.4 Shear strength of unsaturated soils

The principle of effective stress as defined by Terzaghi (1936) is perhaps the single most important concept in understanding saturated soil mechanics (Atkinson & Bransby, 1978). In his publication, Terzaghi (1936) made the following statement to emphasise the importance of effective stress:

"All measurable effects of a change of stress, such as compression, distortion and a change of shearing resistance, are exclusively due to changes in effective stress".

Taking cognisance of its fundamental role in classical soil mechanics, the desirability of extending the principle to describe the behaviour of unsaturated soils is warranted. One of the first attempts at applying an equivalent effective stress approach to unsaturated soils was proposed by Bishop (1959). Bishop defined the effective stress model presented in Equation 2.5:

$$\sigma' = \sigma - u_a + \chi(u_a - u_w) \qquad 2.5$$

Where

σ' = Effective stress (kPa)

σ = Total stress (kPa)

u_a = Air pressure (kPa)

u_w = Pore water pressure (kPa)

χ = Empirical factor related to degree of saturation ranging between 0 and 1

The inclusion of the parameter χ seemed to provide an elegant means of describing 'effective stress' for soils across a range of moisture contents. For a completely dry soil $\chi = 0$ and for a saturated soil $\chi = 1$, thus reducing to the classical definition of effective stress for saturated soils. In addition to Bishop's model, numerous other authors proposed similar relationships aimed at extending the principle of effective stress to unsaturated soils (Aitchison, 1961; Croney *et al.*, 1958; Jennings, 1961; Lambe, 1960; Richards, 1966). Fredlund & Morgenstern (1977) emphasised the fact that by incorporating a soil parameter (χ), the model proposed by Bishop was ultimately a constitutive relationship rather than a description of the stress state of the soil. This flaw is common to the models proposed by the authors mentioned above (Fredlund & Morgenstern, 1977). Furthermore, they stated that the parameter was ultimately impossible to quantify uniquely.

Soon after its publication, Bishop's effective stress model was criticised by Jennings & Burland (1962) who pointed out that while the model successfully predicted the shearing behaviour of unsaturated soil, it could not account for volume change (wetting-induced collapse) characteristics (Toll, 2016; Georgiadis, 2003). Burland (1965), as cited by Toll (2016), went on to highlight that the presence of suction gives rise to two phenomena related to shear strength. In addition to increasing contact stresses between particles, the presence of surface tension also produces a stabilising effect which increases shearing resistance. The importance of separating the stress state variables $(\sigma - u_a)$ and $(u_a - u_w)$ was highlighted by Burland and has since been emphasised by numerous authors (Fredlund & Rahardjo, 1993)

In light of the above-mentioned shortcomings, it becomes evident that the principle of effective stress as being a unique stress state variable governing all mechanical behaviour of soils is not applicable to unsaturated soils. The use of two stress state variables ($(\sigma - u_a)$ and $(u_a - u_w)$) treated separately have thus been shown to adequately describe the shear strength and volume change relationships in unsaturated soils (Fredlund & Rahardjo, 1993). The remainder of this section presents a constitutive relationship describing the shear strength of unsaturated soils in terms of these two stress state variables.

Extended Mohr-Coulomb failure criteria:

Perhaps the most commonly used shear strength equation for unsaturated soils is that proposed by Fredlund *et al*. (1978) as provided in Equation 2.6.

$$\tau = c' + (\sigma - u_a)tan\phi^a + (u_a - u_w)tan\phi^b \quad 2.6$$

Where

τ = Shear strength (kPa)

c' = Effective cohesion (at $(\sigma - u_a)$ & $(u_a - u_w) = 0$) (kPa)

ϕ^a = Angle of friction associated with net normal stress $(\sigma - u_a)$ (°)

ϕ^b = Angle of friction associated with matric suction $(u_a - u_w)$ (°)

The above relationship describes an extended Mohr-Coulomb failure envelope governed by the independent contributions of the stress state variables, net normal stress and matric suction. The contributions to shear strength of the two variables are characterised by the friction angles ϕ^a and ϕ^b. A key feature of the extended failure criterion is that it addresses the two stress state variables separately as suggested by Burland (1965). Figure 2-7 illustrates the failure surface defined by Equation 2.6.

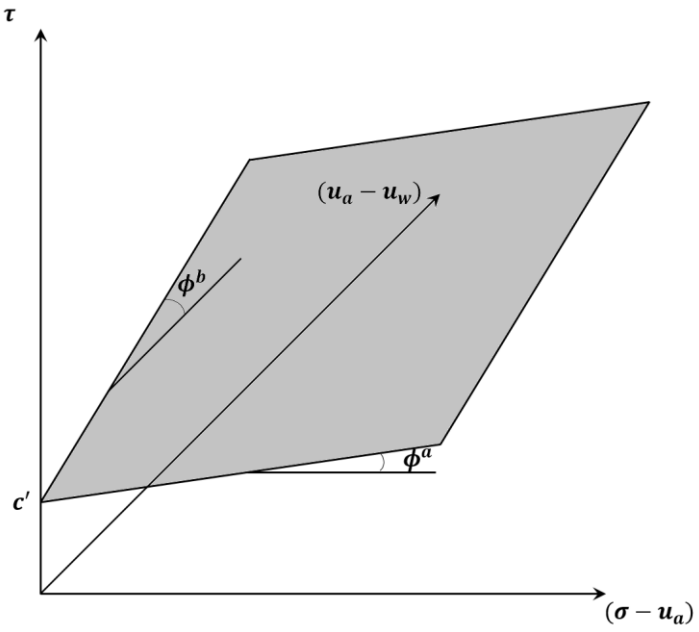

Figure 2-7: Extended Mohr-Coulomb failure envelope (adapted from Toll, 2016)

Fredlund *et al*. (1987) addressed the non-linearity of the proposed failure surface with respect to the τ vs $(u_a - u_w)$ plane, i.e. $(\sigma - u_a) = 0$. In this publication, the variation of ϕ^a with an increase in matric suction was described as follows. At saturation, the effects of pore-water pressure and total normal stress on shear strength are equal, hence the contributions of both stress state variables are characterised by the same friction angle, ϕ^a. Within this region, an increase in net normal stress results in a shear strength gain equivalent to what would be achieved if matric suction was increased by the same amount. Up until the point where the soil begins to desaturate, one friction angle is used in Equation 2.6 and it therefore reduces to the failure envelope associated with saturated soils.

However, if matric suction is increased to a point beyond the air-entry value of the soil, desaturation commences and is accompanied by a decrease in ϕ^b. Following desaturation, the amount of strength gain achieved by increasing matric suction is thus less significant than the strength gained by an equivalent increase in net normal stress. Fredlund *et al.* (1987) noted that above the air-entry value ϕ^b remains relatively constant with further increases in suction. Figure 2-8 illustrates the change in friction angle for different degrees of saturation.

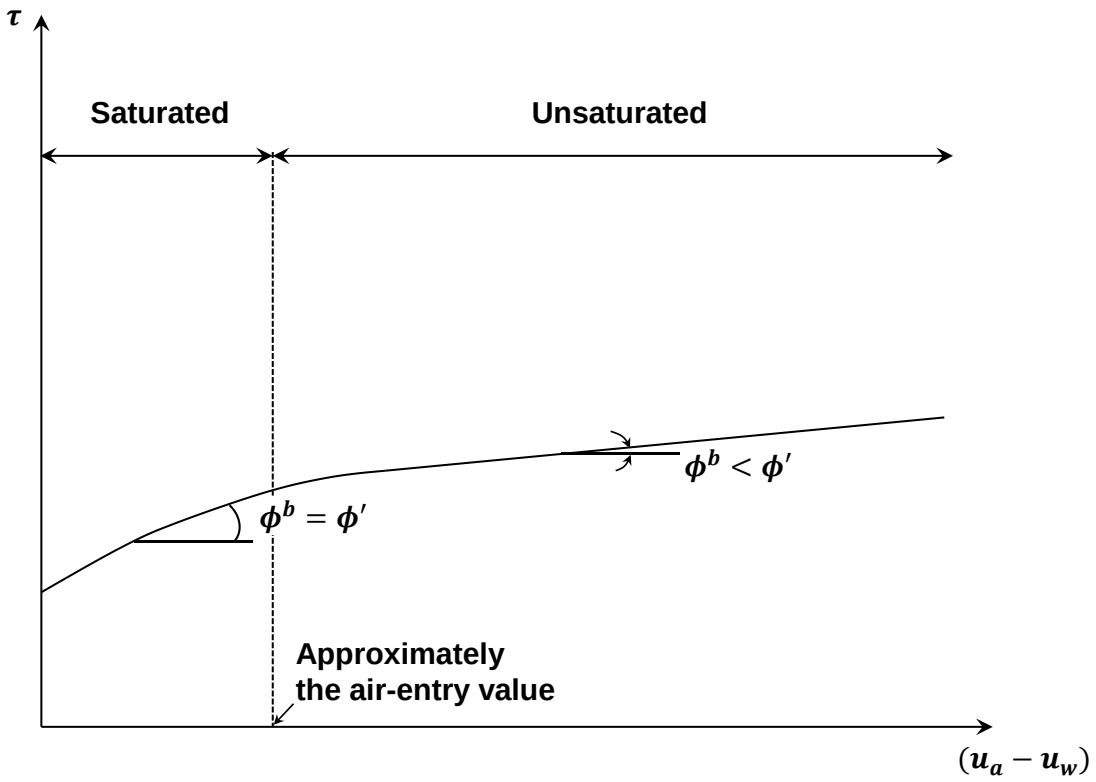

Figure 2-8: Variation of ϕ' with an increase in matric suction (adapted from Fredlund *et al.*, 1987)

When the extended Mohr-Coulomb failure criterion was initially proposed by Fredlund *et al*., (1978), it was suggested that ϕ^a could be taken as being equal to the effective internal angle of friction, measured under saturated conditions. It has however been shown that the assumption of $\phi^a = \phi'$ does not hold for all values of matric suction (Toll 2012). Figure 2-9 presents the results of constant water content triaxial tests (analogous to undrained tests in saturated soils) for two tropical soils.

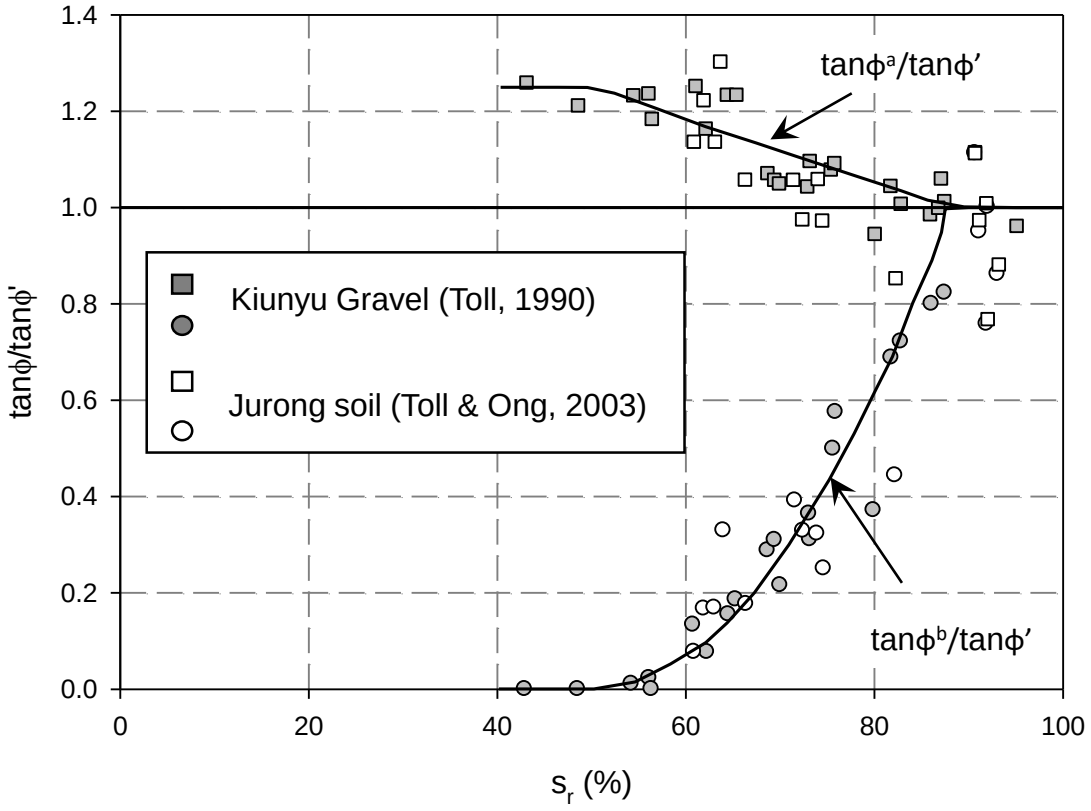

Figure 2-9: Variation of ϕ^a and ϕ^b with a change in saturation (Toll, 2012)

Figure 2-9 highlights the fact that the assumption of $\phi^a = \phi'$ only holds for higher degrees of saturation. Below $S_r \approx 90\%$, a significant increase in ϕ^a can be seen. This phenomenon is of particular importance when evaluating the role of tensile strength in unsaturated soils. Toll (2012) described how the increase in ϕ^a at low moisture contents occurs due to the presence of aggregations in the soil matrix, allowing it to behave as a coarser material. Toll (2012) goes on to explain how these aggregations are able to retain their structure upon shearing due to the presence of suction. However, if the concepts presented in Section 2.1 are revisited, it can be appreciated that the attraction between soil particles are as a result of not only matric suction,

but rather a combination of matric suction and surface tension. In light of its significant contribution to overall shear strength, it can be seen that a proper understanding of tensile strength in unsaturated soils is invaluable.

2.2 THE RELEVANCE OF TENSILE STRENGTH IN GEOTECHNICAL ENGINEERING

As discussed in the previous section, the presence of air in unsaturated soils results in many phenomena which do not occur in saturated soils. It should therefore be appreciated that along with the third phase, unsaturated soils inherit distinct behavioural peculiarities. The following section aims to highlight several instances in geotechnical engineering practice in which the presence of tensile strength is significant. The section concludes with a brief discussion of a strength prediction model which utilises only the tensile strength of a soil to fully define its strength.

2.2.1 Collapsible soils

As early as the 1950s, the problem of collapsible soils was identified (Jennings & Knight (1957)). Schwartz (1985) presented a state of the art paper reviewing engineering practice in South Africa regarding soils with a collapsible fabric. In this publication, a collapsible soil is defined as one which can withstand relatively large applied stresses at low moisture contents but will exhibit large decreases in volume upon wetting, with no increase in applied stress. In short, ‘collapse’ is the additional settlement that occurs if an unsaturated soil with a collapsible fabric is wetted. This concept is illustrated in Figure 2-10. Rogers (1994) argued that defining collapsible soils as occurring only in unsaturated soils is limiting from a geotechnical standpoint. However, since a major portion of collapsible soils does conform to this definition it is valid to understand this branch of collapsible soils. For this reason, the remainder of this section will consider collapsible soils occurring in an unsaturated state as defined by Schwartz (1985).

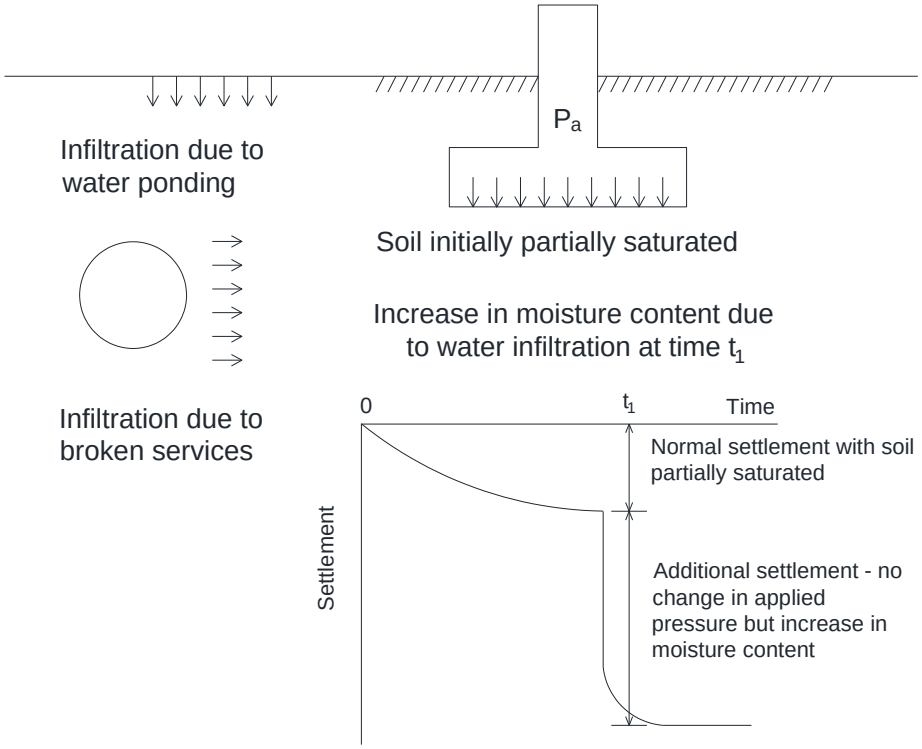

Figure 2-10: Concept of additional settlement due to increase in moisture content (adapted from Schwartz 1985)

In order for collapse to occur Schwartz (1985) outlined several conditions that must be satisfied, all of which are listed below.

1. *The soil must possess a collapsible fabric*. This can generally be identified by a high void ratio (low dry density) and a high shear strength at low moisture contents.

   In light of the mechanisms discussed in Section 2.1, it can be stated that this apparent high value of strength is attributed to the higher values of matric suction which are typical at lower moisture contents. It should be noted that while dry densities and void ratios can alert an engineer to the presence of a collapsible soil, a high dry density (and low void ratio) does not necessarily exclude the possibility of collapse. This point was emphasised by Rust *et al*. (2005) in an investigation of the sandy soils of Mozal, Mozambique.

2. *The soil must be unsaturated.* Research by Jennings & Knight (1957) highlighted the importance of degree of saturation (S_r) on collapse potential by stating that there exists a critical degree of saturation (S_r^{crit}) above which collapse will not occur.

Schwartz (1985) goes on to state that there exists a relationship between S_r^{crit} and particle size distribution. Table 2-1 highlights typical values of S_r^{crit} for different soil types. If the results in Table 2-1 are more closely investigated it can be seen that generally, for a finer material, S_r^{crit} will be higher than for a coarser material.

Table 2-1: Typical values for degree of saturation (adapted from Schwartz, 1985)

Soil type	Critical degree of saturation	Reference
Transported clayey sand Witbank area 35% finer than 0.075 mm	46-51%	Knight (1961)
Transported silty sand Kaalfontein area near Kempton park 40% finer than 0.075 mm	61%	
Fine gravels Fine silty sands Clayey silts	6-10% 50-60% 90-95%	Jennings & Knight (1957)
Berea red sands 25% finer than 0.075 mm	69%	Errera (1977)
Residual granite Coarse grained with 15% finer than 0.075 mm	52%	
Transported sand from Sishen area 10% finer than 0.075 mm	21%	

Again, if the concepts outlined in Section 2.1 are revisited, it is seen that this conforms to the theoretical behaviour of unsaturated soils. Finer materials are able to sustain higher values of matric suction due to the presence of narrow pore spaces. This higher value of matric suction corresponds to a higher increased strength. For coarser materials, only a small amount of matric suction (and therefore strength) can be sustained. For this reason, the moisture content in a coarse material can vary over a large range without the change in strength being sufficient to induce collapse. Figure 2-11 illustrates this concept graphically. The markers in the figure illustrate a hypothetical critical degree of saturation

for both a coarse and fine material. The blue shaded region represents the range over which moisture content can vary, without collapse occurring.

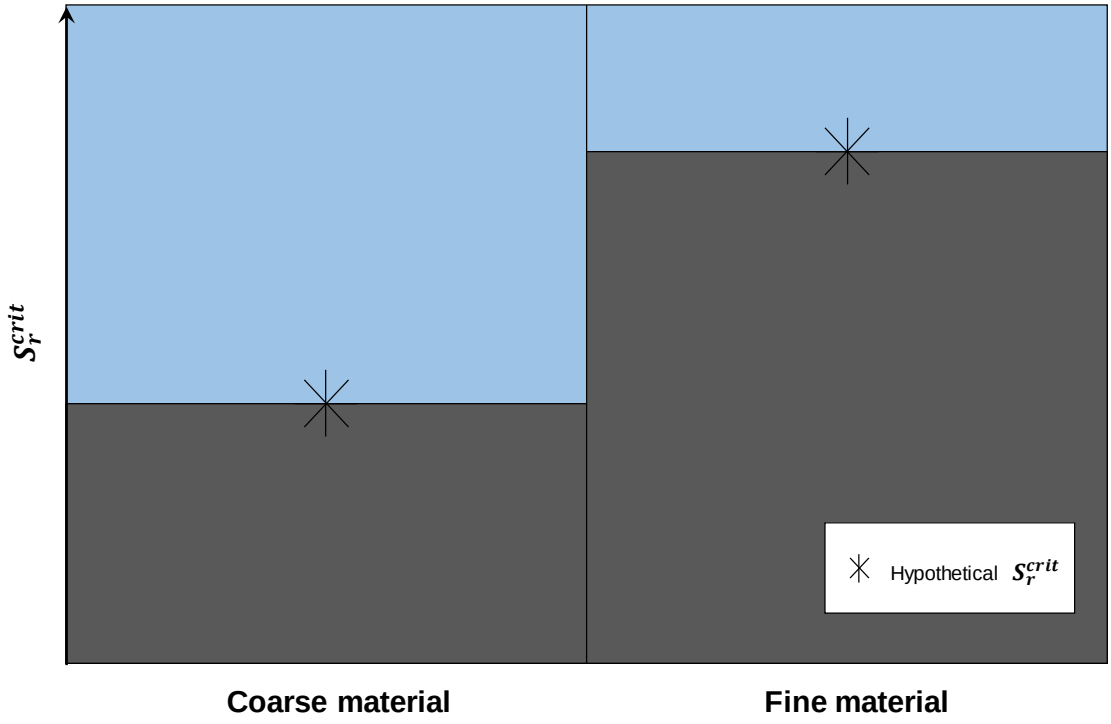

Figure 2-11: Critical degree of saturation for different soil types

3. *There must be an increase in moisture content.* This increase in moisture content, which corresponds to a reduction in matric suction, can be considered to be the trigger for collapse. The rate at which collapse occurs is thus related to the rate of wetting.

4. *Soils must be submitted to a pressure which is greater than their overburden pressure.* This criterion, postulated by Jennings & Knight (1957), states that soil at the ground surface will remain stable regardless of the change in moisture content of the subsoil. This final condition can however be considered a special case as both Jennings & Knight (1957) and Schwartz & Yates (1980) highlight occurrences of non-stable ground surface conditions.

The first of the four conditions listed above refers to the necessity of a collapsible fabric. A collapsible fabric is one which is characterised by a loosely packed structure analogous to a house of cards. In explaining the behaviour of collapsing sands in Southern Africa, Blight (1994) describes how aeolian sands originally deposited in arid and semi-arid conditions now

exist in environments with a moister climate. As a result, partial weathering of the sands has led to small quantities of silt and clay now being constituents of the soil matrix. The metastable, loose packing structure of the soil is held in place by some form of inter-particle bonding. In the case of unsaturated soils (see Condition 2), this bonding or ‘tensile strength’ occurs as a result of matric suction and surface tension, sometimes accompanied by some form of cementation.

The trigger mechanism mentioned in Condition 3 highlights how inundation of the soil matrix will result in a loss of suction and therefore inter-particle bonding. Together with the loss of suction, it is possible that the dissolution of bonding material, e.g. calcium, can occur (Feda, 1994). The loss of inter-particle bonding between the sand grains ultimately results in collapse of the loose soil structure to a more densely packed state. Figure 2-12 illustrates a collapsible soil structure before and after inundation.

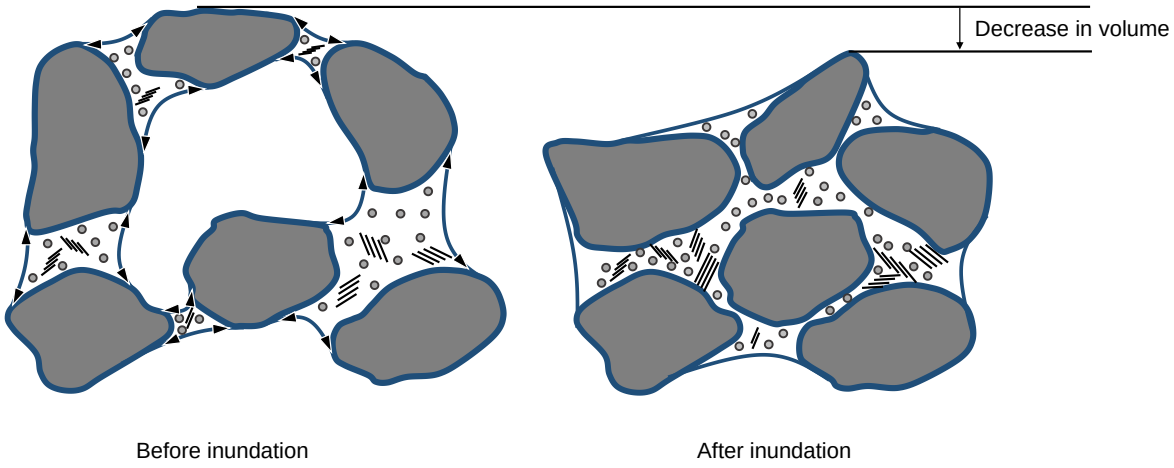

Figure 2-12: Collapsible soil structure before and after inundation

From the descriptions provided above, the role of tensile strength in unsaturated soils in the context of collapsible soils is emphasised. Schwartz (1985) highlighted how the effective stress concept, as defined by Terzaghi is not sufficient for describing partially saturated collapsible soils. An effort therefore needs to be made to better understand and quantify tensile strength in unsaturated soils.

2.2.2 The role of tensile strength in the formation of sinkholes

Of the problem soils encountered in South Africa, none have resulted in failures as catastrophic as those associated with dolomitic soils (Wagener, 1985). Jennings *et al*. (1965) described how subsidence on dolomitic formations can either occur gradually, resulting in structural damage or suddenly in the form of a sinkhole. While both of the occurrences can have substantial economic implications, the formation of a sinkhole occurring without any warning can also be fatal. Figure 2-13 illustrates the aftermath of the formation of a sinkhole which developed on the West Driefontein Mine on the 12th of December, 1962. A disaster which saw a three-storey crushing plant along with 29 employees swallowed by a steep-sided sinkhole measuring 55 m in diameter and 30 m in depth (Wagener, 1985). Since the 1960s numerous other occurrences of sinkholes have taken place in South Africa. In an effort to develop a database of karst related sinkhole and subsidence formation, Richardson (2013) noted that just over 3000 events (sinkholes, subsidences and ground cracks) have occurred in the Gauteng province (this study only considered events prior to the 31st of December, 2011). The frequency of these events, as well as the economic and social implications of their occurrence highlight the importance of understanding the mechanisms associated with their formation.

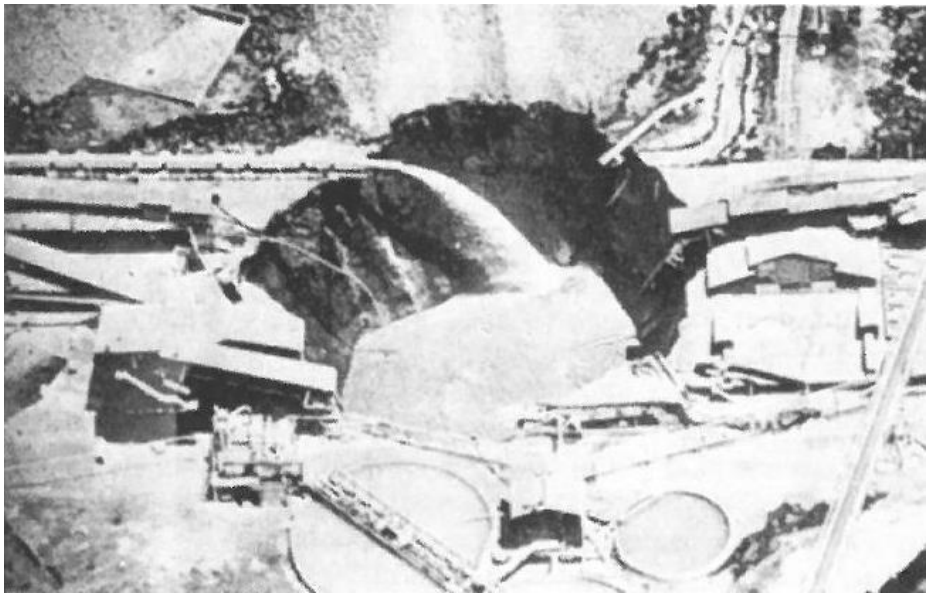

Figure 2-13: Sinkhole at the West Driefontein Mine, 1962 (Wagener, 1985)

Carbonate rocks are primarily comprised of two minerals, namely calcite and dolomite ($CaMg(CO_3)_2$). A carbonate which is composed mostly of calcite is termed limestone whereas one which is dominated by the presence of dolomite is referred to as dolomite rock (Warren,

2000). The geological formations on which sinkholes occur consist predominantly of dolomite rock, interspersed with bands of insoluble chert and, to a lesser degree, bands of shale and banded limestone (Jennings *et al.*,1965). Wagener (1985) described how the exact composition of these formations are largely dependent on the environment in which they were deposited.

The jointed structure of dolomite rock facilitates the movement of water through a network of discontinuities. This pore water usually has a high concentration of CO_2, due partly to its interaction with the atmosphere but mostly due to its interaction with the soil (Jennings *et al*., 1965). The CO_2 rich water results in dissolution and widening of joints and fissures in the dolomite rock, ultimately leading to large cavities being formed. Figure 2-14 illustrates a typical profile of dolomitic geology.

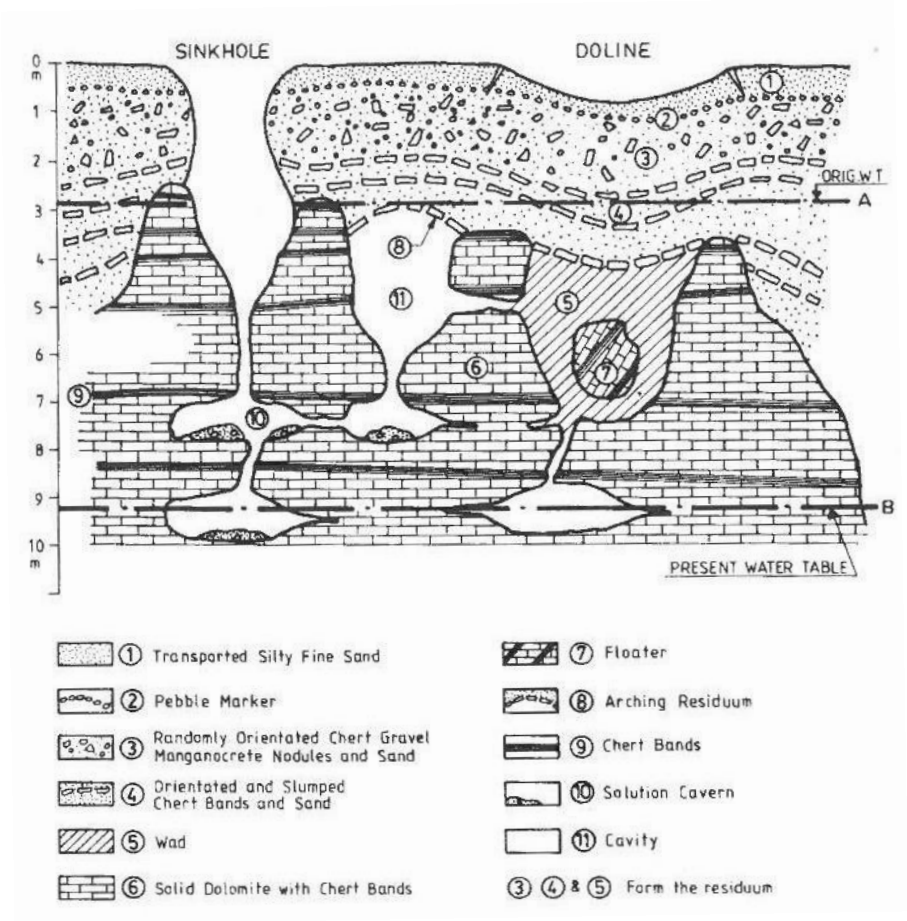

Figure 2-14: Typical profile of a dolomitic formation (Wagener, 1985)

Jennings *et al.* (1965) proposed five concurrent conditions which must be satisfied for a sinkhole to form, all of which are listed below.

1. There must be adjacent material to form abutments which facilitate the formation of a stable arch.
2. Arching must occur in the residuum overlying the karstic topography of the dolomite pinnacles. The development of a stable arch forms as a result of the residuum thrusting against the abutments mentioned in Condition 1. Once the vertical stresses along the intrados become zero, a stable arch will have formed.
3. A cavity must develop below the arch. The development of this cavity occurs as a result of the weathering processes described in the previous section.
4. A reservoir must exist below the arch. The purpose of this reservoir is to accept material which is removed as the cavity is enlarged.
5. Once the cavity has been formed, some disturbing agency is required to disrupt equilibrium and cause collapse of the arch. Successive collapsing of the roof of the void allows it to propagate upwards until a sinkhole appears at the surface.

The first four of the above points are concerned with the conditions required to produce a geological formation susceptible to the development of a sinkhole. Condition 5 highlights that there must be some disruption in the equilibrium of the system to trigger collapse of the originally stable arch. Wagener (1985) described two scenarios which could ultimately result in such a collapse. The two scenarios, dewatering and moisture ingress (static water table condition), are described below.

Dewatering:

Consider Figure 2-14 with an original water table at Position A. Should the water table be rapidly lowered to position B, below the roof of a cavity two concurrent phenomena will take place. Firstly, following the lowering of the phreatic surface, water within the vadose zone (above the water table) will percolate through the joints and fractures of the overlying residuum resulting in piping (Wagener, 1985). Secondly, the lowering of the water table will result in an increase in effective stress of the arching material (Tien, 1996). The combination of these two processes will result in progressive collapse of the roof of the cavity as it propagates upwards, eventually manifesting as a sinkhole.

Water ingress/static water table:

The second scenario considers a static water table established over geological time at position B, below the roof of a cavity. The arches present in this scenario are stable until equilibrium of

the soil along the intrados is upset by the ingress of water from the upper portions of the soil profile. As infiltration occurs, piping, as mentioned previously, is initiated and is accompanied by an increase in the unit weight of the overlying residuum. As the wetting front advances, the final mechanism which triggers collapse of the roof of the cavity is the loss of suction in the soil along the intrados. Jennings *et al.* (1965) highlighted that the disturbing agency mentioned in Condition 5 is often the ingress of water which results in loss of strength of the arching material. In her study, Richardson (2013) found that on the West Rand after 1984, the majority of events occurred as a result of moisture ingress. Richardson (2013) also noted that almost all recorded events occurring in the Tshwane region were due to the ingress of water.

The composition of the material arching over a cavity consists of gravels and chert blocks occurring in a matrix of unsaturated soil, as illustrated in Figure 2-15. The 'cohesive' strength present in this soil due to suction allows it to act as a cementing agent between the large slabs of chert, thereby adding to the stability of the arch (Jacobsz, 2016). If a representative volume of soil at the intrados is analysed, the Mohr circle depicted in Figure 2-15 can be constructed. The major principle stress in this region will be acting in the horizontal direction with the vertical stress being equal to zero, as stated by Jennings *et al.* (1965).

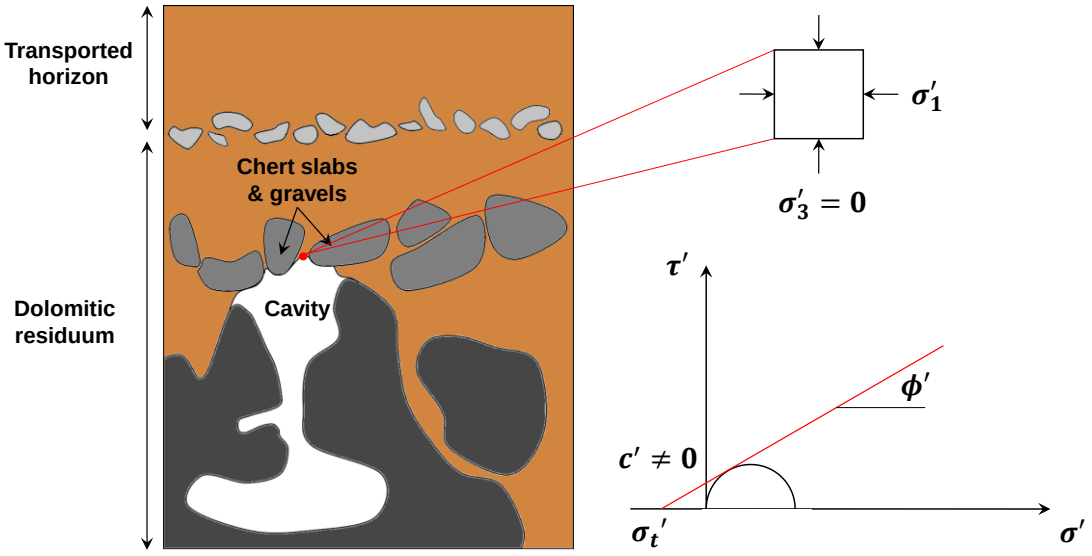

Figure 2-15: Stress analysis at the intrados

If a failure envelope is drawn tangentially to this Mohr circle it can immediately be seen that, for the stress state at the intrados to not violate the yield criterion, the soil must possess some degree of tensile strength. This is highlighted by extrapolating the failure envelope to the

horizontal axis at point σ_t (the tensile strength of the soil). Therefore, the presence of some cohesive strength, which is certainly not zero at this point, implicitly suggests a certain degree of tensile strength for the unsaturated soil in this region. Since the tensile strength of the soil along the intrados largely affects the stability of the arch, being able to understand it and quantify it correctly is invaluable to understanding the formation of a sinkhole.

2.2.3 Use of tensile strength to predict the behaviour of unsaturated soils

From the literature presented thus far, two features of unsaturated soils become apparent. Firstly, for a large portion of the earth's surface, unsaturated soils are unavoidable and, along with their presence come many engineering challenges. These can only be approached with a fundamental understanding of unsaturated soil behaviour. The second point which is highlighted is that its behaviour, being significantly more complex than that of saturated soils, incorporates many more mechanisms which govern its characteristics. A closer investigation on shear strength, presented in Section 2.1.4 demonstrated how two stress state variables (net normal stress and matric suction) are required to predict the strength of unsaturated soils. The quantification of these variables requires specialised laboratory equipment. Additionally, the non-linearity of the failure envelope was emphasised. While this characteristic can be accounted for, it presents an added difficulty to an already complex material.

The following section suggests an alternative model for the shear strength prediction of unsaturated soil. The model referred to as the Griffith failure criterion was derived in the field of fracture mechanics. Griffith (1924) set out to provide an explanation as to the considerable discrepancies observed between the theoretical and observed strengths of solid materials. His study concluded that the observed differences were a result of micro-defects present in the materials, which served as a point of severe stress concentrations from which fracture would initiate. Murrell (1958) illustrated how the theory could be manipulated to derive a failure envelope on the Mohr diagram given by Equation 2.7.

$$\tau^2 = 4\sigma_t^2 - 4\sigma_t\sigma_n \qquad 2.7$$

Where:

τ = Total shear stress (kPa)

σ_n = Normal stress (kPa)

σ_t = Tensile strength (kPa)

Since it was first proposed, Griffith's theory of rupture has been extensively used to study the fracture of rock and, in more recent years, cement stabilised soils (Consoli *et al.*, 2012; Mitchell, 1976). The results of Consoli *et al.* (2012) presented in Figure 2-16 illustrate how the failure envelope predicted (almost perfectly) the shear strength of artificially cement stabilised soils across a range of confining stresses.

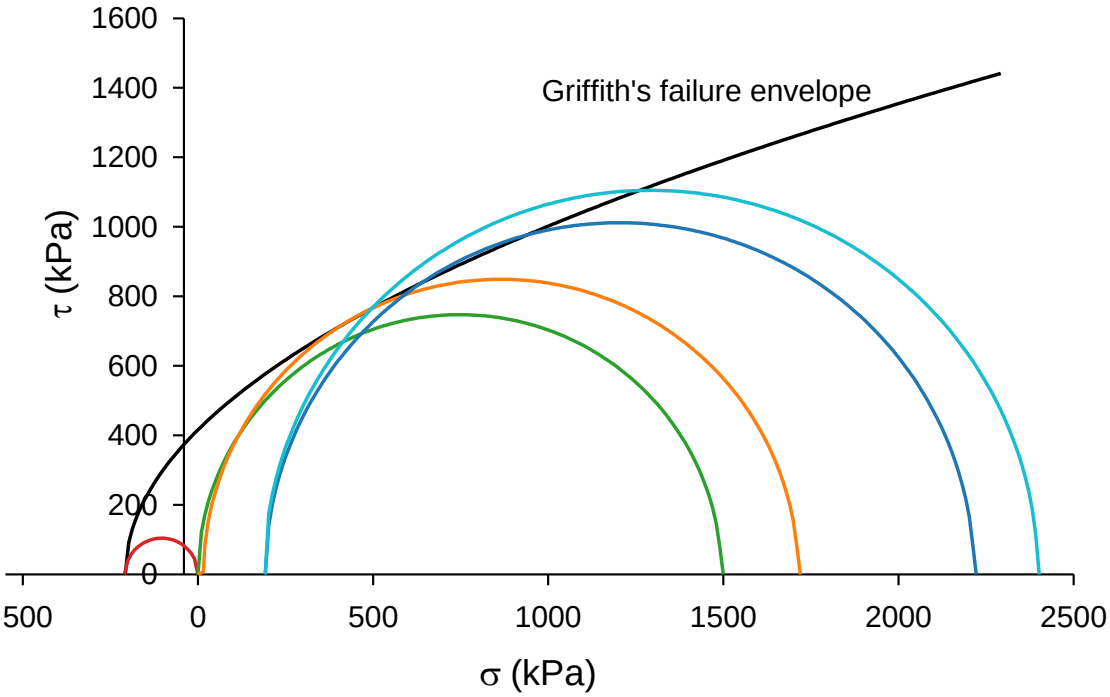

Figure 2-16: Predicted vs. observed shear strength of artificially cemented sand (adapted from Consoli *et al.* (2012))

The attractiveness of the model lies in its simplicity since it requires only the tensile strength of a material to fully define its failure envelope. Considering the constituents of cement-stabilised soils, it can by hypothesised that the failure criterion is applicable to unsaturated soils. For cement-stabilised soils, the adhesion between soil aggregates is provided by cement. Similarly, a force of attraction between particles in unsaturated soils manifests itself through the combination of negative pore water pressure and surface tension. As previously discussed, this interparticle tensile strength is a key factor in defining the shear strength of soils. Another characteristic of unsaturated soil strength is that, at low values of confinement, it exhibits a non-

linear failure envelope. Recognising the above-mentioned characteristics, it is reasonable to hypothesise that the Griffith failure criterion can provide a total stress approach to characterise the shear strength of unsaturated soils.

2.3 LABORATORY TESTING OF UNSATURATED SOILS

While field investigations are useful in characterising the true behaviour of a design during its service life, the control over boundary conditions makes laboratory testing invaluable in the understanding of fundamental soil behaviour. In this section, an overview of conventional laboratory testing procedures in unsaturated soil mechanics is provided. Particular attention is given to tests used to quantify tensile strength as well as the factors which influence it (e.g. matric suction). The section begins with a summary of the various techniques utilised to measure suction. Suction measurement is then discussed in the context of the measurement of Soil Water Retention Curves (SWRCs) which, as previously explained (Section 2.1.3), contains an invaluable amount of information characterising the behaviour of unsaturated soils. Finally, various tensile testing procedures are summarised and the section is concluded with an in-depth discussion of the indirect testing method used for this study, namely the Brazilian Disc Test (BDT).

2.3.1 Soil suction

As mentioned in Section 2.1.2, soil suction is a property of unsaturated soils which is key to understanding their mechanical and physiochemical behaviour. Throughout the development of unsaturated soil mechanics, numerous measurement techniques have been proposed for the measurement of soil suction. Each of these methods can generally be classified according to the component of suction that they measure (e.g. matric or total). Additionally, the suitability of a given measurement device for a specific application is largely dependent on the measurement range of that device. Figure 2-17 illustrates some of the different measurement techniques and the range for which they are applicable.

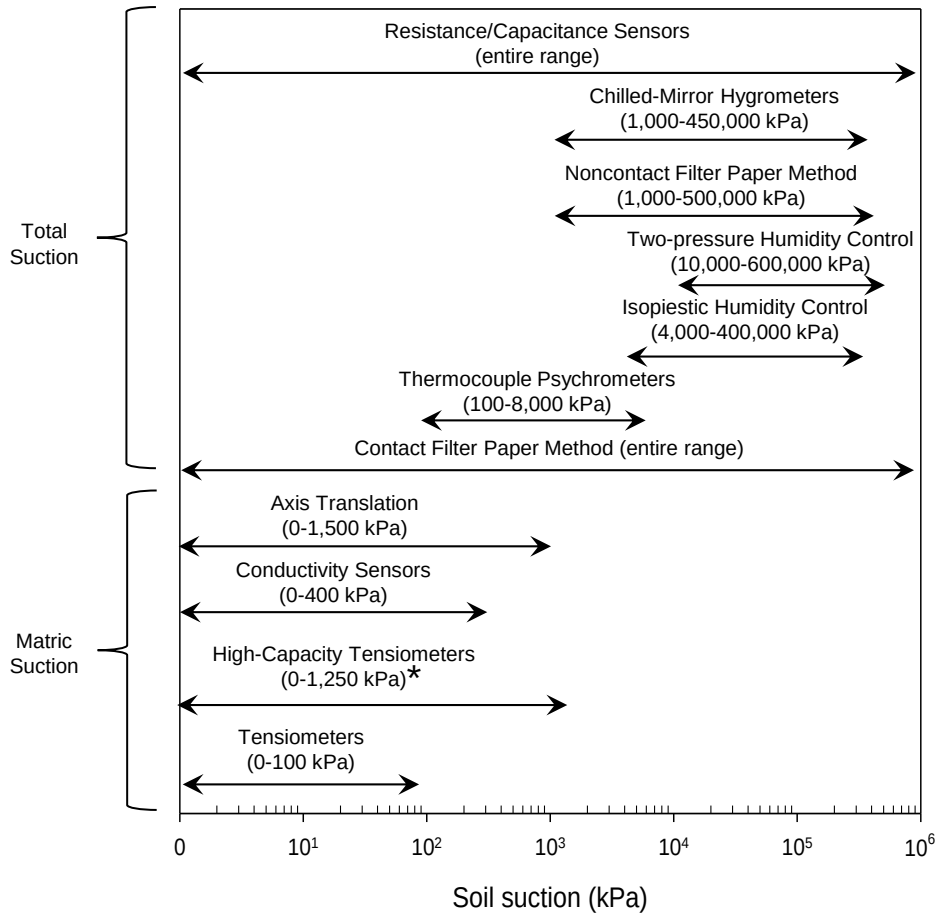

Figure 2-17: Ranges for suction measurement devices (adapted from Lu & Likos, 2004) (*Toll, 2012)

Of the various techniques presented in Figure 2-17, some measure suction directly and others measure a surrogate soil property which is calibrated against soil suction. Direct measurement is performed by measuring the actual pore pressure in a soil mass, whereas indirect techniques measure changes in some other physical property such as humidity (psychrometer), adsorption (filter paper) or electrical resistance (gypsum or thermal block) which is then related to soil suction (Ridley & Burland, 1993). This section provides a detailed description of the two measurement techniques implemented in this study, namely the tensiometer and the filter paper method.

Tensiometers:

Originally introduced by Richards & Gardner (1936) the tensiometer is a measurement device which allows the direct measurement of matric suction. Similar to other direct measurement techniques, it relies on the flow of water between a soil mass and the measurement device. This

flow is facilitated by a High-Air Entry (HAE) ceramic disc which, when saturated, allows for continuity between the water in the measurement device and the soil-water while restricting the flow of air. A standard tensiometer consists of an HAE ceramic disc on one end and a pressure sensor on the other, connected by a water reservoir (Lu & Likos, 2004). Figure 2-18 schematically illustrates the various components of a tensiometer in contact with a soil sample.

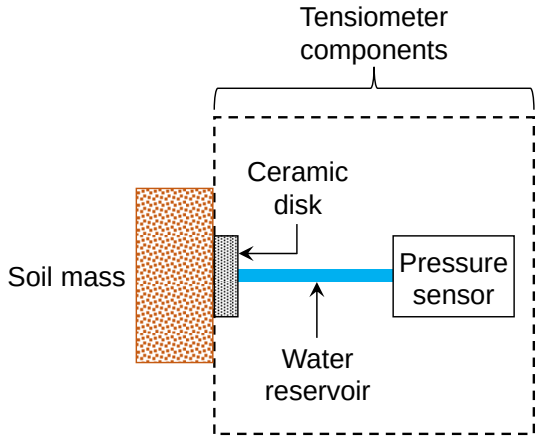

Figure 2-18: Illustration of the different components in a tensiometer

The movement of water is dependent on the pressure gradient between the soil mass and the tensiometer. A soil specimen with a certain matric suction will therefore result in a flow of water from the tensiometer to the soil until the water pressure inside the tensiometer is equivalent to the pressure of the soil-water. Conversely, if the soil is then wetted up, the direction of water movement will be reversed until equilibrium is reached (Lu & Likos, 2004). For conventional tensiometers, the time taken for equilibrium to be established (response time) can, at best, take several hours (Ridley & Burland, 1993).

The capacity of a tensiometer is governed by two factors, namely air-entry and cavitation. Air-entry refers to the process whereby a pocket of air is drawn into the water reservoir at the contact point between the tensiometer and the soil surface. This process is prevented through the use of a High-Air Entry (HAE) ceramic disc. The purpose of this ceramic disc is to allow continuity of the soil-water with the water in the reservoir while restricting the flow of air. Cavitation refers to the nucleation of air bubbles in the water reservoir which are formed when the value of matric suction exceeds the tensile strength of water. Irrespective of how it occurs, once air bubbles are introduced into the reservoir, any subsequent flow of water will cause expansion or contraction of the air bubbles (depending on the direction of flow) resulting in non-transmission of suction to the measuring device (Ridley & Burland, 1993).

While early versions of the tensiometer were limited by a cavitation pressure of approximately 100 kPa (Ridley & Burland, 1993; Toll, 2012), subsequent developments have allowed for so-called 'high-capacity' tensiometers to be constructed. The basis of their design involves minimising potential nucleation sites through the use of extremely small water reservoirs (Lu & Likos, 2004). This feature, used in conjunction with a relatively high-capacity ceramic and the thorough saturation of that ceramic, allows for matric suction in excess of 100 kPa to be measured (Toll, 2012). Ridley & Burland (1993) are credited with the design of the first high-capacity tensiometer, which was reported to measure matric suction of approximately 1200 kPa. Furthermore, a response time of less than five minutes was observed, illustrating a substantial improvement from earlier versions of the device. Figure 2-19 illustrates the various components of a high-capacity tensiometer.

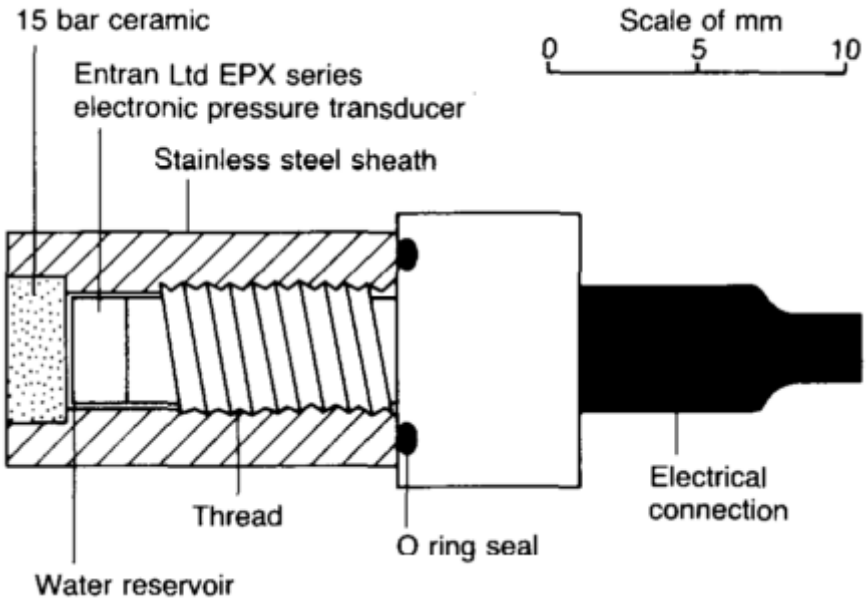

Figure 2-19: High-capacity tensiometer (Ridley & Burland, 1993)

It should be noted that while the above-mentioned design makes it possible to measure matric suction in excess of a megapascal, the sophisticated setup becomes irrelevant if the ceramic disc is not properly saturated, which becomes increasingly difficult with an increase in air-entry value.

The filter paper method:

A useful approach to measuring soil-water potential, which has existed for a considerable amount of time, is the filter paper method. First proposed by Gardner (1937), it is a relatively simple method, capable of measuring both total and matric suction over a wide range (see Figure 2-17).

The procedure is an indirect measurement technique whereby soil moisture is transferred from an unsaturated soil specimen to an initially dry piece of filter paper. This transfer of moisture continues until equilibrium of suction is reached, after which point the moisture content of the filter paper is gravimetrically determined and related to soil suction (Lu & Likos, 2004). Equalisation of suction is achieved either through the flow of vapour or liquid. When the filter paper is placed in direct contact with the soil, equilibrium is reached through the flow of liquid thus resulting in the measurement of matric suction.

Alternatively, the soil specimen and filter paper can be placed inside a sealed container (but not in contact), which will allow for equilibration to occur through the transfer of vapour. In such a case, total suction will be measured (Toll, 2012). Figure 2-20 illustrates the general test setup for both the contact and non-contact filter paper methods.

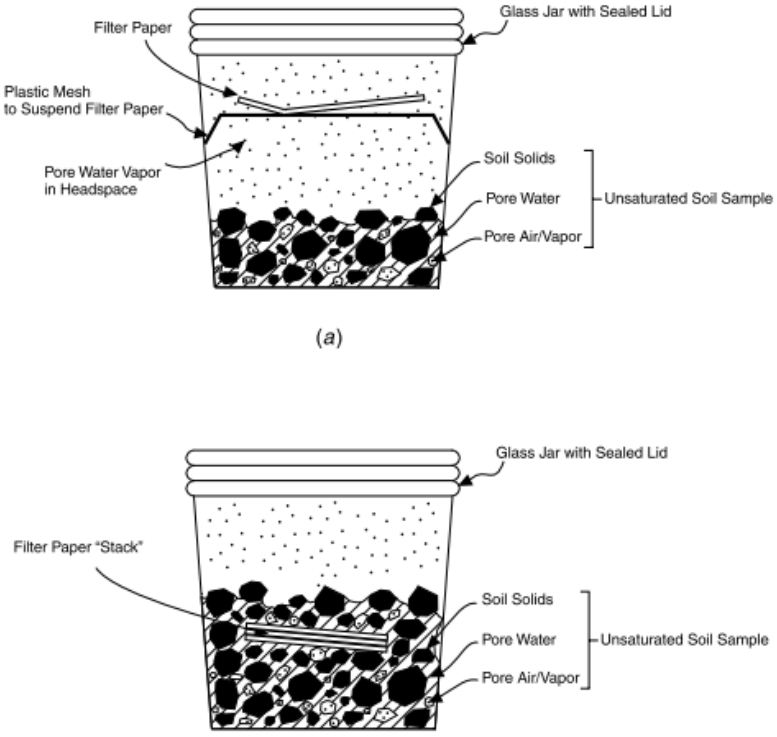

Figure 2-20: General setups for filter paper methods: a) non-contact method for total suction measurement and b) contact method for the measurement of matric suction (Lu & Likos, 2004)

The appeal of this approach to suction measurement is related to its simplicity and low cost. This simplicity is however not without its drawbacks, the most significant being its slow response time which generally takes up to seven days (Chandler & Gutierrez, 1986). Despite the existence of more technologically advanced techniques, the filter paper method is still a useful and reliable approach to suction measurement.

2.3.2 Methods for the determination of the Soil Water Retention Curve (SWRC)

As discussed in Section 2.1.3, Edgar Buckingham is credited as being the first researcher to publish results on soil-water retention behaviour (Narasimhan, 2005). The results presented in his publication were measured through the use of the hanging-column or tension plate test. The test setup incorporates a porous disc connected to a water reservoir which is left exposed to the atmosphere. Connection between the porous stone and water reservoir is achieved through a flexible tube or 'hanging-column' of water (Radcliffe & Šimůnek, 2010). Figure 2-21 provides a graphical illustration of this setup.

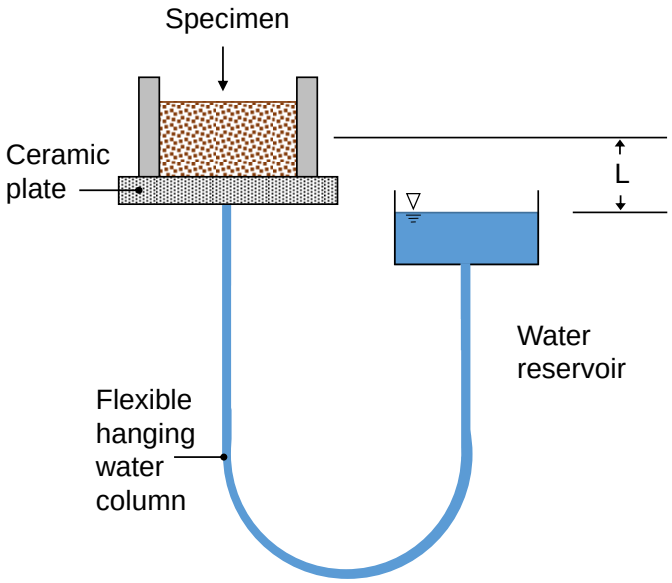

Figure 2-21: Hanging-column apparatus (adapted from Radcliffe & Šimůnek (2010))

For the hanging-column method, a saturated soil specimen is placed in contact with the porous stone, initially at an elevation equal to the water level of the reservoir. The reservoir is then lowered by a specific amount (L) resulting in a pressure difference between the reservoir and soil-water. This pressure gradient initiates the flow of water from the specimen to the reservoir which continues until equilibrium is reached. At this point, the specimen is removed from the

porous disc and weighed such that its gravimetric moisture content can be calculated. This process is repeated by incrementally lowering the reservoir to obtain a series of discrete pairs of moisture content and matric suction. This approach to SWRC measurement is one which allows a high level of accuracy since the magnitude of matric suction can simply be measured as the difference in elevation (L) (Radcliffe & Šimůnek, 2010).

Since Buckingham's original publication, more sophisticated approaches to soil-water retention measurement have been proposed. However, disadvantages which are common to most of these techniques include:

- the long duration required for equilibration to occur at a specific value of suction and
- the need to measure a series of discrete points to obtain a full SWRC.

Recognising the above shortcomings, Toker *et al*. (2004) proposed a new technique for the continuous measurement of the SWRC, capable of measuring a full curve from one soil specimen in a fraction of the time required for previous methods. A description of this method, referred to as the MIT technique, is provided in the following discussion.

The MIT technique:

Conceptually a simple procedure, the MIT technique (Toker *et al*., 2004) involves the preparation of a saturated soil specimen which is dried out under controlled conditions, with measurements of matric suction and mass being continuously recorded. The test setup (illustrated in Figure 2-22) makes use of a tensiometer (not dissimilar to the one proposed by Ridley & Burland (1993)) to measure matric suction of the soil. The specimen, placed in contact with the tensiometer is positioned on top of an electronic laboratory scale which continuously records the mass of the sample as moisture is removed. Following the completion of the test, these mass readings make it possible to back-calculate gravimetric moisture content, thereby allowing for a complete SWRC to be measured.

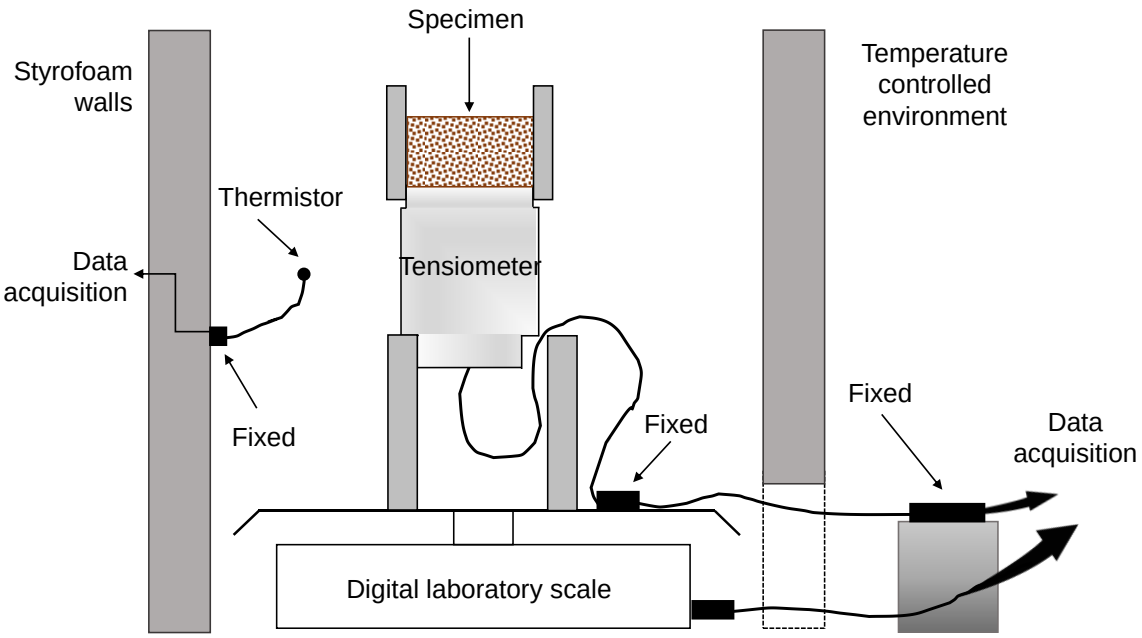

Figure 2-22: Test setup for the MIT technique (adapted from Toker *et al.* (2004))

The method presents substantial advantages over previous approaches to soil retention measurement. Arguably, the most significant benefit of the MIT technique is the time taken for a complete SWRC to be measured. While previous methods generally require up to seven days for the measurement of a single point on the SWRC, the MIT technique allows for the measurement of a complete curve in 3-5 days (inclusive of sample preparation) (Toker *et al.*, 2004).

2.3.3 Tensile testing of unsaturated soils

The measurement of matric suction and its relationship to moisture content is a useful tool in analysing the mechanical behaviour of a soil. However, the presence of matric suction, together with water surface tension brings about a mechanical property which bears significant practical applications in the field of geotechnical engineering, namely tensile strength. The measurement of tensile strength of unsaturated soils can generally be subdivided into direct and indirect tests.

Ideally, it is intuitive that direct tension tests would be preferred since they involve uniaxially loading a soil specimen in pure tension. For several decades, tensile measurement techniques have been developed in both the agricultural sector and in geotechnical engineering. A method described by Heibrock *et al.* (2003) involved loading a vertically aligned tubular sample until tensile failure occurred at the centre of the specimen. The method involved the preparation of a cylindrical sample (90 mm in height with a 24 mm diameter) at a specific density and moisture

content. The specimen was then coated in wax and left to equilibrate for a period of 48 hours. Following the equilibration period, an 8 mm hole was drilled in the cylinder to create a tubular sample. Thereafter, a filter textile was placed in the centre of the tube with an epoxy resin being used to fill the upper and lower portions of the sample's core. Embedded in each epoxy filled segment was a dowel with a hook at one end which ultimately facilitated the tensile loading of the sample. Finally, the wax coating was carefully removed and the specimen carefully placed in the loading apparatus (a modified triaxial rig). Figure 2-23 a) depicts the setup used by Heibrock *et al.* (2003) while Figure 2-23 b) provides a cross-sectional schematic interpretation of their description.

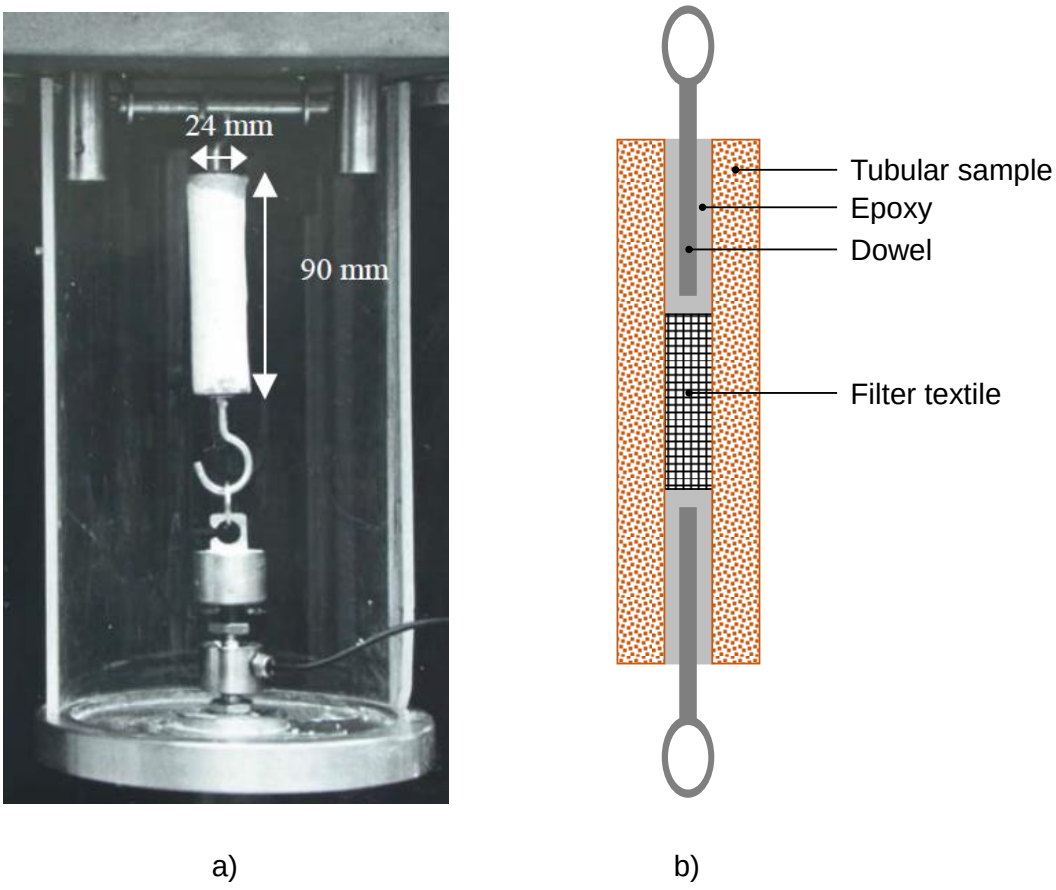

Figure 2-23: a) Test setup as used by Heibrock *et al.* (2003) and b) a cross-sectional schematic interpretation of their setup

Lu *et al.* (2005) pointed out that this approach is useful for measuring the tensile strength of cohesive materials. For granular materials, however, a certain amount of sample confinement is required to directly measure the tensile strength. Kim (2001) presented a direct testing procedure which facilitated confinement and thus allowed for the tensile strength of unsaturated

sands to be measured. A summary of this testing method as provided by Kim & Sture (2008) is included in the following discussion.

The test is based on a device originally proposed by Perkins (1991), which was a displacement controlled method involving the placement of a cubical specimen within a split box, one half of which was restrained and the other free to move. The action of moving one half of the split box resulted in the mobilisation of tensile strength in the soil. This concept is illustrated in Figure 2-24.

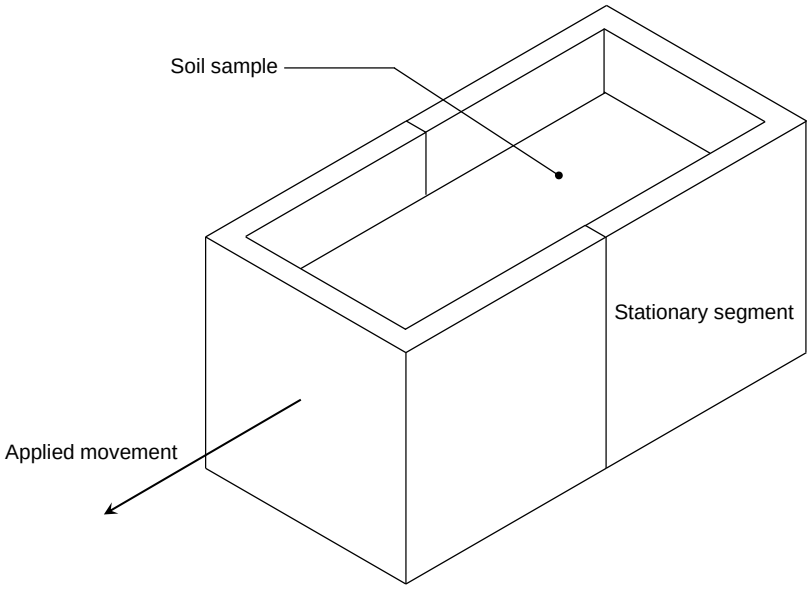

Figure 2-24: Working principle of the device proposed by Perkins (1991)

A shortcoming of this method, as mentioned by (Kim & Sture, 2008), was that the flat contact surface between the box and soil did not promote interlocking and was liable to slippage.

Kim (2001) addressed the shortcomings of Perkins' apparatus by incorporating triangular wedges (covered in sandpaper) placed adjacent to the side walls with an angle greater than the dilation angle of the soil. This modification reduced the relative movement between the box and the sample. Kim's modified setup made use of a load-controlled system whereby a tensile force was induced by a bucket incrementally filled with water. The bucket was attached to the moveable half of the split box via a pulley system. Figure 2-25 illustrates the modified test setup as proposed by Kim & Hwang (2003).

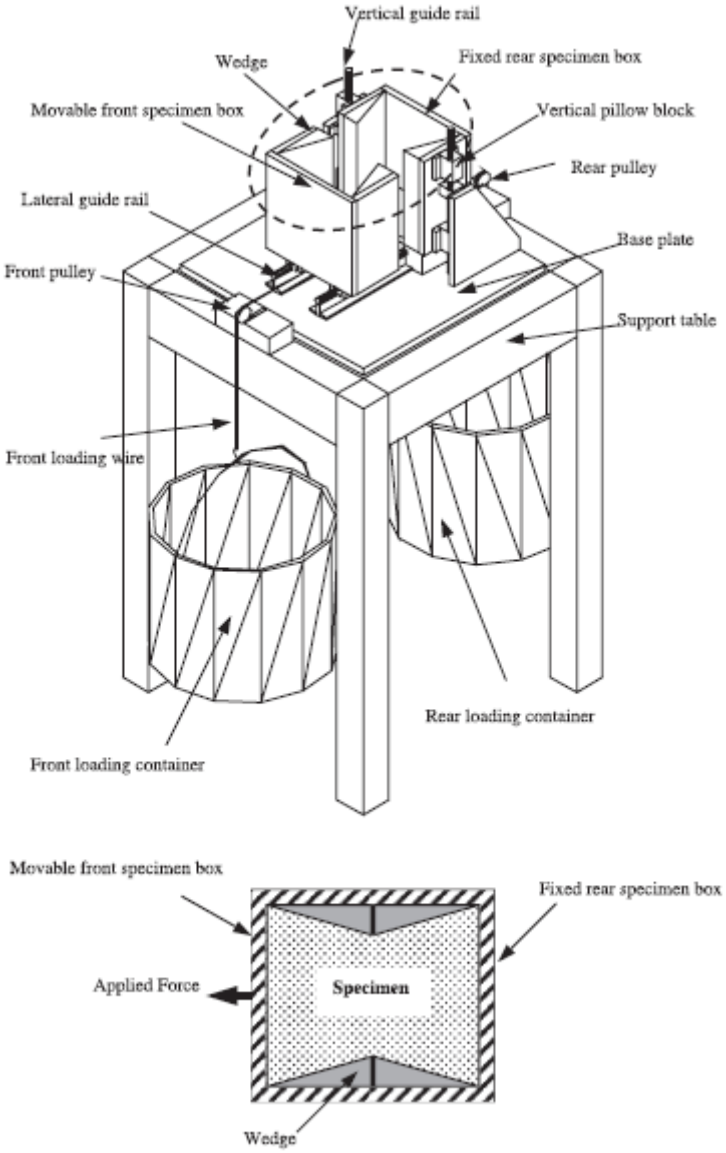

Figure 2-25: Direct tension test proposed by Kim & Hwang (2003)

A shortcoming of this method, as mentioned by Lu *et al.* (2005), is that due to the large volume of the specimen it becomes challenging to prepare multiple samples with consistent porosities. Additionally, it is intuitive that for a larger volume of soil, obtaining an even distribution of moisture within the sample will be difficult and time consuming.

Recognising the limitations of the above-mentioned procedure, Lu *et al.* (2005) proposed a new technique for the direct measurement of the tensile strength of unsaturated sands. The principle on which this technique is based is to allow the weight of the specimen to induce tensile stresses in the soil, thereby mobilising its tensile strength. The apparatus shown in Figure 2-26 consists of a tubular split mould, attached at one end (left side in Figure 2-26) to an adjustable plate. When the sample is placed inside the tubing the two halves of the mould are clamped together.

The mould is placed on the adjustable table and, just prior to testing, the clamps are removed. The adjustable plate is then slowly tilted until the gravitational pull on the lower portion of the sample and mould are sufficient to induce a tensile failure along the centre of the specimen. The angle of inclination of the setup is measured and the tensile strength of the soil can be calculated using Equation 2.8. A photograph of the setup at failure is provided in Figure 2-27.

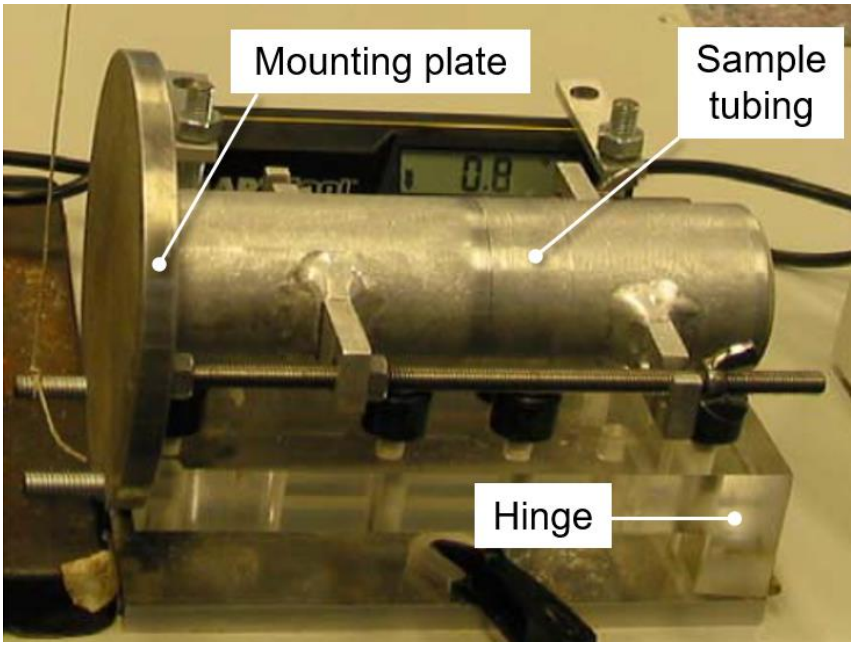

Figure 2-26: Testing equipment for direct tension test Lu *et al.* (2005) (Goulding, 2006)

$$\sigma_t = \frac{W sin\beta}{A} \qquad 2.8$$

Where:

σ_t = Tensile strength (kPa)

W = Weight of the free half of the sample mould and sample fragment (kN)

β = Angle of inclination (°)

A = Cross-sectional area of sample (m^2)

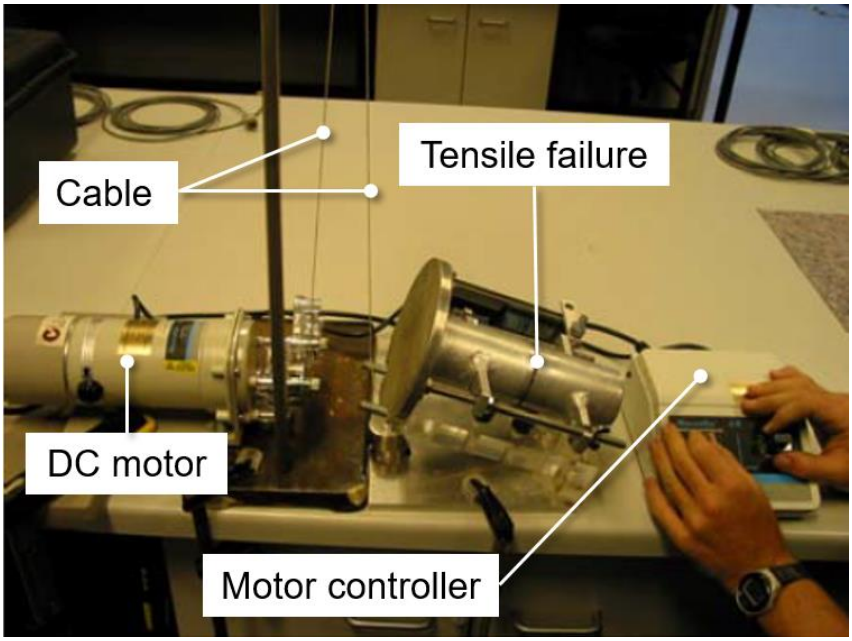

Figure 2-27: Testing equipment for direct tension test at failure Lu *et al.* (2005) (Goulding, 2006)

While the procedure proposed by Lu *et al.* (2005) was shown to repeatably measure the tensile strength of unsaturated sands, it could be argued that the method would be less suitable for cohesive soils. Whereas Lu *et al.* (2005) reported maximum strengths only slightly exceeding a kilopascal, the tensile strength of a cohesive material could easily be an order of magnitude higher. In such a case, this method may not be capable of inducing tensile stresses sufficient to produce a tensile failure. Furthermore, a challenge which is common to any direct tensile testing procedure is the ability to 'grip' the specimen such that it can be pulled apart. In the case of the method proposed by Heibrock *et al.* (2003), the test relies on the adhesion between the tubular sample and epoxy resin and between the epoxy and dowels through which force is applied. For the method proposed by Kim (2001), traction between the sample mould and soil was achieved through the use of triangular wedges coated in sandpaper. Although not explicitly stated in their publication, the approach presented by Lu *et al.* (2005) would have had to ensure adhesion between the soil mass and tubular mould to avoid the sample simply slipping out as the table was inclined.

While this difficulty can be addressed for each test as it is used for a specific soil, no blanket solution can be applied since the adhesive characteristics between a soil mass and the testing equipment will differ significantly for different soil types.

In light of the above-mentioned shortcomings and due to its relative simplicity, an indirect testing procedure predating all tests mentioned thus far has gained popularity. The remainder of this chapter discusses the Brazilian Disc Test (BDT), taking into account the theories on which it is based and its development across a range of disciplines.

2.3.4 The Brazilian Disc Test (BDT)

The Brazilian Disc Test is a method commonly used to determine the indirect tensile strength of various materials. While Carneiro (1943) is credited with introducing the test, it was later recognised that Akazawa (1943) had independently developed a similar procedure, published in Japanese, two months after Carneiro's publication. Due to its relative simplicity, the test has gained popularity across a number of disciplines, being used to test rock, concrete, cement-stabilised soils and, to a lesser extent, unsaturated soils. The concept of the test is to load a disc specimen along its vertical axis, resulting in the development of tensile stresses perpendicular to the line of load application. This setup is illustrated in Figure 2-28. The tensile strength of the material can then be calculated by the elastic solution given in Equation 2.9, originally proposed by Timoshenko (1934).

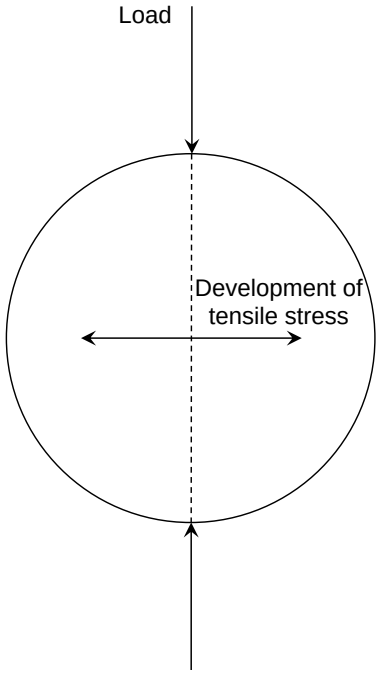

Figure 2-28: Working principle of the BDT

$$\sigma_t = \frac{2P}{\pi DL} \quad 2.9$$

Where:

σ_t = Tensile strength (kPa)

P = Applied concentrated load (kN)

D = Diameter of disc specimen (m)

L = Thickness of disc specimen (m)

Since its inception, the test has received widespread attention across various disciplines, often with its validity being questioned. A key aspect of the Brazilian Disc Test is that, according to the Griffith fracture criterion, cracking must initiate in the centre of the specimen if the result is to be in anyway representative of a *tensile* failure (Erarslan *et al.*, 2012; Li & Wong 2013). Despite this crucial condition for the successful implementation of the test, researchers have repeatedly highlighted that this is often not the case. Fairhurst (1964) stated that, for small contact angles (i.e. the area over which load is applied), failure may occur away from the centre of the disc. Furthermore, Hudson *et al.* (1972) indicated that cracking would always initiate directly under the loading points when flat loading platens were used. In light of these concerns, many variations of the test have been implemented, with particular attention given to the loading conditions. Figure 2-29 illustrates some typical loading configurations.

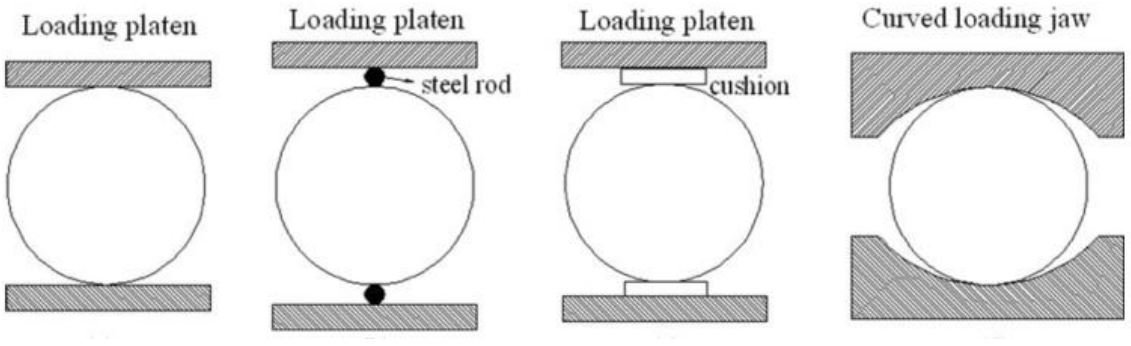

Figure 2-29: Typical loading configurations used for the Brazilian Disc Test (Li & Wong, 2013)

Hondros (1959) presented solutions for the distribution of both radial and circumferential stresses along the loaded diameter of a sample subjected to a load distributed across a finite arc. The solutions, applicable to both plane stress and plane strain conditions, are provided in Equations 2.10 and 2.11. The variables used in these calculations are illustrated in Figure 2-30.

$$\sigma_\theta = \frac{P}{\pi RL\alpha}\left\{\frac{\left[1-\left(\frac{r}{R}\right)^2\right].sin2\alpha}{1-2\left(\frac{r}{R}\right)^2.cos2\alpha+\left(\frac{r}{R}\right)^4} - tan^{-1}\left[\frac{1+\left(\frac{r}{R}\right)^2}{1-\left(\frac{r}{R}\right)^2}.tan\alpha\right]\right\} \quad 2.10$$

$$\sigma_r = -\frac{P}{\pi RL\alpha}\left\{\frac{\left[1-\left(\frac{r}{R}\right)^2\right].sin2\alpha}{1-2\left(\frac{r}{R}\right)^2.cos2\alpha+\left(\frac{r}{R}\right)^4} + tan^{-1}\left[\frac{1+\left(\frac{r}{R}\right)^2}{1-\left(\frac{r}{R}\right)^2}.tan\alpha\right]\right\} \quad 2.11$$

Where:

P = Applied load (kN)

R = Radius of disc specimen (m)

L = Thickness of disc specimen (m)

2α = Angular distance over which P is assumed to be distributed (Radians)

r = Distance from the centre of the disc (m)

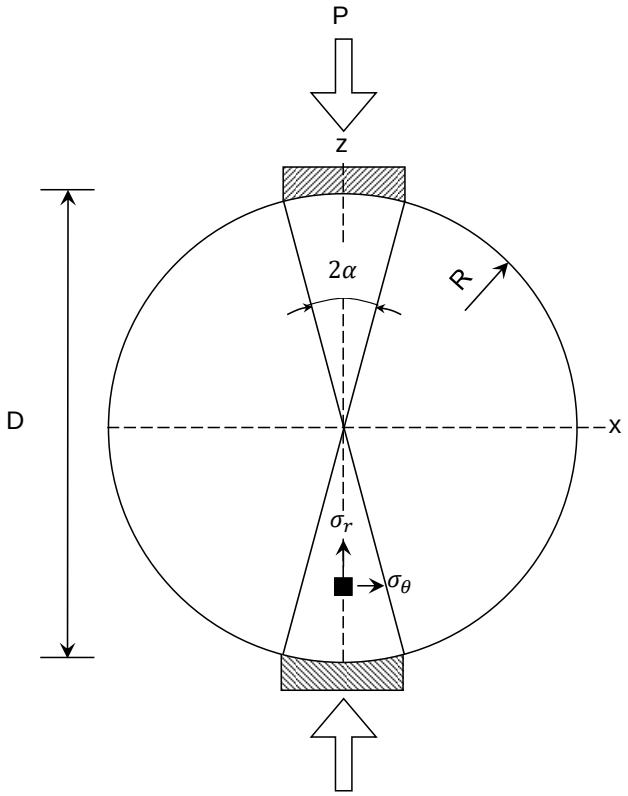

Figure 2-30: Illustration of the Brazilian Disc Test under uniformly distributed finite arcs (adapted from Li & Wong (2013))

Erarslan *et al.* (2012) investigated the effect of loading conditions for Brazilian Disc Tests performed on Brisban tuff. The study incorporated both an experimental and numerical component, and considered BDTs performed with standard Brazilian jaws as well as various loading arcs as shown in Figure 2-31. The magnitudes of tensile strength in this study were calculated using Equation 2.10 for the centre of the disc sample (i.e. $r = 0$). Results obtained from the numerical analyses are included in Figure 2-32 for a) standard jaws and b) 30° loading arcs.

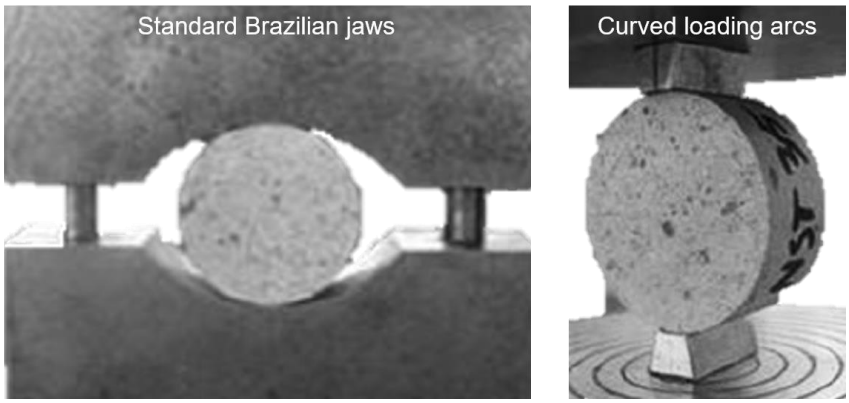

Figure 2-31`: Standard Brazilian jaws and curved loading arcs considered (adapted from Erarslan *et al.* (2012))

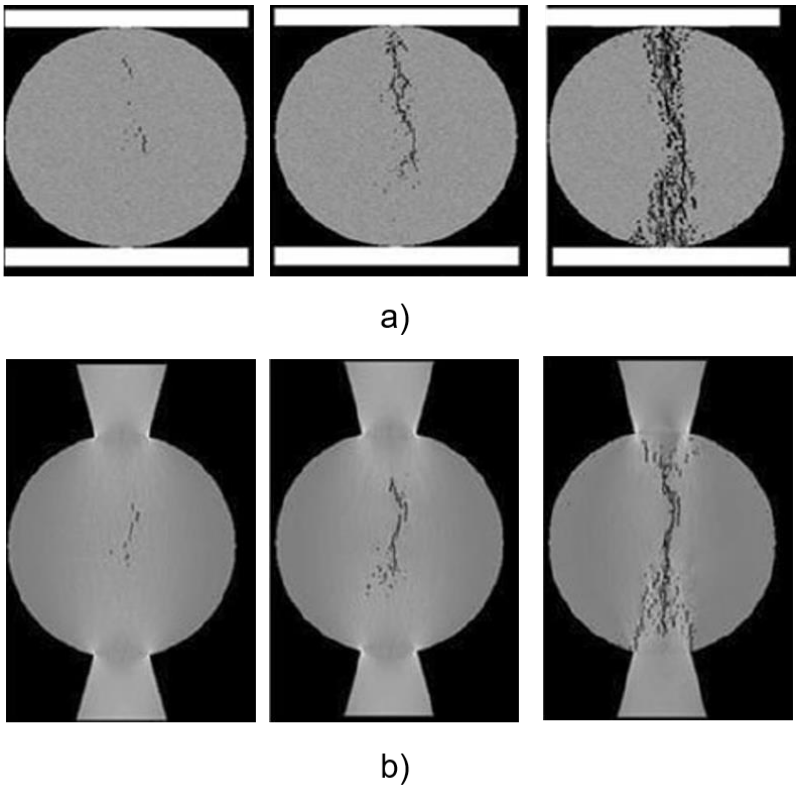

Figure 2-32: Numerical analyses illustrating crack initiation and propagation for a) standard Brazilian jaws and b) 30° curved loading arcs (adapted from Erarslan *et al.* (2012))

The results of the study concluded that the use of standard Brazilian jaws produced a catastrophic, crushing failure and with the most scattered results, while the use of 30° curved loading arcs resulted in the finest, most centrally located cracks. These results emphasise the importance of ensuring a distributed load application

While the procedure presented by Carneiro (1943) was originally intended for the testing of concrete, the research presented thus far is a testament to the vast development achieved in the field of rock mechanics. By comparison, relatively little development or usage has been made of the method for the testing of soils. That being said, the procedure has occasionally been implemented for the testing of a variety of soils (Dexter & Kroesbergen, 1985; Beckett *et al.*, 2015; Vesga & Vallejo, 2006; Krishnayya & Eisenstein, 1974). For this dissertation, advancements in the field of rock mechanics were used to develop the test for its successful application to soils.

2.4 SUMMARY

The information provided in this chapter highlights how, for unsaturated soils, a significant amount of tensile strength can be generated due to the presence of surface tension and matric suction. The increase in overall shear strength of the soil mass due to these inter-particle forces of attraction was shown to bear practical significance to engineering problems commonly encountered in practice.

Despite being such a fundamental property of the strength of unsaturated soils, the ability to repeatably measure tensile strength for different soil types across a range of moisture contents remains a complex task. Due to the difficulty associated with the measurement of tensile strength, research on the behaviour of various soil types subjected to tensile stresses has not received much attention.

For these reasons, the aim of this study was to first develop a testing procedure which could be successfully applied to a range of soil types, at different moisture contents. The results obtained from the established setup would then facilitate the investigation of the behaviour of unsaturated soils subjected to tensile stresses.

3 EXPERIMENTAL PROCEDURE

The primary focus of the experimental work carried out was the indirect measurement of tensile strength using the Brazilian Disc Test (BDT). Consequently, refinement of this testing procedure to ensure repeatable measurements was prioritised. To quantify sample surface deformation during loading, a measurement technique known as Digital Image Correlation (DIC) was used in conjunction with the BDT. An additional testing procedure implemented for this research topic was the measurement of Soil Water Retention Curves (SWRCs). The desired outcome of the SWRC was merely to give a qualitative indication of the variation in matric suction with moisture content and to highlight the transition between saturation regimes. This chapter begins with a description of all aspects related to the BDT, addressing the overall layout of the test setup, the instrumentation that was used, as well as procedures implemented to prepare disc specimens for testing. The chapter is concluded with a general overview of the techniques used to measure SWRCs.

3.1 MATERIAL TYPES

The materials tested in this study were chosen with two objectives in mind. Firstly, it was decided that the unsaturated properties of the materials tested should bear some relevance to a practical engineering problem. Two cases where unsaturated soil mechanics is of particular importance in South Africa include:

- the stability of a soil arch spanning a cavity prior to the formation of a sinkhole and
- slope stability problems, which are important for many geotechnical engineering designs.

Considering the above-mentioned cases, one of the materials chosen was taken from a transported soil horizon overlying dolomitic bedrock from the Centurion area, south of Pretoria. Figure 3-1 illustrates the soil profile from which disturbed samples were taken. Han & Vanapalli (2016) stated how, for a granular material, capillarity is the dominant mechanism contributing to the mechanical behaviour of a soil. The transported Centurion soil was found to contain a significant amount of clay, thereby distinguishing its behaviour from the other two materials. However, as presented in Section 2.1.4, for lower values of saturation, the angle of friction associated with net normal stress was shown to increase. This phenomenon was attributed to the fact that, at higher suctions, aggregations of finer particles are able to retain their structure upon shearing, thereby allowing the soil to behave as a ‘coarser’ material. The inter-particle bond between these larger aggregations is then strongly dependent on the effect of capillarity. Since capillarity is directly related to particle size (i.e. the smaller the particle

size, the higher the suction as discussed in Section 2.1.2), it was decided that all particles greater than 1 mm would be removed prior to testing. Truncating the grading at 1 mm would therefore allow for only the portion of material *significantly* contributing to arch stability to be investigated.

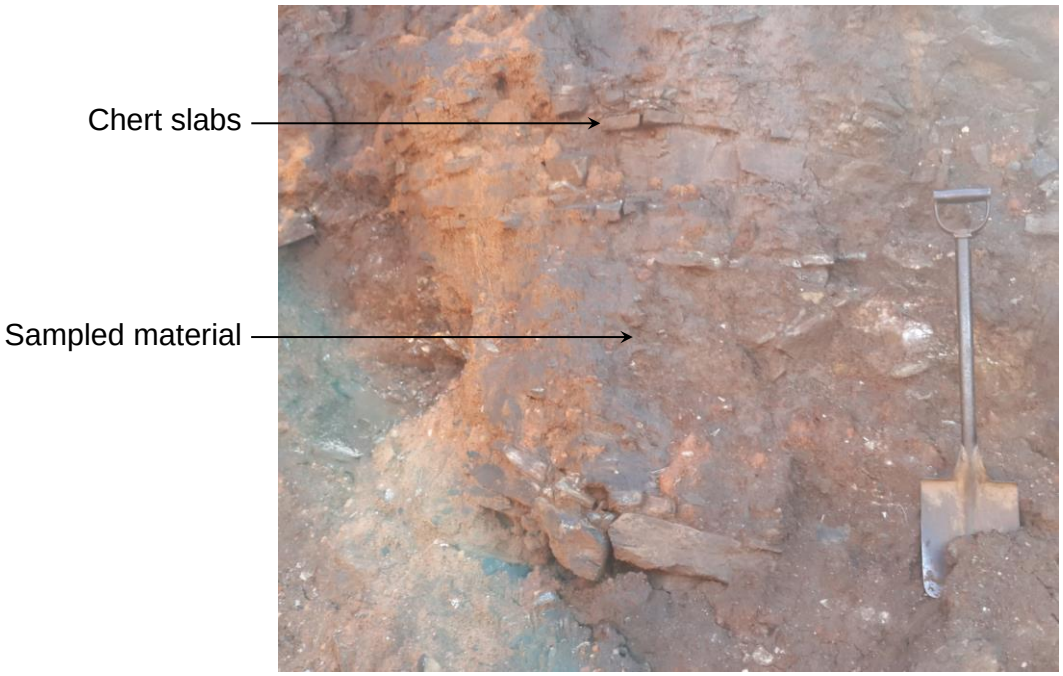

Figure 3-1: Dolomitic soil profile

In the mining industry, the construction of Tailings Storage Facilities (TSF) relies heavily on the stability of these facilities' outer slopes. Fourie (1996) illustrated how the presence of matric suction (and therefore interparticle tensile strength) significantly increases a slope's resistance to shallow failures. Two different tailings materials were therefore considered for this study namely, iron and gold tailings. On a TSF, the location where soil strength is of particular importance is close to the day wall where material is deposited. It was thus decided to investigate the soil near the point of deposition, where slope stability is of concern.

The second objective considered when choosing material types was related to the effect of particle size distribution on matric suction. The materials were chosen to represent three distinctly different textural classes. Particle size distributions for all three materials are included in Figure 3-2, with their mineralogical compositions presented in Figure 3-3. Additionally, the specific gravity of each material is given in Table 3-1.

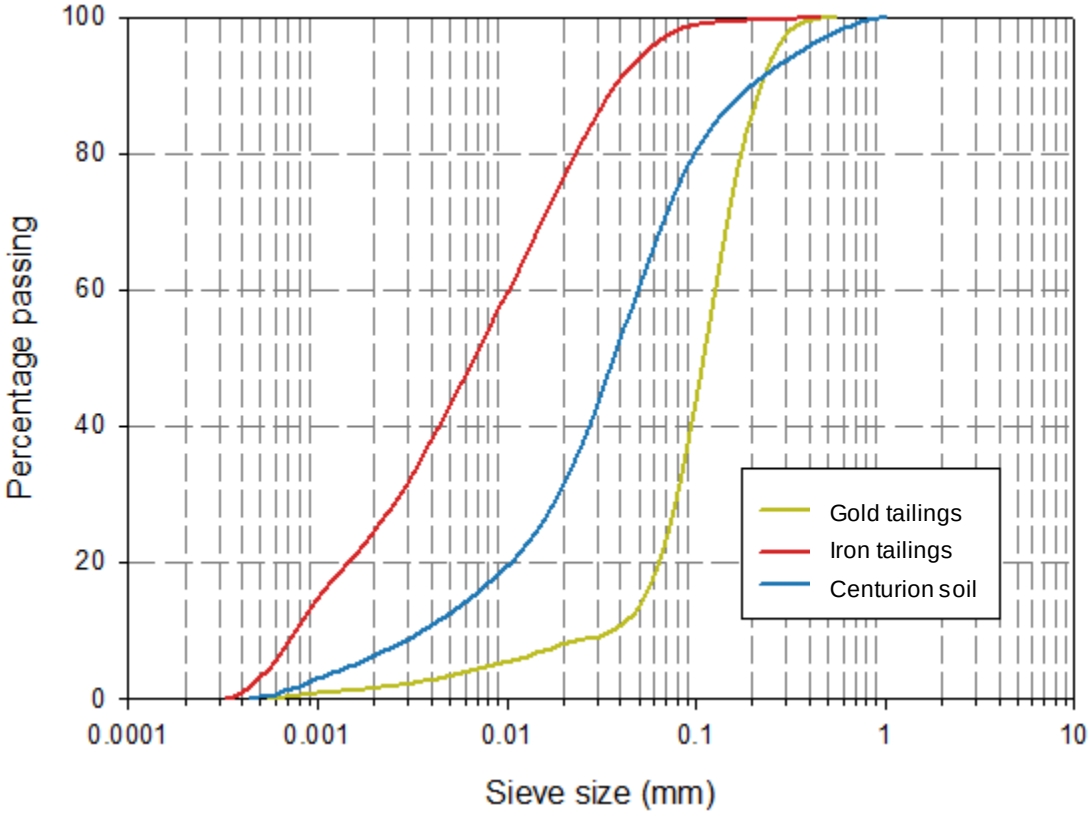

Figure 3-2: Particle size distributions of materials tested

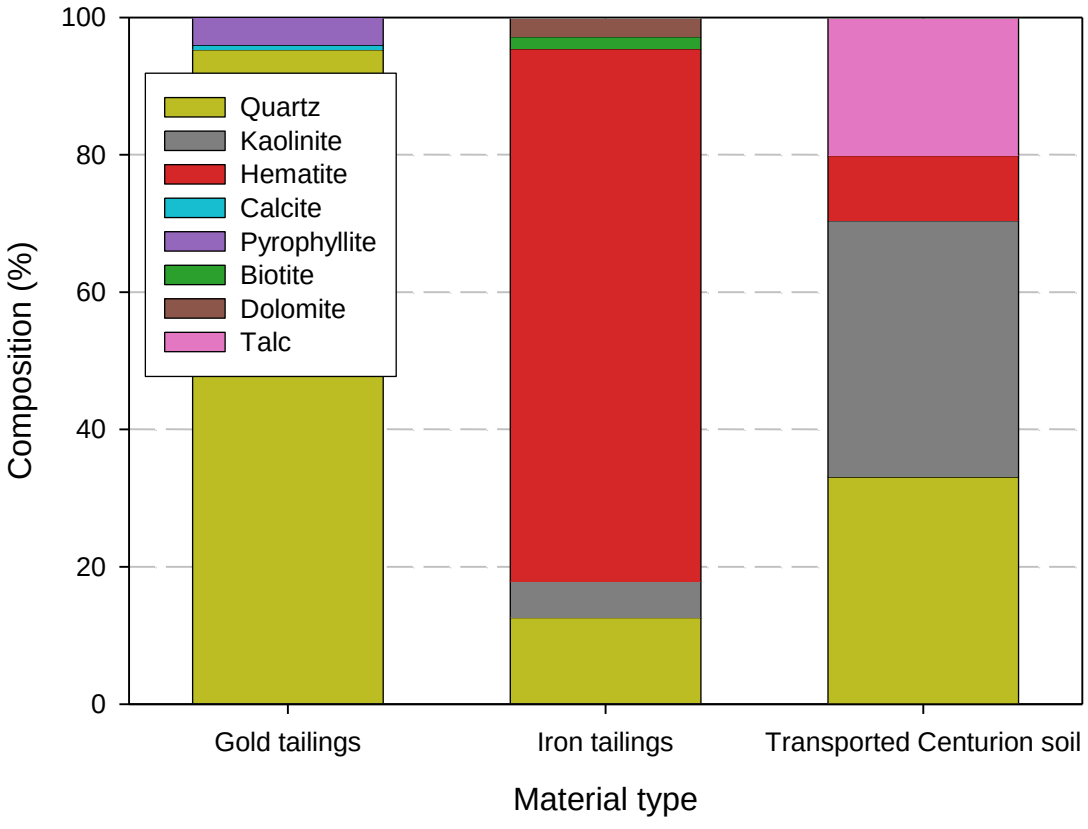

Figure 3-3: Mineralogical composition of materials tested

Table 3-1: Specific gravity for soils tested

Material	G_s
Gold tailings	2.69
Iron tailings	3.89
Centurion soil	2.75

From Figure 3-2 it can be seen that the particle size distribution curve for the Centurion soil illustrates a small clay size fraction i.e. less than 10% passing the 0.002 mm sieve. In contrast, the X-Ray Diffraction (XRD) results presented in Figure 3-3 show that this material contained 37% kaolinite. The discrepancy between these two results is likely due to poor dispersion of the clay minerals.

3.2 TEST SETUP

Due to the wide range of the soils' grading and mineralogical characteristics, it was anticipated that measured tensile strengths would differ significantly for the three materials. Preliminary studies on gold tailings revealed that typical values of tensile strength could be less than 5 kPa (Gaspar & Jacobsz, 2016). Conversely, the relatively fine grading of the iron tailings and the high percentage of clay mineralogy in the Centurion soil provided an indication that tensile strengths for these materials could be significantly higher. Vesga & Vallejo (2006) measured tensile strengths for kaolinite clay of up to 450 kPa. It was therefore decided that two separate setups should be implemented, differing only by the positioning and characteristics of the load cell used. For the testing of weaker materials, a customised setup was designed to ensure, as far as possible, accurate measurements at a high resolution. For stronger specimens, the main concern was being able to measure high loads. The resolution of the load cell was thus less of a concern and so a conventional loading press could be utilised. This section therefore focusses on the design of the setup used to test weaker specimens.

3.2.1 Brazilian Disc Test (BDT)

BDTs were carried out using a conventional triaxial loading frame modified to ensure correct loading conditions. The first aspect considered was the design of loading platens. As mentioned in Section 2.3.4, an important feature of a correctly performed BDT is that cracking should initiate in the centre of the sample. To ensure this condition was satisfied, the effect of loading conditions was investigated analytically using Equations 2.10 and 2.11. Presented in Figure 3-4, the circumferential (σ_θ) and radial (σ_r) stresses are plotted as a function of sample depth

for varying values of the contact angle α. The horizontal axis illustrates increments of stress with tension being plotted as positive. The vertical scale is expressed as a multiple of the sample radius, with R representing the total radius of the sample and r the distance from its centre.

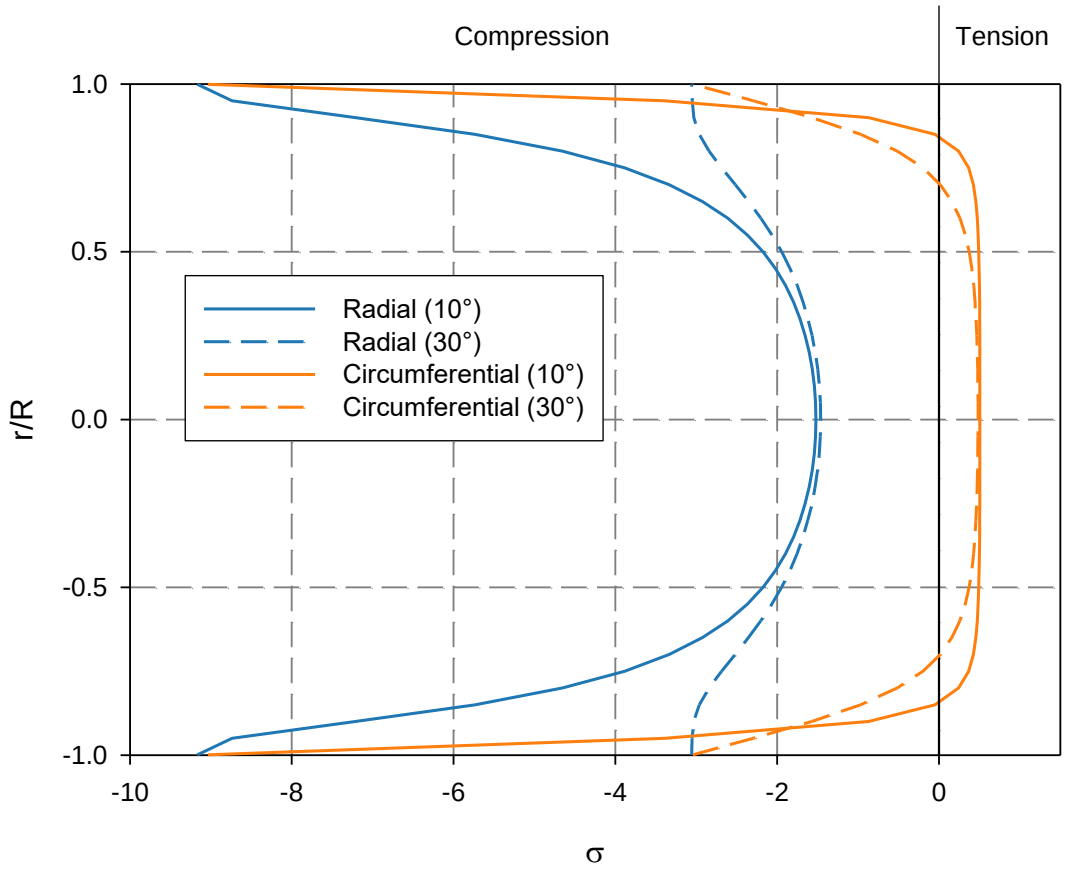

Figure 3-4: Distribution of circumferential and radial stresses acting along the sample diameter for contact angles (α) of 30° and 10°

From the distributions presented in Figure 3-4, two key characteristics of the loading conditions become apparent. The first is that a variation in the half contact angle α has a negligible effect on the magnitude of stress (circumferential or radial) achieved in the centre of the disc. However, a decrease in α results in significant compressive stress concentrations at the contact points on the sample. It should be noted that tensile stresses computed at the centre of the disc using either Equation 2.10 as proposed by Hondros (1959) or Equation 2.9 as proposed by Timoshenko (1934) produce the same result.

Upon inspection of Figure 3-4, it can be stated that the choice of contact angle 2α should be governed by the compressive to tensile strength ratio of the material being tested. This is to

ensure that the material is strong enough in compression to sustain the stress concentrations at the ends of the disc, so that tensile strength can be fully mobilised at the centre. If the ratio of maximum compressive to tensile stresses occurring at the ends and centre of the sample are plotted as a function of the half contact angle α, a theoretical criterion can be derived to determine the value of α that should be applied for a specific material. This relationship is provided in Figure 3-5. For example, concrete is generally assumed to be ten times stronger in compression than it is in tension. For this ratio of σ_r to σ_θ, the minimum required value of α would be approximately 9°.

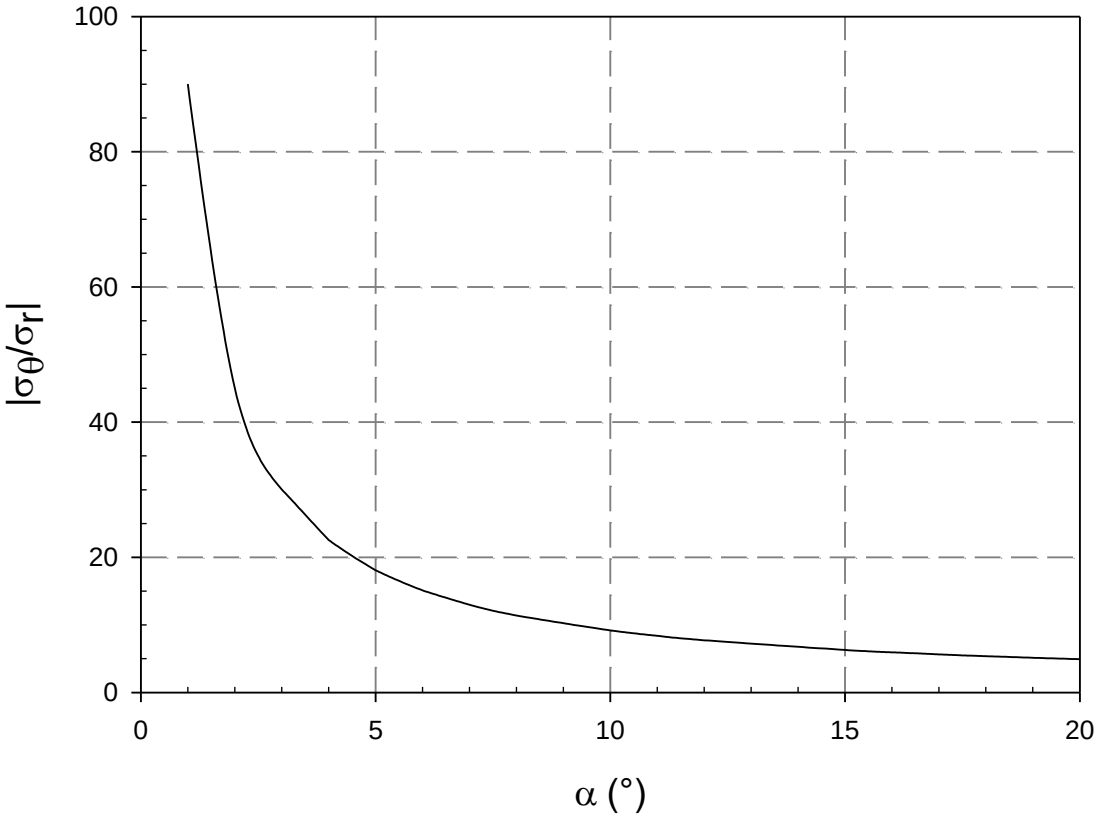

Figure 3-5: Relationship between contact angle and compressive-to-tensile strength ratio

In recognition of the high stress concentrations associated with smaller values of α, the occurrence of invalid failure mechanisms originating away from the centre of the disc, as noted by Fairhurst (1964) and Hudson *et al.* (1972) can be investigated through the use of Mohr diagrams. Consider first a Mohr circle constructed for an element of soil at the centre of the disc. In light of the fact that stresses achieved at the centre are independent of the contact angle, Mohr circles at this point, constructed for varying values of α would be equivalent. Using the

tensile strength of the soil as determined from the minor principle stress of the above-mentioned Mohr circles, failure envelopes can be derived for the soil using either Griffith's failure criterion or the more commonly used Mohr-coulomb failure envelope. If then an element of soil at 0.95R is investigated for varying values of α, the Mohr-circles presented in Figure 3-6 can be constructed.

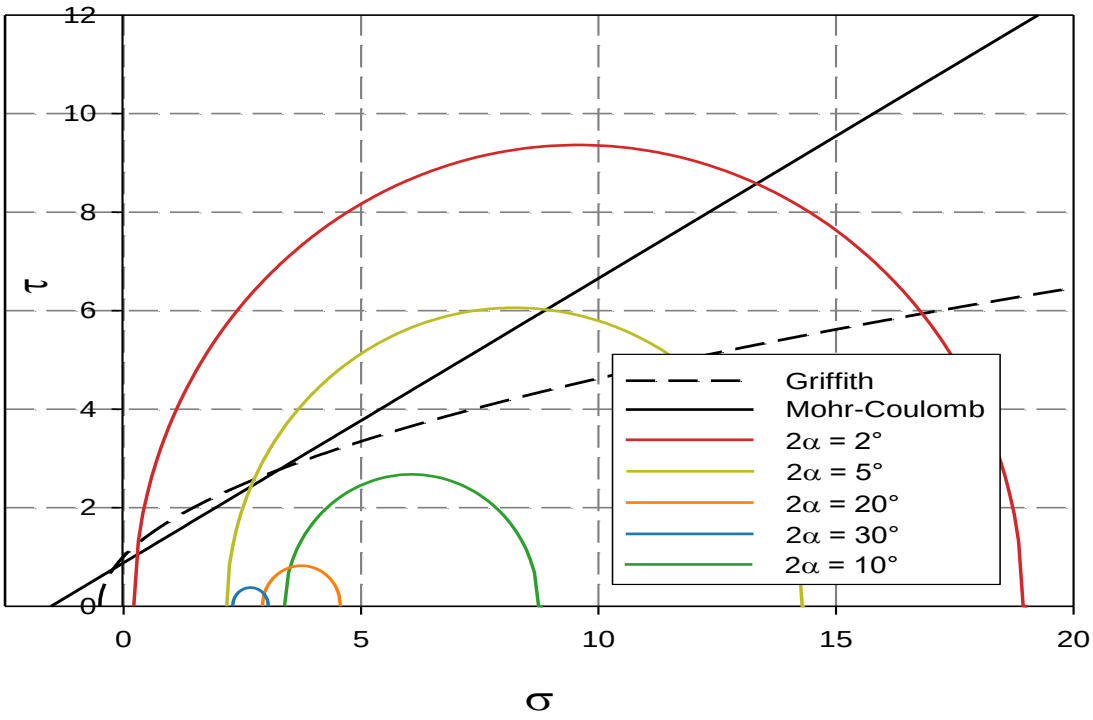

Figure 3-6: Mohr-circles constructed for an element of soil at 0.95R for varying values of α

From the results presented in Figure 3-6, it becomes clear that, with a decrease in α, the stress state for an element of soil near the contact points expand towards the yield surface. The size of each Mohr circle continues to increase with a reduction in α, until such point that the state of stress violates either failure criteria. The above illustration provides an explanation as to the invalid failure mechanisms observed by previous researchers. This knowledge of the effect of loading conditions can be used to prevent shear failures occurring at the ends of the specimen before tensile strength is mobilised at its centre, thereby ensuring the validity of the Brazilian Disc Test. Due to the results presented in Figure 3-4, Figure 3-5 and Figure 3-6, as well as the conclusions reached by Erarslan *et al.* (2012), it was decided that 30° curved loading strips would be used for this study. The loading strips were manufactured to have a radius of 27 mm, 2 mm greater than the sample radius. This allowed for the initial deformation of the sample to occur without the edges of the loading strip cutting into the soil. Figure 3-7 illustrates the curved loading strips.

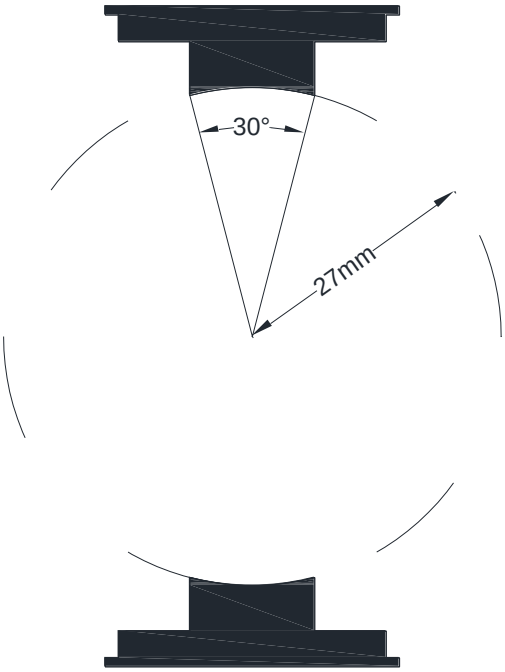

Figure 3-7: Curved loading strips

Loading of the samples was achieved through the upward movement of the bottom platen at a constant rate. This pushed the specimen into the top (stationary) platen inducing a force along the vertical axis of the sample. The force was then transmitted through a loading shaft beneath the bottom platen to a load cell. The initial test setup ensured alignment of the load shaft and load cell through a housing.

Taking cognisance of the low strengths measured in preliminary studies (Gaspar & Jacobsz, 2016) the effect of friction in the above setup was investigated. Specifically, friction between the loading shaft and load cell housing was considered. Since relative movement of these two components could only occur as a result of the deflection of the load cell, it could be argued that the friction resulting from this minute movement would be negligible. In spite of this argument, a decision was made to include a linear bearing in the test setup positioned between the shaft and load cell housing. The addition of this component was achieved with little extra effort or cost, yet it significantly improved the stability of the system and ensured that friction would not significantly affect load measurements. Figure 3-8 shows the test setup after the inclusion of a linear bearing.

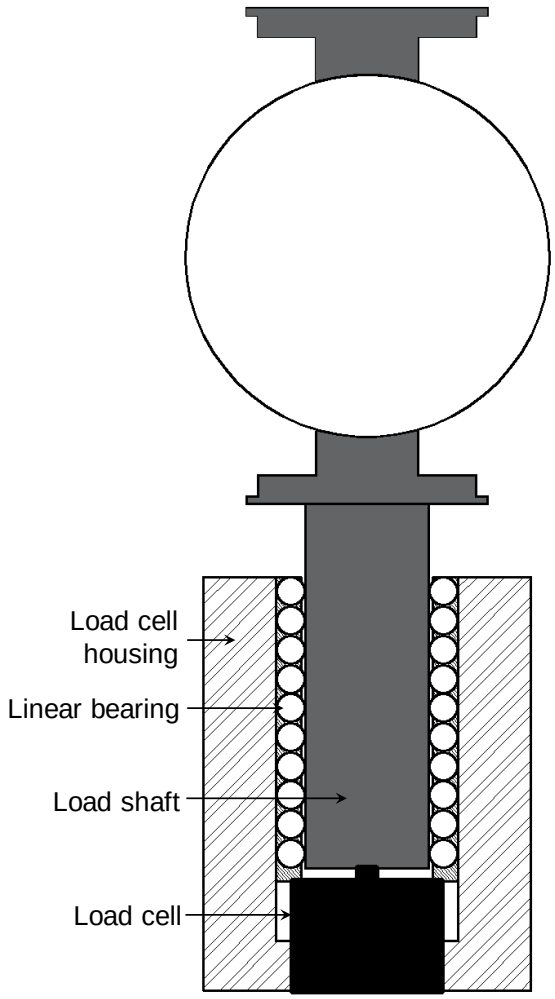

Figure 3-8: Final setup with inclusion of linear bearing

Final modifications to the loading frame involved the use of a Linear Variable Differential Transformer (LVDT) and calibration markers to be used in conjunction with DIC. The purpose of the LVDT was to measure the relative movement between top and bottom platens. Two L-shaped brackets, fitted to the top stationary platen, allowed for calibration markers to be included on either side of the sample testing area. All aforementioned modifications to the loading frame were then enclosed in a box, the purpose of which was to minimise the effect of changing ambient lighting on the results of the DIC. The box was constructed with an L-shaped cut-out along its right side, which allowed for a laptop to be slotted in view of the digital camera used for DIC. Placing a portion of the laptop screen in view of the camera allowed for photographs taken of the sample to be precisely correlated with an exact time, load and vertical displacement reading, all of which were displayed on the laptop screen. Figure 3-9 illustrates the final setup of the loading frame.

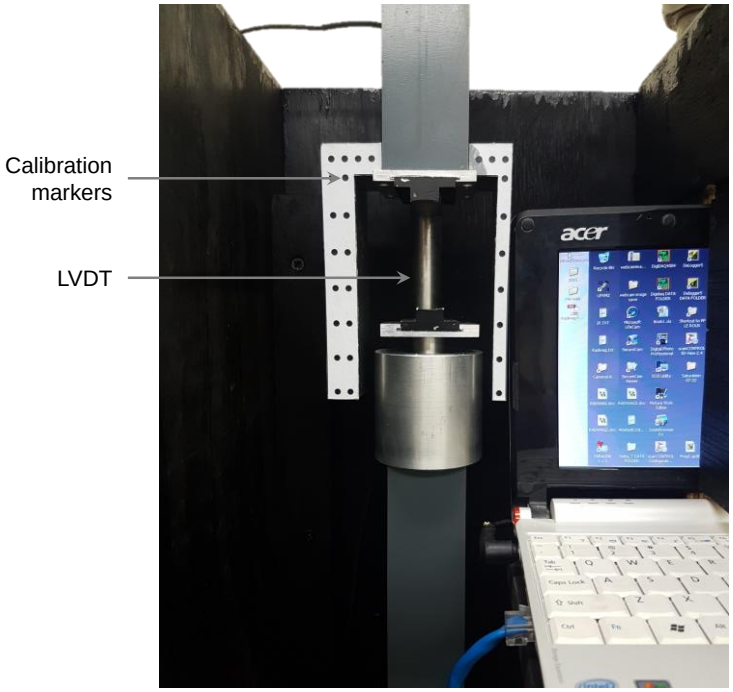

Figure 3-9: Final setup of loading frame

The BDTs were performed using an HBM C9C load cell with a maximum capacity of 200 N. Since the loads that would be measured were expected to amount to generally less than 5% of the load cell capacity, it was deemed necessary to determine whether the resolution of the device was adequate. The resolution check was performed by placing a known mass onto the load cell, monitoring the response of the load cell and then removing the mass. Starting with a mass of 200 mg, this process was repeated with progressively heavier weights until a significant response in the output of the load cell was observed. Figure 3-10 indicates the response of the load cell for 1 g, 2 g, 5 g and 10 g with the zero line representing the output of the load cell with only the loading platform on top of it.

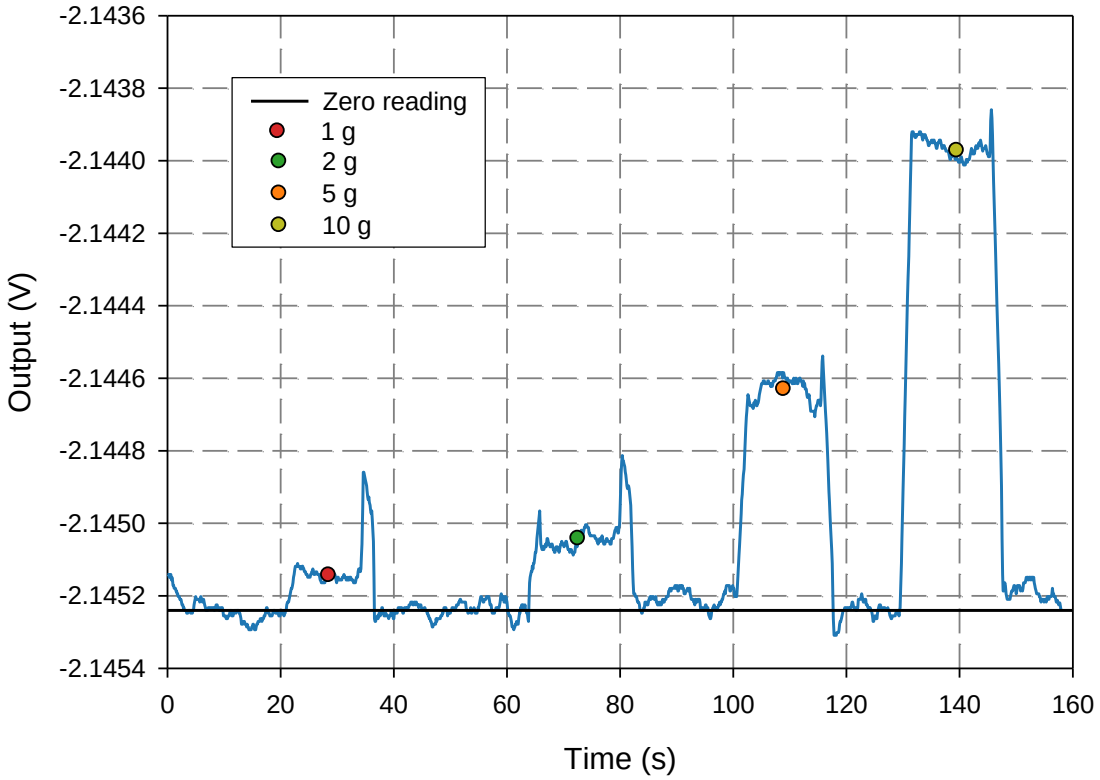

Figure 3-10: Results indicating the resolution check of the load cell

From Figure 3-10 it can be seen that the first point at which the output voltage deviated significantly from its zero reading was after the placement of 1 g. The load cell resolution, taken as being approximately 0.01 N, was considered to be sufficiently accurate at small loads. Having investigated the adequacy of the load cell resolution, a calibration was performed in its lower range (bottom 5% of its capacity) using a dead load system. The results of this calibration are included in Figure 3-11.

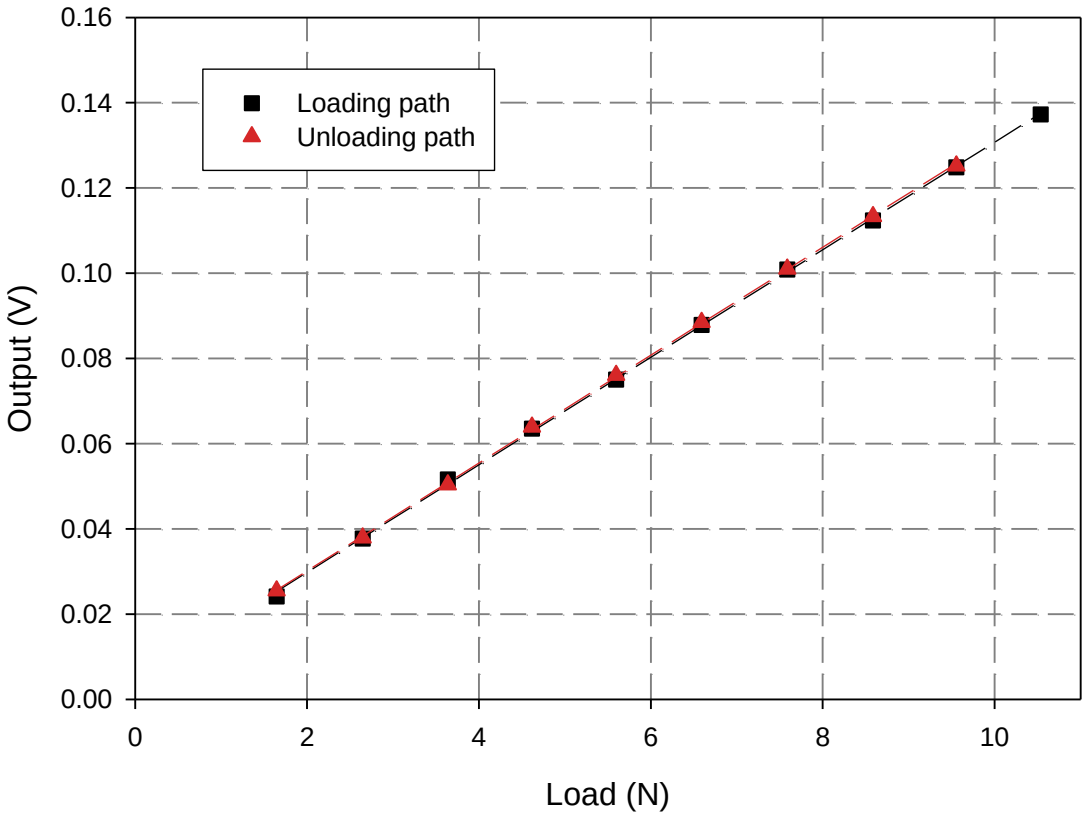

Figure 3-11: Load cell calibration in lower range

The final component of the BDT test setup was the digital camera used to perform DIC during each test. The camera used was a Canon 100D digital camera fitted with a 40 mm fixed lens, positioned 280 mm away from the sample surface. When positioning the camera, care was taken to ensure that the lens was aligned with the centre of the soil sample and that the camera was placed perpendicular to the front surface of the specimen. Figure 3-12 provides a schematic of the entire setup of the BDTs indicating the various components as well as the position of the camera relative to the loading frame.

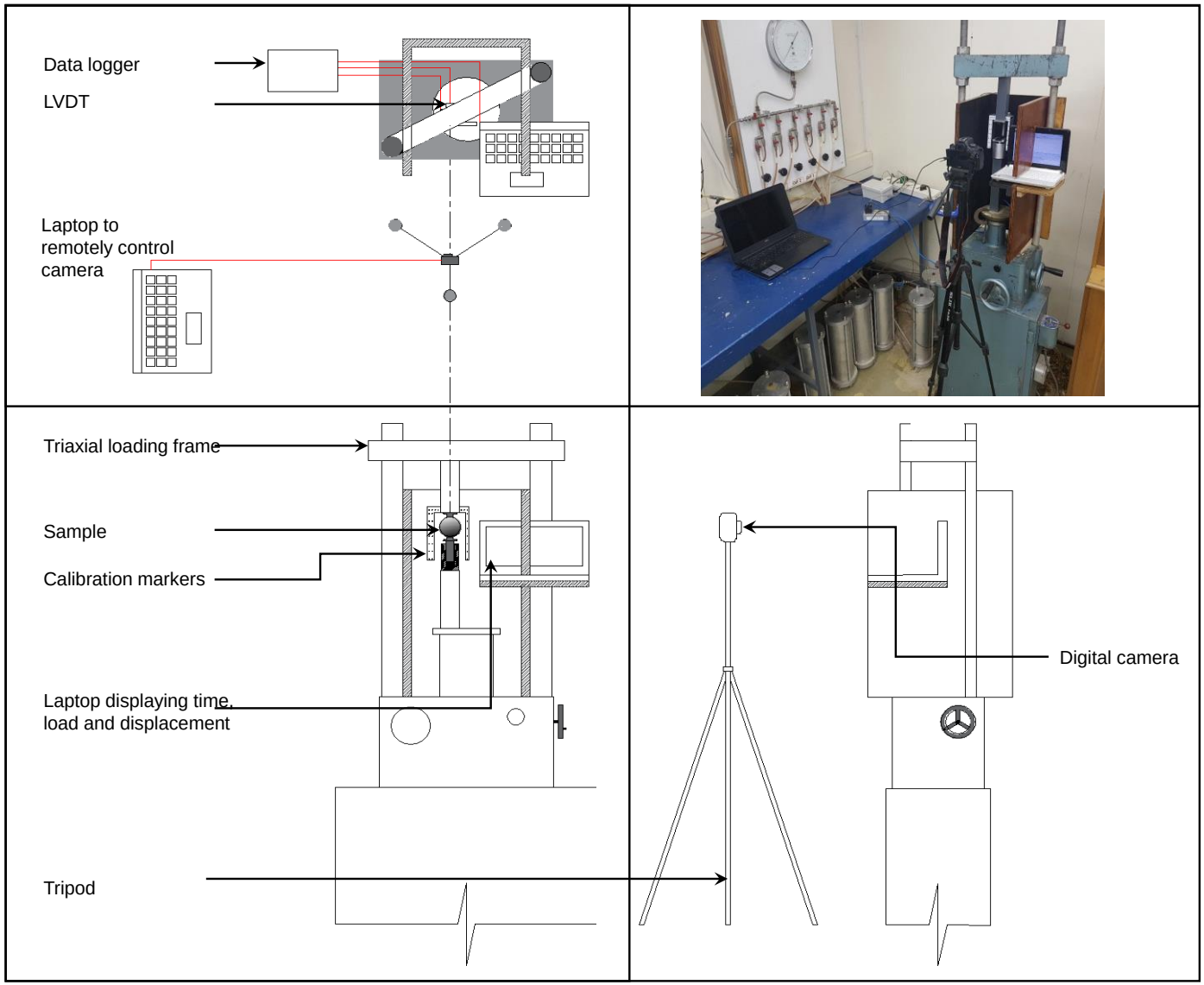

Figure 3-12: Schematic of final setup

As previously mentioned, samples exceeding the capacity of the above-mentioned load cell were tested on a conventional loading press with all other aspects of the layout presented in Figure 3-12 remaining unchanged. Despite being recently calibrated by the manufacturers, calibrations of the load press were redone both with respect to its load and vertical displacement readings. While the load output of the press was found to be accurate, its measurement for vertical displacement was not. As a result, the LVDT used in the previously mentioned setup was attached to the loading press and displacement readings, used for the interpretation of test results, were taken from this instrument.

3.2.2 Digital Image Correlation (DIC)

Digital Image Correlation (DIC), sometimes referred to as Particle Image Velocimetry (PIV), is a photogrammetric technique whereby a sequence of digital images is analysed, such that surface displacements can be measured. To implement the technique, a region of interest is specified in the first photograph of the sequence, and this region is divided into several subsets (or patches). The position of these subsets is tracked in each photograph, thereby allowing for soil displacement to be calculated as deformation of the specimen takes place. For this research project, DIC was applied to create virtual strain gauges at predetermined positions on the sample.

The desired outcome for the use of virtual strain gauges was to determine:

a) the stage of the test where cracking had begun and
b) the distribution of horizontal strain along the loaded axis of the sample.

Due to the inherent nature of the test, it is known that strains across the diameter of the sample would not be uniform. As a result, the ideal approach to obtaining a representative value of strain at the centre would be to calculate strain from two patches immediately adjacent to the crack. However, positioning subsets so close to the centre would increase the likelihood of a crack forming within a subset, making it unrecognisable in subsequent photos. Furthermore, since the purpose of the strain analyses was to identify a change in behaviour rather than the value of strain itself, subsets were positioned on the outermost portion of the sample to achieve outcome a). For outcome b), patches were positioned on either side of the centre line of the sample at a spacing which would facilitate strain calculations along its *entire* diameter. Figure 3-13 illustrates the positions of the subsets used for outcomes a) and b).

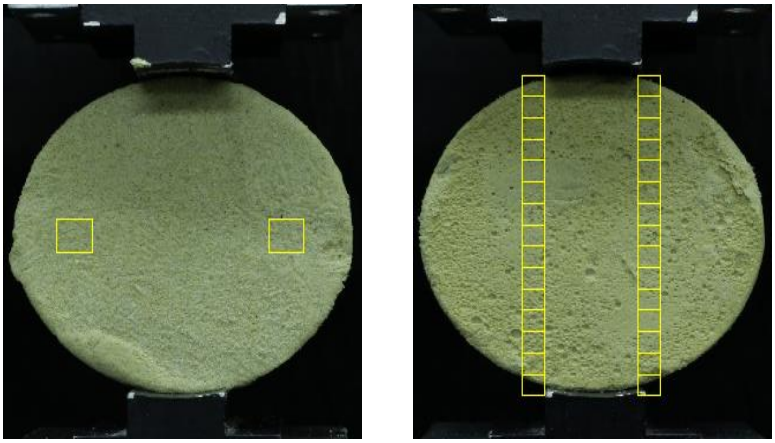

(a) (b)

Figure 3-13: Subset positions to determine a) time of crack initiation and b) strain distribution along sample diameter

The precision of DIC is a function of patch size, with larger patches producing higher precision. However, larger patches reduce the level of detail that can be obtained in a region of high strain gradients, since the strains are calculated from fewer points (White *et al.*, 2003). For outcome a), strain at only one position of the sample was required and therefore a large patch size of 100 px was chosen. In contrast, a greater amount of detail was required to determine the distribution of strain along the loaded axis and as a result, a smaller subset size of 64 px was selected. To illustrate the effect of varying patch sizes on calculated strains, a sensitivity analysis was performed on the calculation of horizontal strain (Outcome a)) for a range of subset sizes. Figure 3-14 shows the results of this analysis.

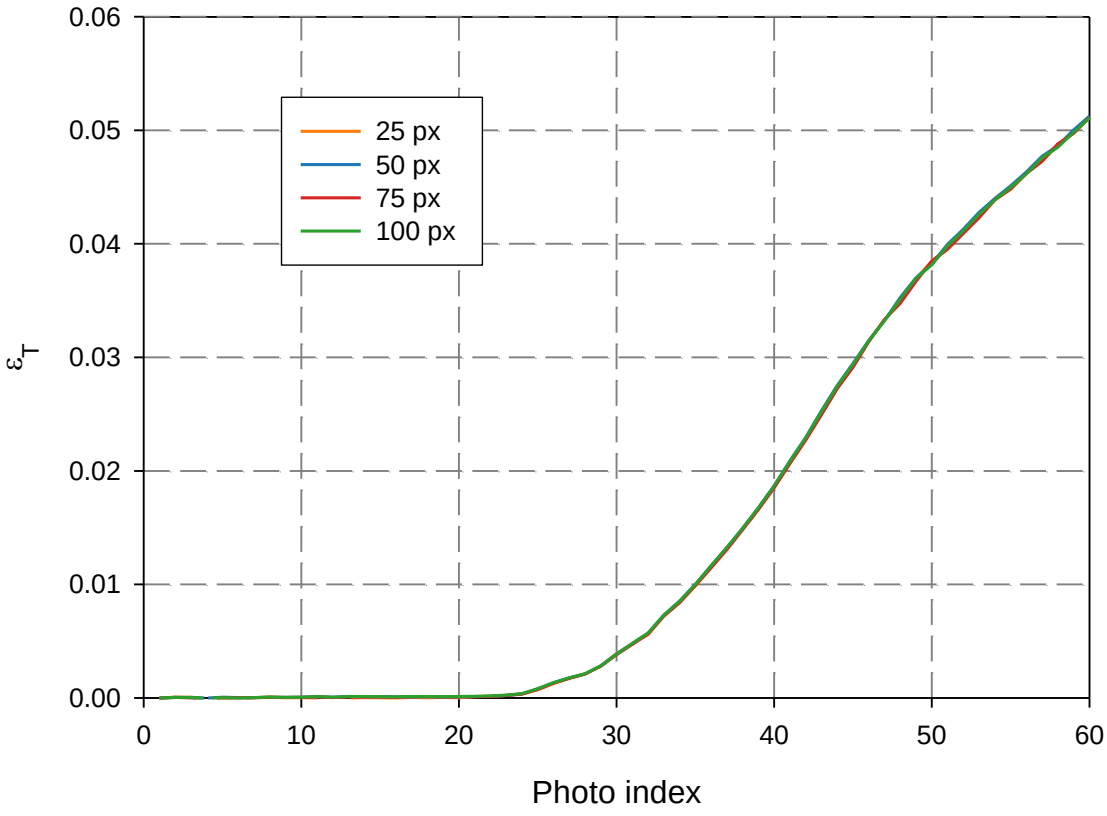

Figure 3-14: Effect of patch size on strain computations

From Figure 3-14 it can be seen that for a practical range of patch sizes, the effect on the computed strain was found to be negligible. The final aim for using DIC was to produce contour plots of strain over the entire sample surface to locate the exact position at which cracking initiated. For this final analysis, a greater amount of detail was required (particularly at the centre of the sample) and so the patch size was reduced even further to 20 px. To provide an indication of the level of detail, Figure 3-15 illustrates the grid of subsets used to determine the strain for these contour plots.

Figure 3-15: Mesh used to produce contour plots of strain

3.2.3 Determination of the Soil Water Retention Curve (SWRC)

The relationship between matric suction and moisture content is one which houses an abundance of information that can be used to interpret various characteristics of unsaturated soils. However, as stated in Section 2.1.3, the initial state of the sample has a significant impact on the SWRC that is ultimately measured. For this research project, SWRCs were required to provide a qualitative indication as to the variation in matric suction with moisture content, as well as to approximately highlight the transition between different saturation regimes. These relationships were used to interpret trends in tensile strength for varying moisture contents for the three materials. It should be noted that since the initial state of SWRC and BDT samples were not equivalent, no attempt was made to draw quantitative correlations between the results of these two tests.

For gold and iron tailings, the SWRCs were gathered from parallel research projects being conducted at the University of Pretoria by Le Roux (2016) and Chapman (2016) respectively. For the Centurion soil, testing was conducted by the author. This section provides an overview of the procedures utilised to measure the SWRCs of all three materials.

The method implemented for this dissertation is based on the MIT technique proposed by (Toker *et al.*, 2004). The procedure involved preparing a sample at 100% saturation with three high capacity tensiometers embedded in it. The soil mass was placed on an electronic scale and allowed to dry out, with measurements of matric suction and mass being recorded continuously. Mass readings were later used to back calculate the gravimetric moisture content of the soil as

it dried out. This testing procedure was carried out in an enclosed, insulated chamber such that temperature could be kept constant for the duration of the test. Figure 3-16 highlights the key components of this setup.

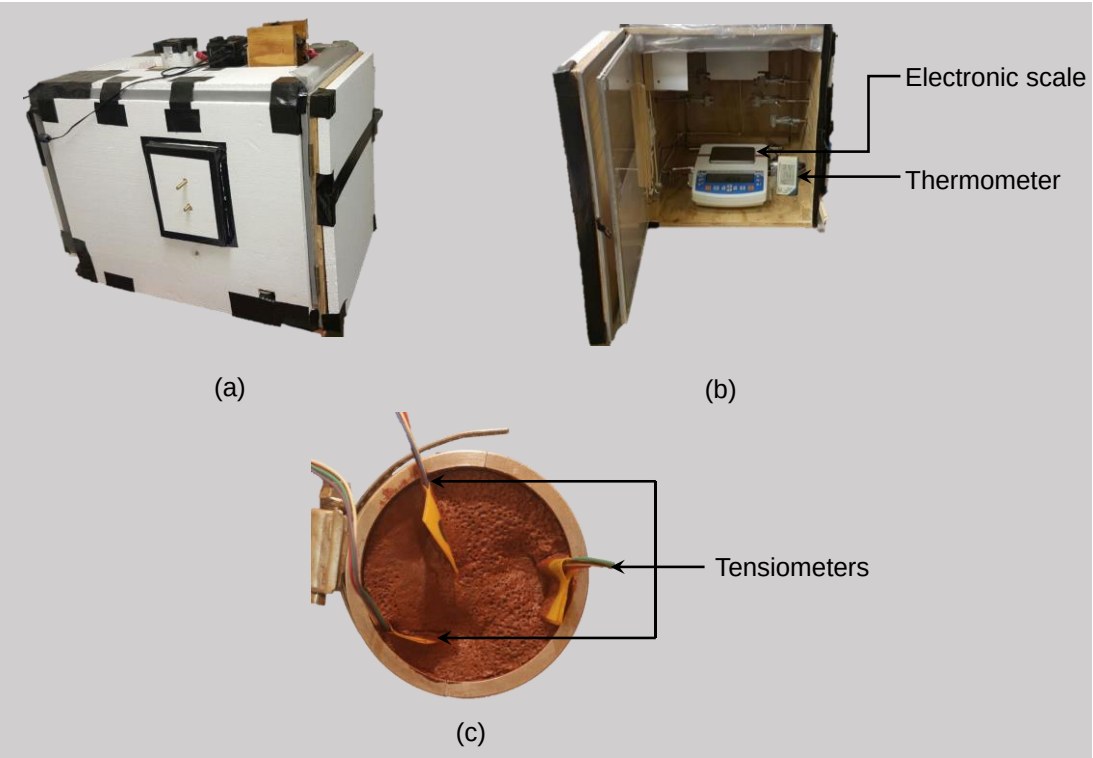

Figure 3-16: a) Insulated chamber, b) positioning of electronic scale and thermometer within the chamber and c) the positioning of tensiometers within the soil mass

The MIT technique was used up until cavitation of the tensiometers occurred. To obtain complete SWRCs for the soils, the filter paper method discussed in Section 2.3.1 was used to measure matric suction at magnitudes exceeding the cavitation pressure of the tensiometers.

Matric suction of the samples was measured by placing a piece of filter paper in direct contact with the sample prepared at some predetermined moisture content. The sample and filter paper were then sealed to prevent evaporation and were subsequently left for equilibration of moisture between the soil and filter paper to occur. Following the equilibration period, the wet mass of the filter paper was recorded and used to determine its gravimetric moisture content, which was then related to a value of matric suction through the calibration curves provided by Hamblin (1981). For the experimental work carried out in this dissertation, Whatman No. 42 filter paper was used. An equilibration period of seven days was implemented, and filter paper mass measurements were recorded (to five significant digits) on an electronic laboratory scale.

3.3 SAMPLE PREPARATION PROCEDURE

3.3.1 Brazilian Disc Test (BDT)

In developing a sample preparation procedure, the first factor considered was that of specimen size. It was established that it would be beneficial to use a diameter that is conventionally adopted in triaxial testing. In South Africa, typical sample diameters are 50, 100 and 150 mm. Use of a 'standard' sample diameters would allow for the tensile results of BDTs to be related to those from confined and unconfined compression tests, allowing the failure envelope of a given soil to be fully defined. The final decision on sample size was based on the fact that the tensile strength of unsaturated soils is relatively low in comparison to materials on which BDTs are commonly performed (concrete, rock, etc.). Consequently, a soil sample containing any defects would likely result in failure occurring at a defect rather than at the centre of the specimen where maximum tensile strength is mobilised. When preparing larger specimens, there would be a tendency towards a higher number of defects and, as a result, the smallest standard diameter of 50 mm was chosen. Using an aspect ratio of 2:1 (diameter:length), which is typical for BDTs) a final sample size of 50 mm in diameter and 25 mm in length was selected. Clayton *et al*. (1995) provided the recommendation that the minimum sample dimension should be in the order of 5-10 times larger than the maximum particle size of the soil. Considering the particle size distributions presented in Figure 3-2 it can be seen that this criterion is far surpassed, thereby validating the choice of a smaller specimen size.

The preparation procedure comprised of two aspects, namely the manufacture and preparation of sample moulds, as well as the preparation of a slurry. Sample moulds consisted of three separate components including a cylinder split in half, a base plate into which the cylinder could be seated, as well as an O-bracket which was used to clamp the two halves of the cylinder together. Figure 3-17 illustrates the three individual components.

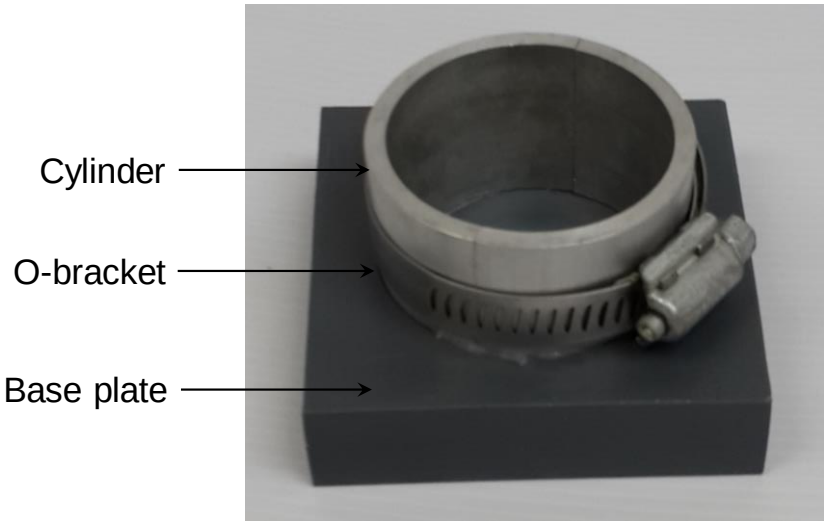

Figure 3-17: Sample mould

Prior to the deposition of slurry, each mould was lined with petroleum jelly along all adjoining surfaces to ensure water tightness of the assembly. The inside of each mould was then sprayed with a lubricant to allow for the easy removal of the sample at the end of the preparation process.

Once the mould setup had been finalised, preparation of the sample commenced. Each sample was prepared from a reconstituted slurry at a gravimetric moisture content governed by the workability of each material. Chosen moisture contents of each soil type are included in Table 3-2. The slurry was deposited into a mould in three separate lifts and vibrated for 20 seconds after each lift. It should be noted that the intention of vibrating after each lift was to ensure even distribution of the material within the mould, rather than to achieve any particular density. Figure 3-18 presents an idealised schematic on the effect of this short vibration period on the distribution of material within the mould. An improvement in sample homogeneity was observed by comparing samples prepared with and without the vibration stage. Vibrated samples showed fewer air inclusions and were more homogeneous.

Table 3-2: Slurry moisture contents

Material type	Gravimetric moisture content (%)
Gold tailings	27
Iron tailings	40
Dolomitic residuum	60

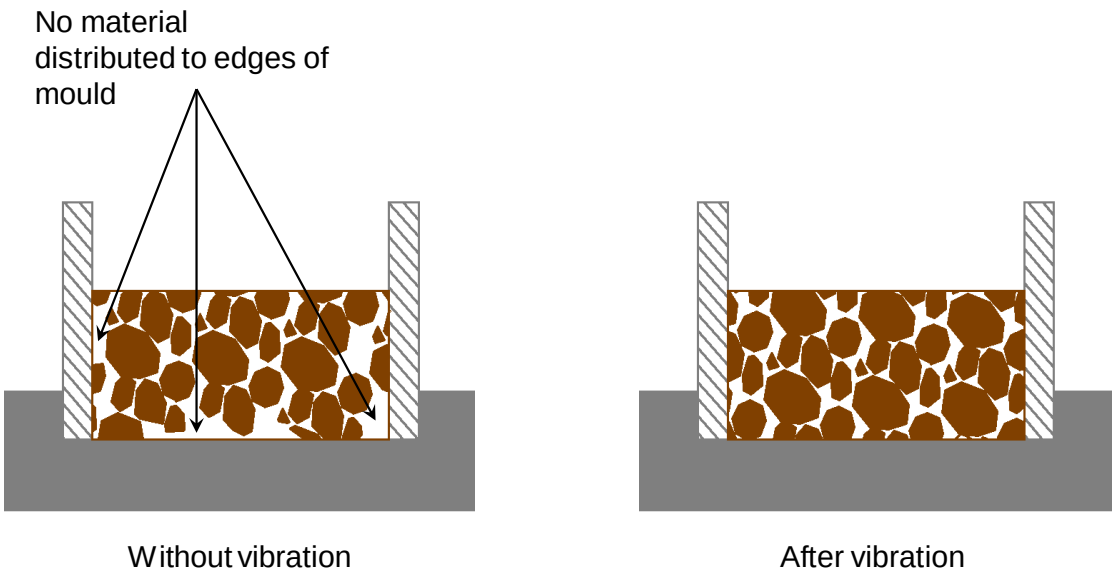

Figure 3-18: Effect of vibration on sample uniformity

Following the deposition of slurry, moulds were placed in an oven at 65°C and allowed to dry out to the desired moisture content. Mass readings of each specimen were periodically taken to determine the amount of moisture loss, and thus the moisture content of the sample. Once a sample had reached the targeted moisture content, it was demoulded and trimmed to a height of 25 mm. A final mass reading of the sample was then taken, together with four height and two diameter measurements, all of which were used to determine the unit weight of each individual sample. Finally, before being stored, samples were wrapped with a combination of both cling film and aluminium foil, as suggested by Heymann & Clayton (1999), to minimise the amount of moisture loss prior to testing. All samples were left overnight (approximately 16 hours) to allow moisture and thus matric suction to equilibrate throughout the sample.

3.4 TESTING PRODECURE

3.4.1 Brazilian Disc Test (BDT)

After being left to equilibrate for a given period of time, the disc samples were unwrapped and placed on top of the bottom loading strip. Once the sample had been put in place, care was taken to ensure that the top and bottom loading platens were properly aligned before loading commenced. To ensure proper alignment of the setup, the bottom loading platform was manually raised until there was approximately a 1 mm gap between the top of the disc specimen and the top loading strip. When in this position, a close-up photograph of the setup was taken

and the bottom platen was adjusted until a rectangle could be drawn connecting the edges of the top and bottom loading strips. Figure 3-19 illustrates a typical photograph of the disc specimen following proper alignment.

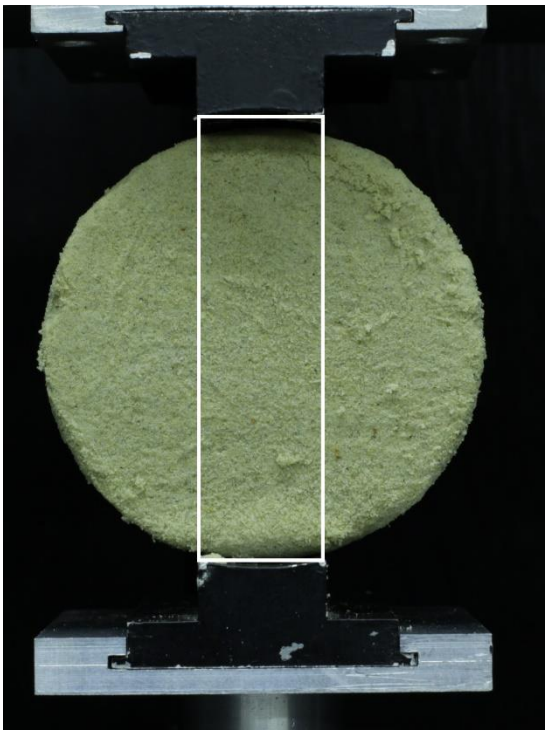

Figure 3-19: Alignment of sample prior to loading

Once the sample had been properly aligned, the digital camera, set to take a photograph every five seconds, was remotely triggered and loading of the specimen commenced. The strain rate used for the BDTs was chosen to avoid excessive loss of moisture throughout testing. A study conducted by Wulfsohn *et al.* (1998) on the triaxial testing of unsaturated soils discussed the effect of loading rate on strength measurements. Wulfsohn *et al.* (1998) stated that while the compressive strength of an unsaturated soil can be significantly altered by the loading rate if it exceeds some critical value, the tensile strength is however not significantly affected. A strain rate of 0.5 mm/min was therefore utilised for the testing of all three materials.

Immediately following failure of a sample, the mass of the two broken halves was recorded and the material was placed in an oven to dry at 105°C. Once the material had completely dried out the oven was turned off, opened slightly and allowed to cool down to room temperature. The purpose for doing this was to avoid the dried-out soil samples absorbing any ambient moisture after being removed from the oven. This would likely occur if samples were removed while

they were at an elevated temperature. This intermediate step allowed for an accurate measurement of the mass of solids for each specimen which was used to determine their moisture contents. Any correlations made between moisture content and strength during the analysis of results were based on these final measurements of gravimetric moisture content.

4 EXPERIMENTAL RESULTS AND DISCUSSION

The following chapter presents a discussion of results for Brazilian Disc Tests (BDTs) performed on three soil types. Results are subdivided according to material and, for each soil, tensile behaviour is investigated in terms of stress vs vertical compression, as well as strain development during loading. For the latter two factors, differences in behaviour across different saturation regimes are highlighted. The results of each material are concluded with a discussion on the effect of moisture content and matric suction on the tensile strength of unsaturated soils. With the exception of the transported Centurion soil, the Soil Water Retention Curves (SWRC) discussed in this chapter were taken from the results of two parallel research projects at the University of Pretoria conducted by Le Roux (2016) and Chapman (2016). The chapter concludes with a general discussion on the behaviour of the three materials

The BDT results provided in this chapter are presented in terms of calculated tensile stress vs imposed vertical compression. Tensile stresses presented for each test were calculated using the elastic solution given in Equation 2.9. The values of vertical compression represent the relative movement between the two loading strips. Furthermore, all strain results are presented with tensile strain as positive.

4.1 GOLD TAILINGS

The first granular material considered for this study was gold tailings (material properties included in Chapter 3). Being the coarsest material tested, the magnitude of matric suction that could be developed at high moisture contents was minimal. As a result of this low suction, it was found that samples could not be prepared in the capillary regime without collapsing under their own weight. For this reason, the results presented in this section have targeted the pendular regime and the dry and the wet sides of the funicular regime. Typical tensile stress vs vertical compression curves for these three zones are plotted in Figure 4-1.

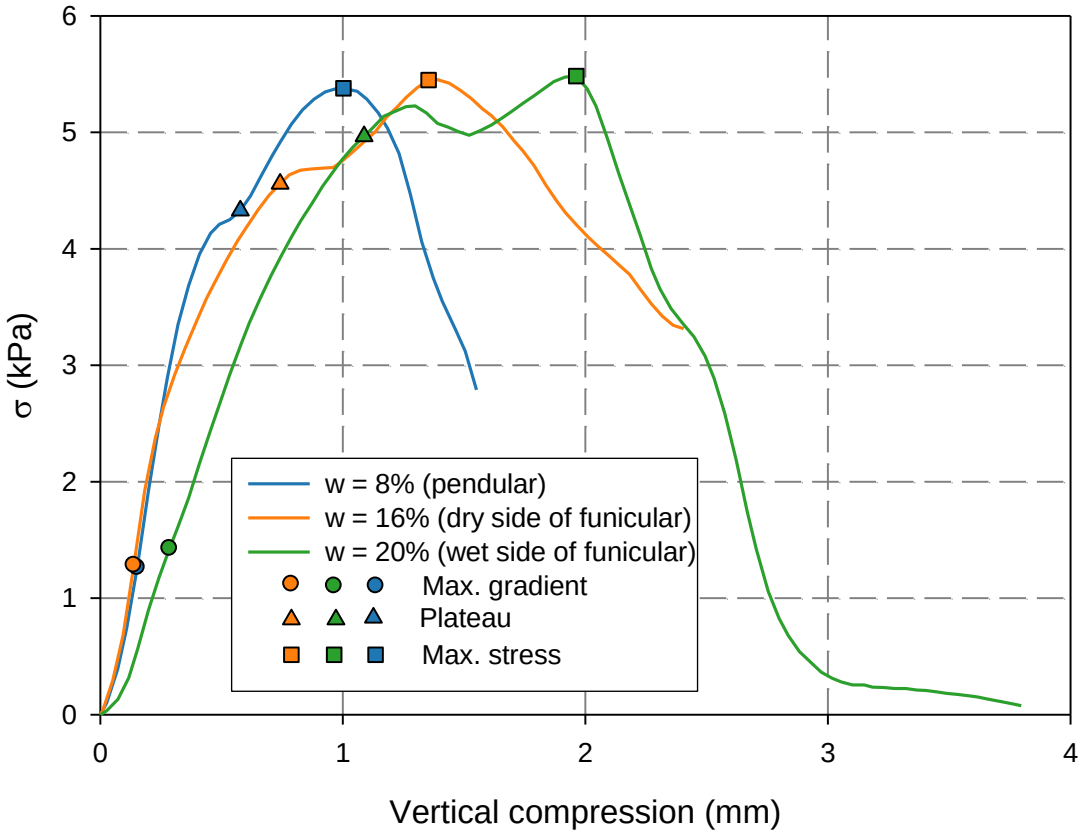

Figure 4-1: Stress vs compression relationship for gold tailings across different saturation regimes

From the curves presented in Figure 4-1, three distinct changes in behaviour can be identified. Initially, each curve rises steeply as load is applied. In this region, the gradient of the stress-compression curve increases slightly until the first inflection point is reached. After the curve reaches this maximum gradient, it slowly begins to flatten until it reaches a plateau/initial peak. Finally, each curve goes on to achieve a second (maximum) peak load before dropping rapidly.

Conventional interpretation of the Brazilian Disc Test states that the maximum achieved load should be used to calculate the indirect tensile strength of a material. However, the results of split cylinder tests conducted on Fibre Reinforced Concrete (FRC), presented by Denneman *et al.* (2011), illustrated a 'double peak' result similar to that presented in Figure 4-1. The conclusions of their study stated that the maximum peak value was related to secondary cracking mechanisms. Denneman *et al.* (2011) stated that the initial peak represented the linear elastic limit state and that from it, a best estimate of tensile strength could be calculated.

The presence of two inflection points occurring before maximum load illustrated in Figure 4-1, as well as the conclusions made by Denneman *et al.* (2011), raise the question of whether conventional interpretation is adequate to quantify the tensile strength of weakly bonded

unsaturated soils. To investigate this aspect, tensile strain development in the sample during loading was examined and is discussed in the following section.

4.1.1 Tensile strain development

Measurements of tensile strain development were recorded using Digital Image Correlation (DIC) as described in Section 3.2.2 and the results of these measurements are provided in the following discussion. Figure 4-2 and Figure 4-3 present the results of the strain analyses performed on samples at gravimetric moisture contents of w = 8% and w = 20% respectively. Within the results presented for each sample, three sub-figures are included to highlight different aspects at three critical stages of the tests. The stages presented are as follows:

1. Maximum gradient on the stress vs compression curve.
2. Initial peak/plateau (this is also the instance at which a crack first becomes visible).
3. Maximum measured load.

Part (a) of the figures contains the stress vs compression behaviour as presented in Figure 4-1, along with markers at the three points discussed above. Part (b) illustrates the distribution of horizontal tensile strain along the loaded axis of the sample at each of the three stages. The vertical axis of the results presented in Part (b) is expressed as a multiple of sample diameter, with D representing the total diameter and d, the distance from the top of the sample. Finally, shaded contour plots of horizontal tensile strain at each stage is provided in Part (c). Contours are superimposed on the corresponding photographs of the sample to emphasise specimen condition at each stage.

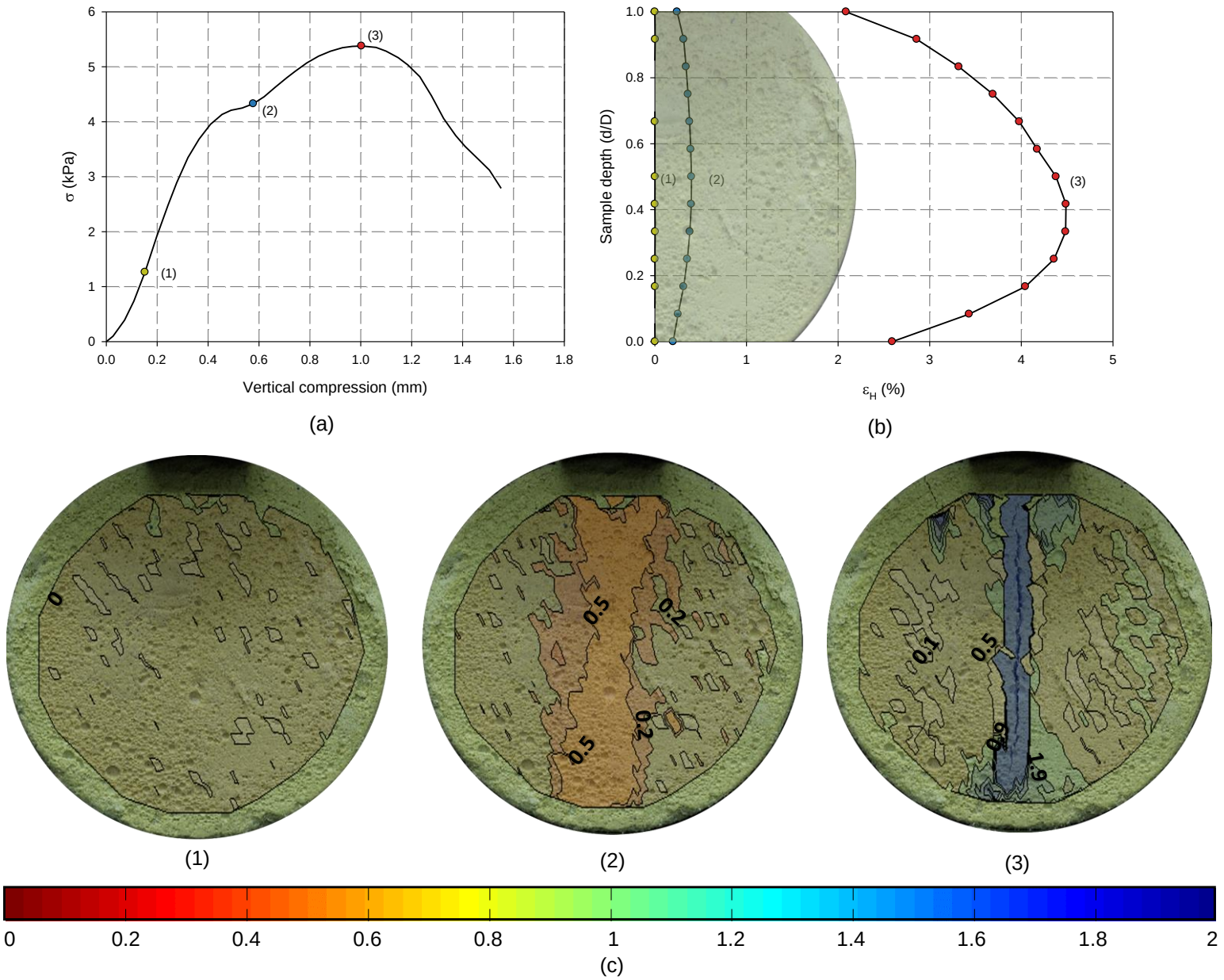

Figure 4-2: Strain analysis for sample at w = 8%

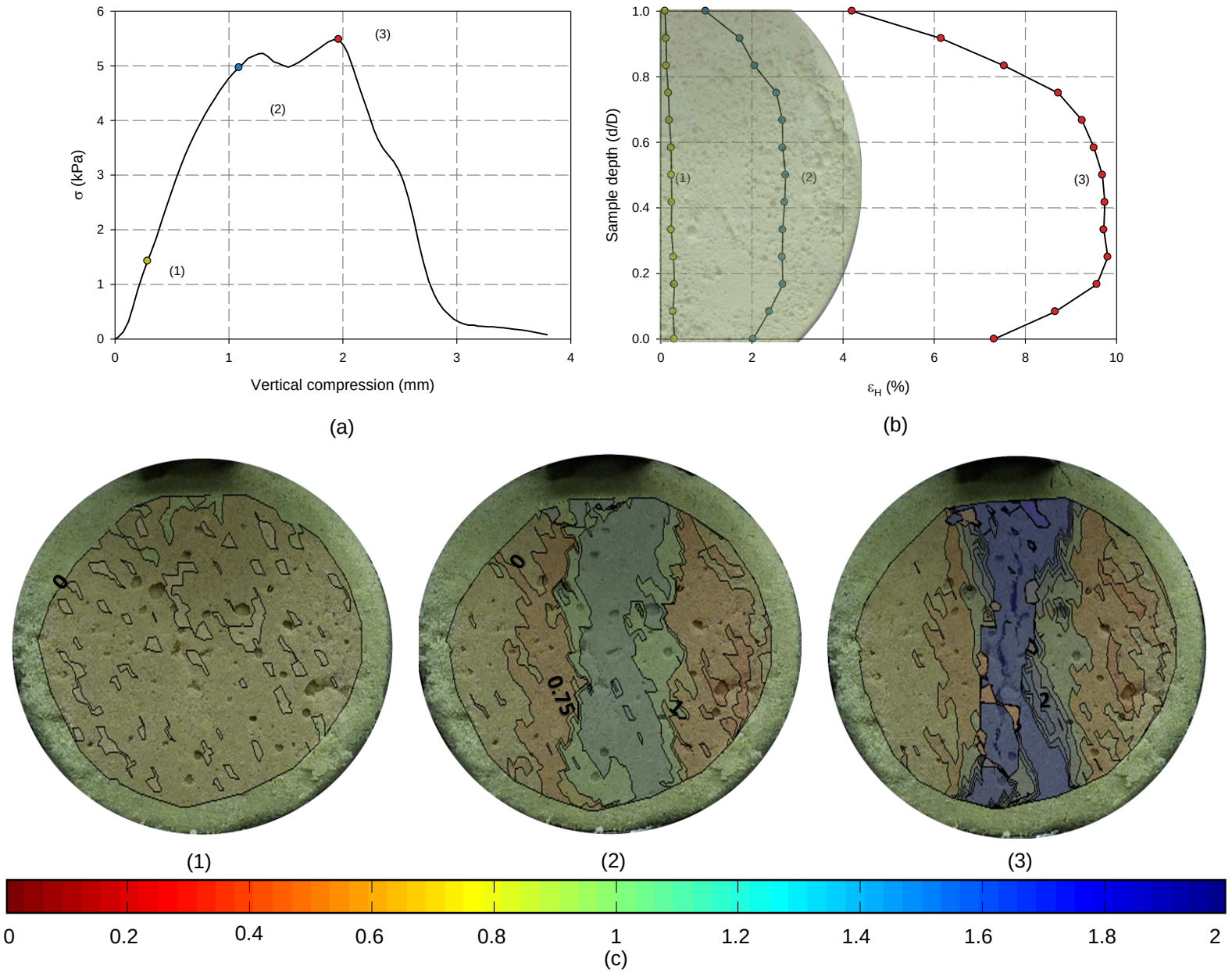

Figure 4-3: Strain analysis for sample at w = 20%

From the results presented in the above figures, several trends can be identified. Figure 4-2 b) and Figure 4-3 b) illustrate how the distribution of tensile strain approximates parabolic distributions, with peak values reached in the centre of the disc. This behaviour is reinforced by the contour plots in the second frame of Figure 4-2 c) and Figure 4-3 c). Together, these two figures validate the measured strengths as being due to the mobilisation of *tensile* strength. It is worth noting that these trends in tensile strain development correlate well with the plots of circumferential and compressive stresses along the loaded axis of the sample presented in Figure 3-4. This shows that the assumption of elastic conditions in the interpretation of BDTs is a valid approximation.

At the instance where a surface crack became visible, the sample had begun to split at its centre. According to Griffith's failure criterion (Section 2.2.3), this is the unique point on the specimen at which the conditions for tensile failure at a value equal to the uniaxial tensile strength are met (Li & Wong, 2013). Taking cognisance of the fact that the sample is no longer intact at this stage, it can be stated that any further loading of the disc will be unrelated to its maximum tensile strength. As a result, the remainder of the test can be disregarded. However, defining failure as the point at which a crack becomes visible is a crude interpretation of the test, since it is known that stresses along the depth of the sample are not constant (Li & Wong, 2013). It has thus been proposed that the point at which the stress-compression curve achieves a maximum gradient be investigated more closely in terms of horizontal strain development.

Figure 4-4 a) and b) contain the stress-compression curves for samples at w = 8% and w = 20% respectively, together with tensile strain development across the centre of the sample plotted on the secondary vertical axis.

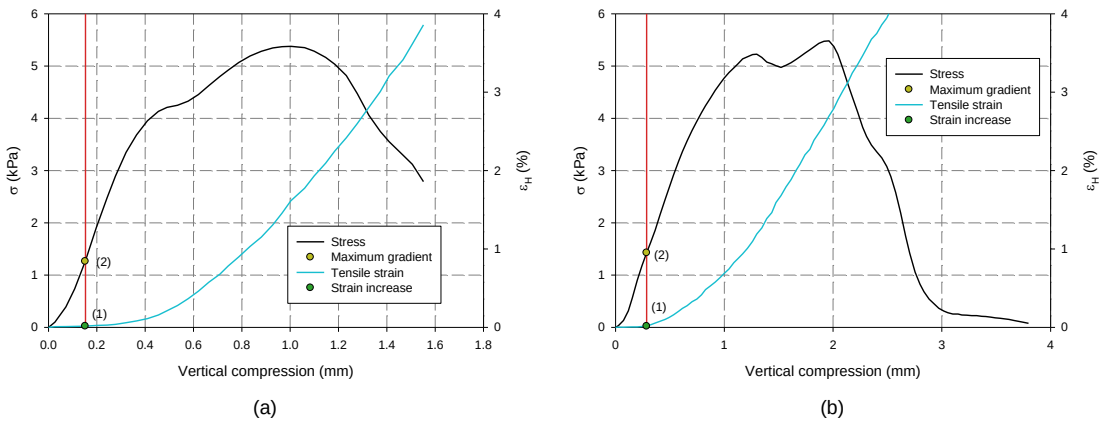

Figure 4-4: Tensile stress and horizontal tensile strain development across the sample centre vs displacement for a) w = 8% and b) w = 20%

From these results it can be seen that, at the point where tensile strain begins to deviate from zero (Point 1), the stress vs compression curve reaches its maximum gradient and the rate of the stress-compression plot (i.e. the rate at which the sample is able to carry load) begins to diminish. A similar relationship observed in concrete was described by Karihaloo (1995) from the perspective of fracture mechanics. Karihaloo (1995) described how the non-linearity in a load-deformation curve following this point of inflection was due to the formation of micro-cracking.

At this stage of the test the sample has reached a state of first yield, prior to which tensile splitting cannot occur. Following first yield (Point 2), progressive failure of the sample ensues and micro-cracks begin to grow and coalesce until a surface crack becomes visible. Beyond this stage of the test, the elastic solutions for the BDT are no longer strictly valid.

Identifying the maximum gradient of the stress-compression curve can easily be repeatably determined from calculation. In contrast, the approach of locating the stage at which tensile strain begins to increase is more subjective. Having defined the stage of the test where tensile strength is mobilised using both approaches, (i.e. locating the point where a) the maximum gradient of the stress-compression curve is reached or b) tensile strain begins to increase), it was seen that either method produced almost identical results for 75% of the tests carried out. Therefore, the point of maximum gradient on the stress-compression curve has been found to define the stress at first tensile yield. This stress is sufficiently conservative to be used as the criterion for tensile failure in this weak granular soil.

To emphasise the danger of adopting the maximum achieved load as being indicative of the tensile strength of a weak material, consider the results for a test conducted at an intermediate moisture content of w = 12%. Figure 4-5 illustrates the stress vs compression results, together with an image of the sample at a key stage of the test.

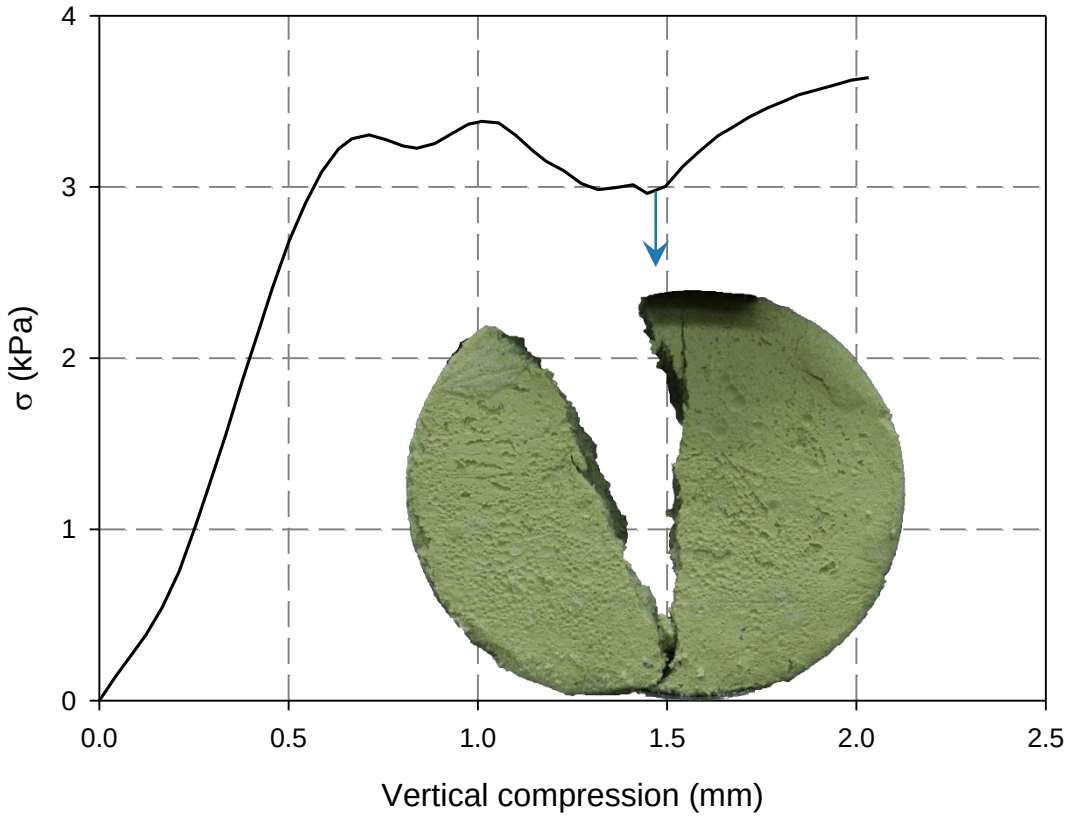

Figure 4-5: Stress vs displacement for sample at w = 12%

Indicated in Figure 4-5 is the stage of the test where only half of the sample remained between the two loading strips. It is clear from this figure that the increase in load measured after this point is certainly not as a result of tensile splitting, but rather due to the compression of one half of the sample. The above result strongly emphasises the magnitude of error associated with blindly adopting the maximum achieved load as an indication of the tensile strength.

4.1.2 Transition in material behaviour

The results presented in the preceding sections illustrate that within the moisture content range considered, similar behaviour was observed for the samples tested, both with respect to inflection points in the stress-compression curve and in terms of the ductile responses seen in the strain analyses. However, in addition to these results, a final group of tests was conducted on samples which were allowed to dry out almost completely and which were therefore tested at very low values of saturation. Figure 4-6 illustrates the stress-compression-tensile strain results for a sample at w = 0.17%. Shaded contour plots are provided in Figure 4-7 for three stages of the test.

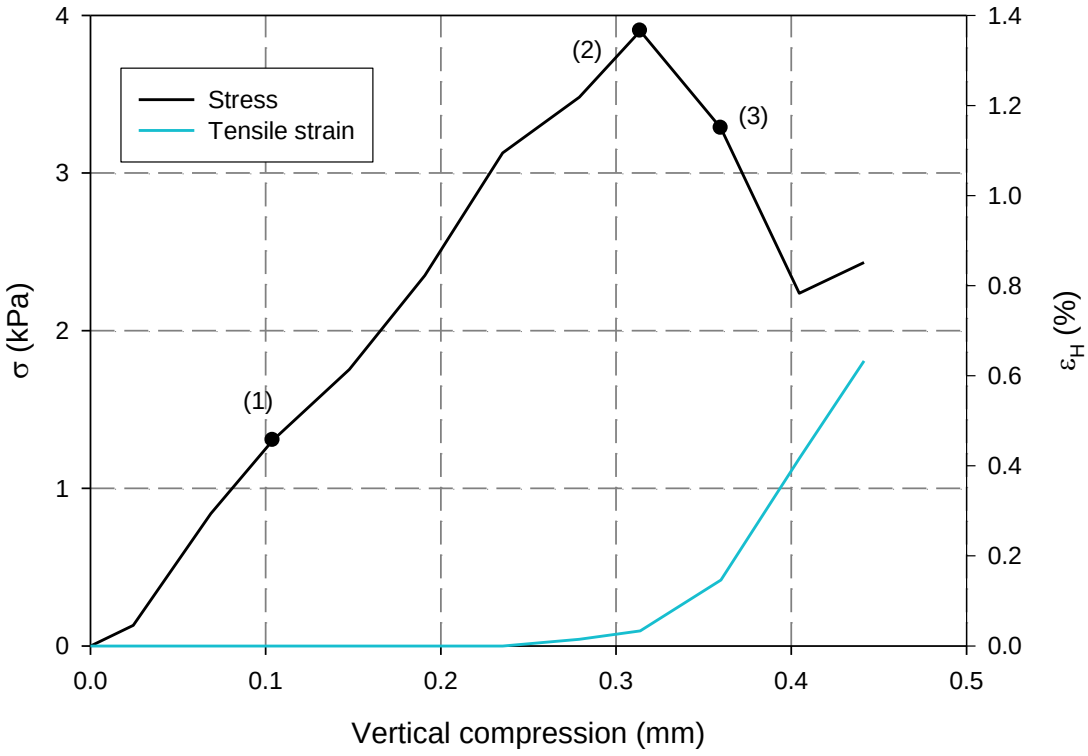

Figure 4-6: Stress vs displacement vs tensile strain for a sample at w = 0.17%

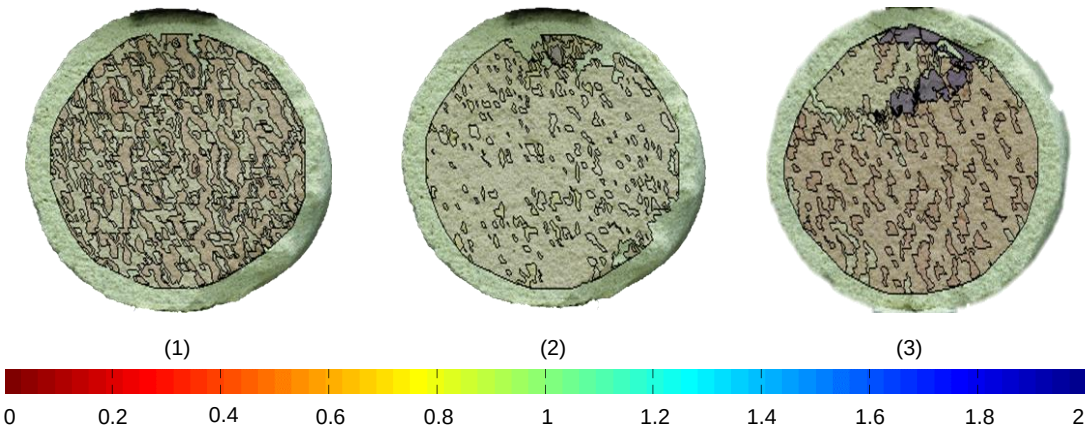

Figure 4-7: Contour plots of tensile strain for a sample at w = 0.17%

The results in Figure 4-6 illustrate a more brittle behaviour from what has been discussed thus far. The stress-compression results exhibited a linear relationship and showed little change before the maximum load was reached. Similarly, little change in the development of tensile strain across the centre of the sample is observed up until the peak load. At this point, tensile strain is seen to increase rapidly, thereby indicating a tensile failure.

Consideration of the contour plots in Figure 4-7 do however illustrate that the observed failures appear to not have been a result of tensile splitting.

These results highlight a strain concentration initiating close to the top loading strip rather than at the centre of the sample. However, these measured displacements occurred as a result of a small piece of material breaking off from the surface rather than the failure of the entire specimen. In spite of this, examination of the results presented in Figure 4-6 highlights the following two aspects:

1. the stress-compression curve remains linear up until the peak load (validating use of Equation 2.9 for this region) and
2. horizontal tensile strain across the centre of the specimen remained close to zero for the linear portion of the stress-compression curve, increasing sharply at the point of maximum stress.

Taking these characteristics into account it can be stated that the observed failures are in fact indicative of the mobilisation of tensile strength.

An explanation for the measured surface displacements is due to the extreme brittleness of a weak unsaturated granular material at this low moisture content. Due to its lack of ductility, a stress concentration significant enough to cause surface cracking could be brought about by either the slightest imperfection in the sample geometry or the smallest misalignment in the placement of the sample on the loading strip. Figure 4-8 illustrates these two issues graphically.

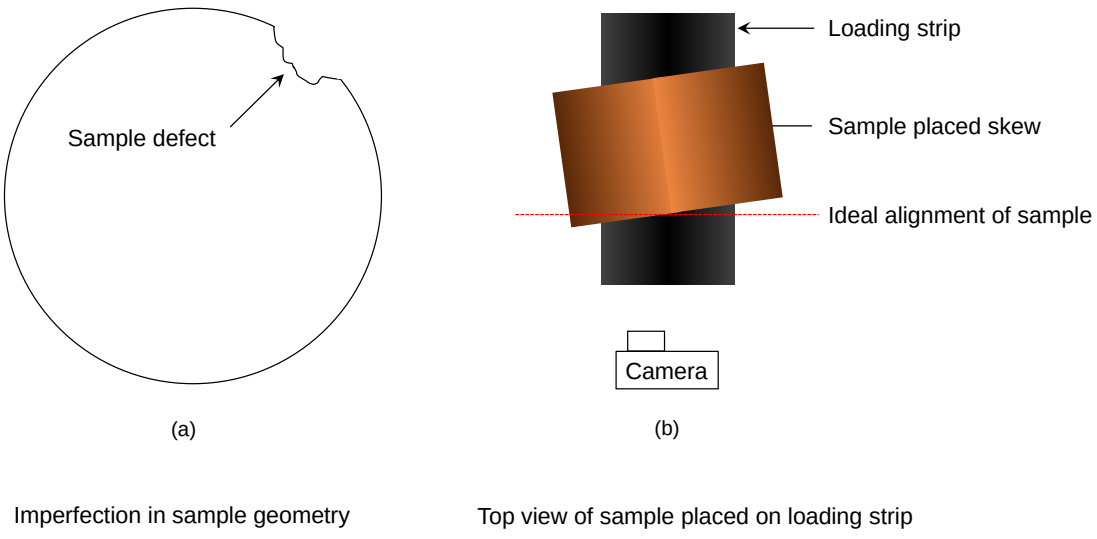

Figure 4-8: Causes of premature surface displacements

The above results illustrate that while the measurement of surface displacements is useful, for weak brittle materials it can be misleading. If it is clear that cracking initiates in the centre of the sample, it can be stated that the observed failure has occurred as a result of tensile splitting. However, if initial displacements occur away from the centre, the result should be analysed more closely before its validity can be confirmed. Furthermore, the results highlight how below a certain threshold moisture content, a dramatic loss in ductility is observed.

4.1.3 Relationship between tensile strength and moisture content

The following section presents the measured tensile strengths as a function of moisture content. For the purposes of qualitatively highlighting the variation in matric suction across different saturation regimes, an SWRC as determined by Le Roux (2016) has also been included. Figure 4-9 a) illustrates tensile strength as a function of moisture content, with the SWRC presented in Figure 4-9 b).

Examining the SWRC in Figure 4-9 b) it can be seen that, in the funicular regime, matric suction remains relatively constant. This result is reflected in the measured tensile strengths which showed little variation across the moisture contents considered in this regime. Despite increased scatter of tensile strength in the pendular regime, it was observed that strengths tended to increase with a rise in matric suction (again echoing the trend of the SWRC). The amount of scatter present at such low moisture contents was attributed to the extreme brittleness of the material in the pendular regime. As was described in the preceding section, below a certain moisture content, the susceptibility of samples to stress concentrations make it difficult to repeatably measure tensile strength in this range.

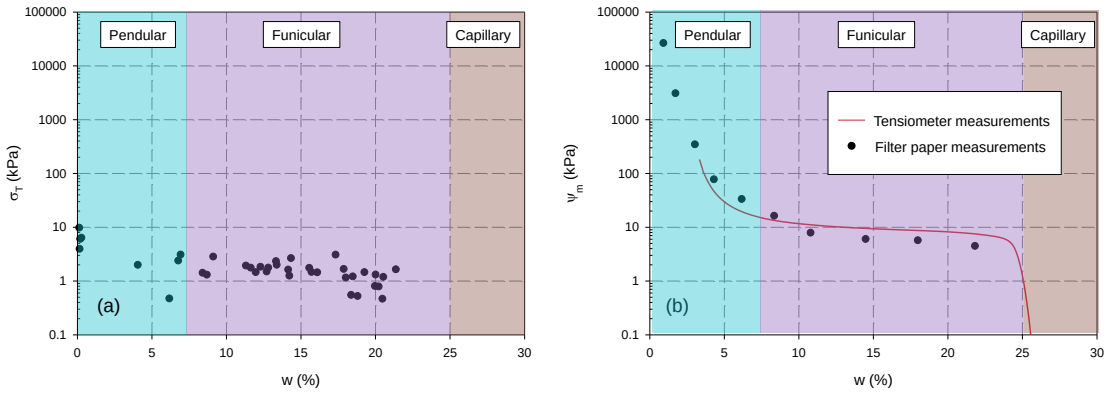

Figure 4-9: a) Relationship between moisture content and tensile strength and b) the SWRC for gold tailings (Le Roux, 2016)

4.2 IRON TAILINGS

For the two finer materials tested, the problem of preparing a stable sample in the capillary regime was not a concern. However, whilst it was possible to prepare samples so close to their saturated moisture content, the setup used did not facilitate a tensile splitting mechanism at such wet conditions. The problem encountered for these tests related to the compressive vs tensile strength ratio of the material (as discussed in Section 2.3.4). For such a high degree of saturation, it was found that upon loading, the sample tended to barrel into an elliptical shape until its radius along the vertical axis exceeded that of the loading strip. At this stage, the edges of the strip began cutting into the sample, compressing it excessively with no cracking occurring along the loaded axis. Figure 4-10 provides contour plots of shear strain for three stages of a test conducted on a sample at S_r = 83% (w = 23.7%).

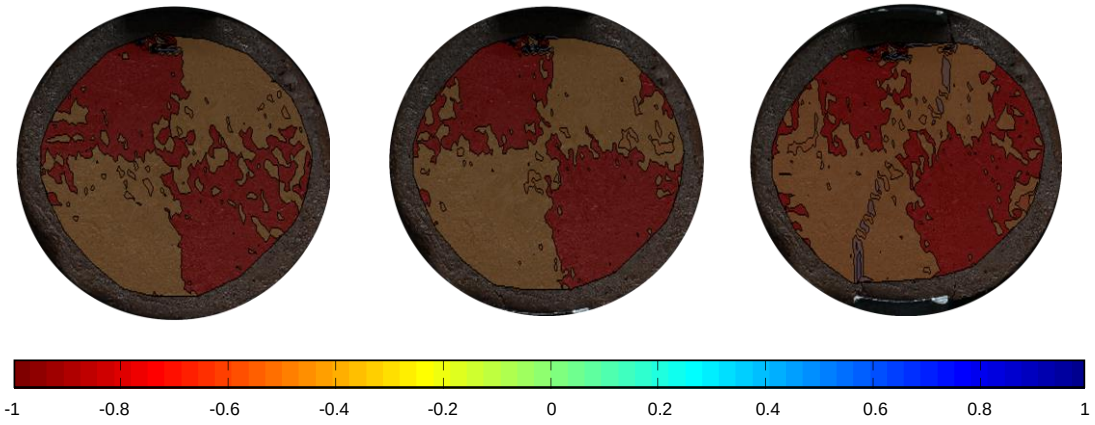

Figure 4-10: Shear strain development for iron tailings sample at S_r = 83% (w = 23.7%)

Due to the aforementioned complications, samples at progressively drier moisture contents were prepared and tested to determine the upper bound of saturation that successfully resulted in a tensile failure. Figure 4-11 presents the stress vs compression results for this group of tests.

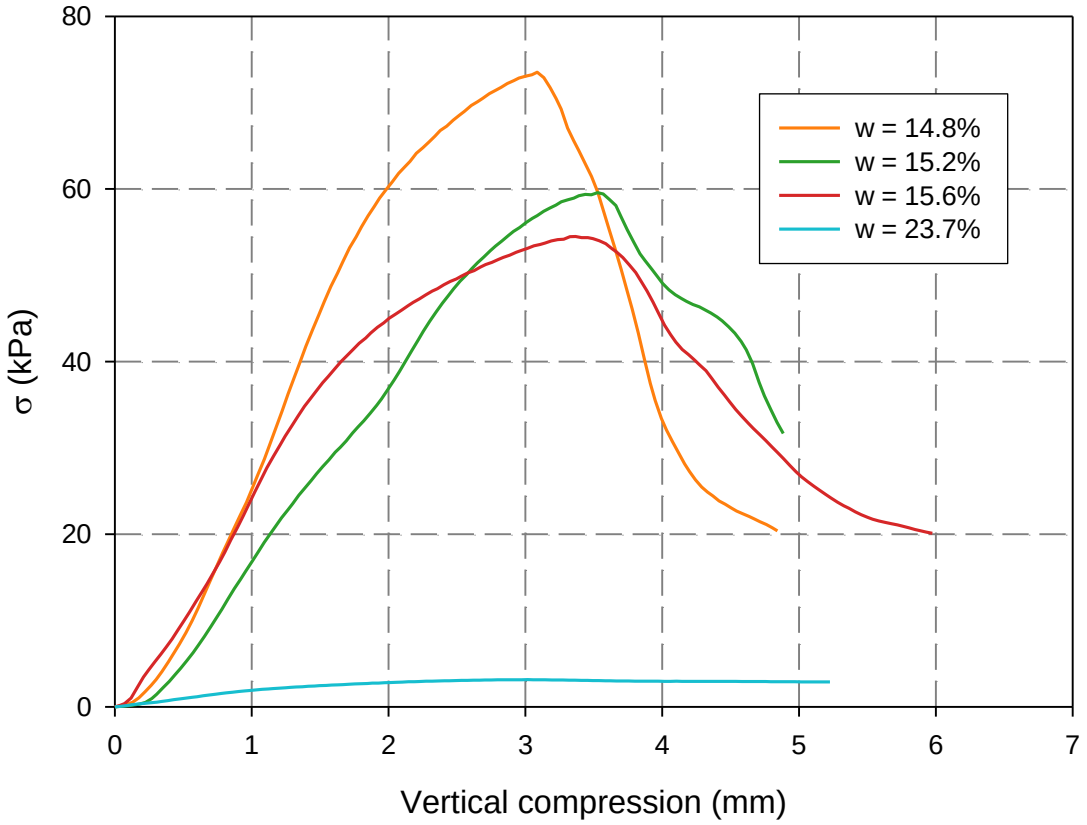

Figure 4-11: Tests performed at high degrees of saturation to determine the upper moisture content resulting in a tensile failure

In addition to determining the maximum moisture content that would result in a tensile failure, the above test results illustrate the effect of moisture content (and thus matric suction) on the strength of a fine-grained soil. While the two wettest results presented in Figure 4-11 are certainly not indicative of tensile strength, it is interesting to note that a decrease in moisture content of 8.1% resulted in an increase of 51 kPa in the peak load. Furthermore, a difference in moisture content of just 0.4% between the two driest samples allowed the failure mechanism to transition from a 'punching' type failure to a tensile failure. From the results presented in Figure 4-11, it was revealed that 14.8% was the wettest gravimetric moisture content for which the test setup used would result in a tensile splitting failure. Figure 4-12 contains the stress vs compression results for tests performed on samples in the pendular regime and the dry and wet sides of the funicular regime.

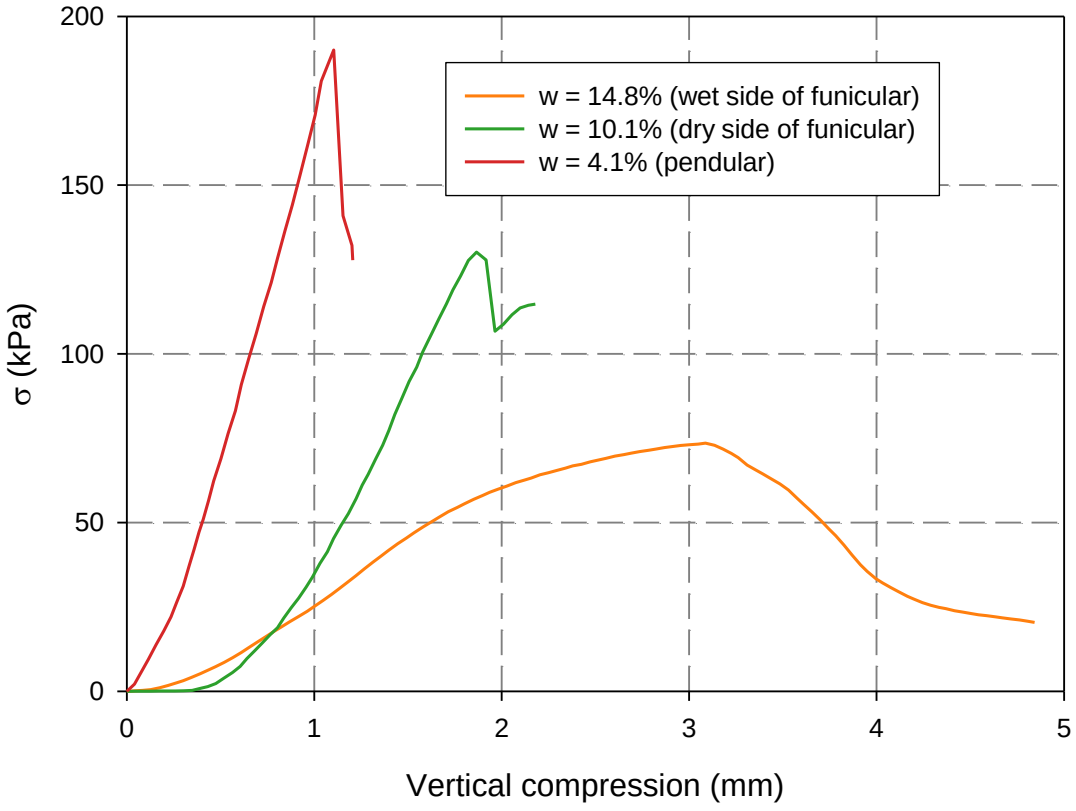

Figure 4-12: Stress vs compression relationship for iron tailings across different saturation regimes

The changes in behaviour observed for iron tailings are more clearly defined in Figure 4-12. At high degrees of saturation, samples tended to respond in a ductile manner, rising at a shallow gradient and reaching a peak load at a relatively high vertical compression. As the material was dried out, stress-compression curves rose at noticeably steeper gradients and achieved maximum stresses at lower magnitudes of compression. Similar to what was observed for gold tailings, the ductile response of wettest sample presented in Figure 4-12 contains an inflection point occurring before the peak load. Furthermore, it was noted that the two drier samples displayed a relatively linear stress-compression relationship up until the peak stress was reached.

The relationships observed in the above results were investigated further by performing strain analyses as described in Section 3.2.2. The results of this investigation are provided in the following section.

4.2.1 Tensile strain development

The transition from ductile to brittle behaviour revealed by the tensile stress vs compression curves was echoed by the results of the strain analyses. For the same samples presented in the preceding section, Figure 4-13 illustrates the development of tensile (horizontal) strain at the centre of the sample for the three regimes.

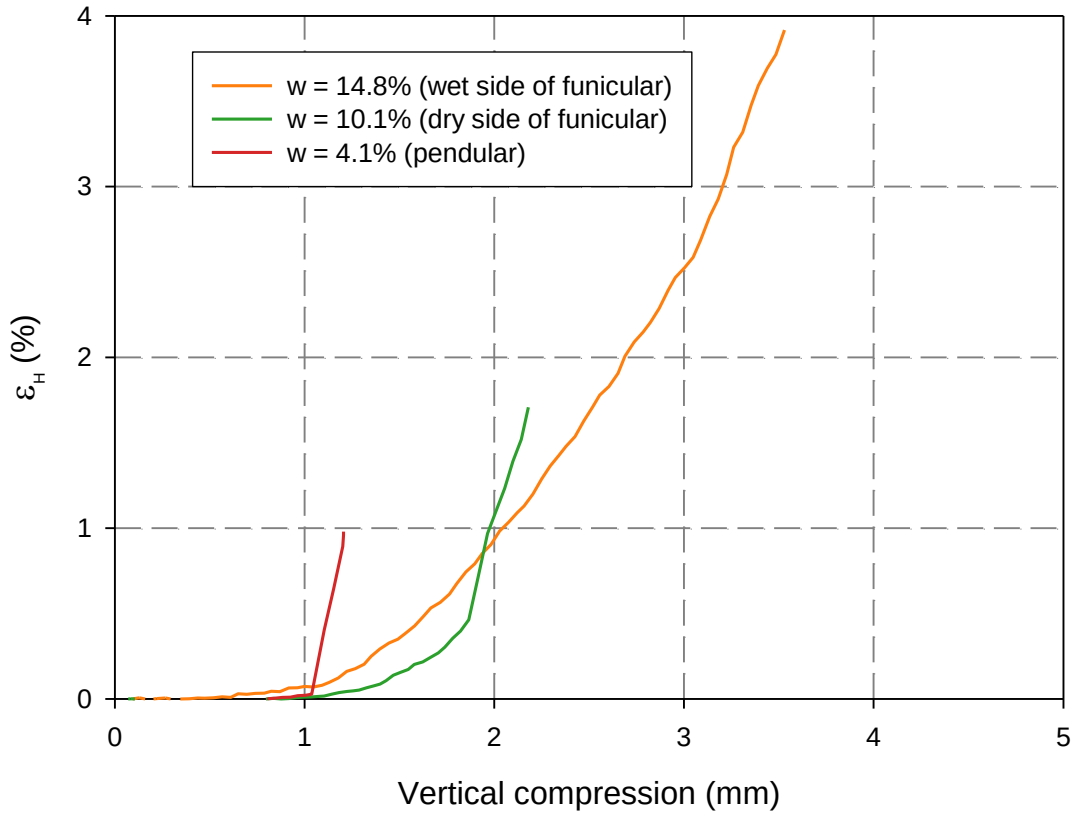

Figure 4-13: Tensile strain development for iron tailings across different saturation regimes

Similar to the observed stress vs compression trends, the computed strain results illustrated a transition from ductile to brittle behaviour with a reducing degree of saturation. Furthermore, in addition to the stage at which tensile strain begins to increase (defined previously as the point of first yield), one discernible characteristic of the strain results is that a sharp increase in gradient became progressively more distinct as moisture content was reduced.

To illustrate the relationships between tensile stress and strain behaviour, the results for the wettest and driest samples presented in Figure 4-12 and Figure 4-13 are combined. Figure 4-14 and Figure 4-15 illustrate the tensile stress and strain vs vertical compression results for the two tests, with horizontal tensile strain plotted on a secondary vertical axis. Furthermore, a strain

contour plot of the sample at the stage where maximum load is reached is included to qualitatively illustrate the position at which cracking initiated. Finally, to highlight the difference in the soil's ability to deform under loading, plots containing strain along the samples' diameter are provided in Figure 4-16.

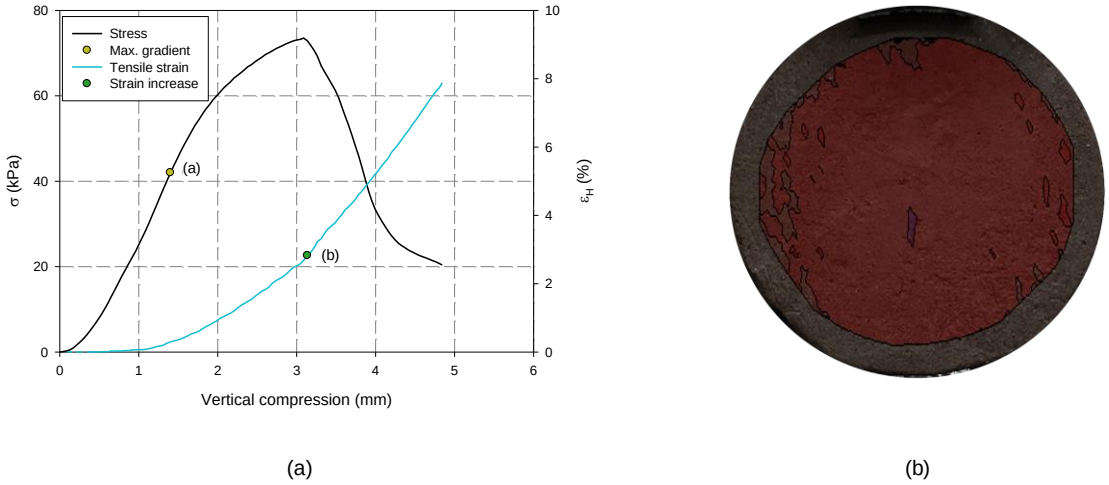

Figure 4-14: a) Stress vs compression results and b) contour plots of horizontal tensile strain for a sample at w = 14.8%

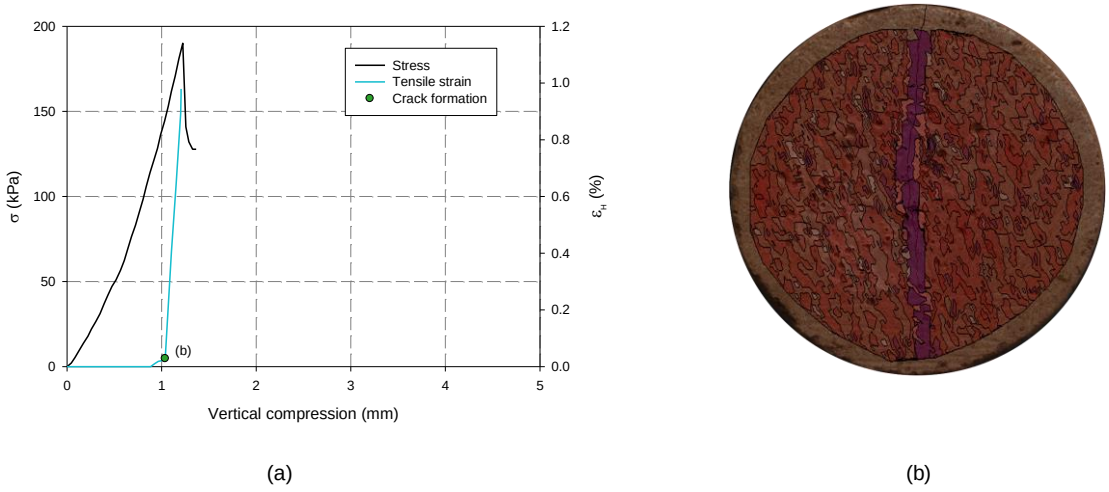

Figure 4-15: a) Stress vs compression results and b) contour plots of horizontal tensile strain for a sample at w = 4.1%

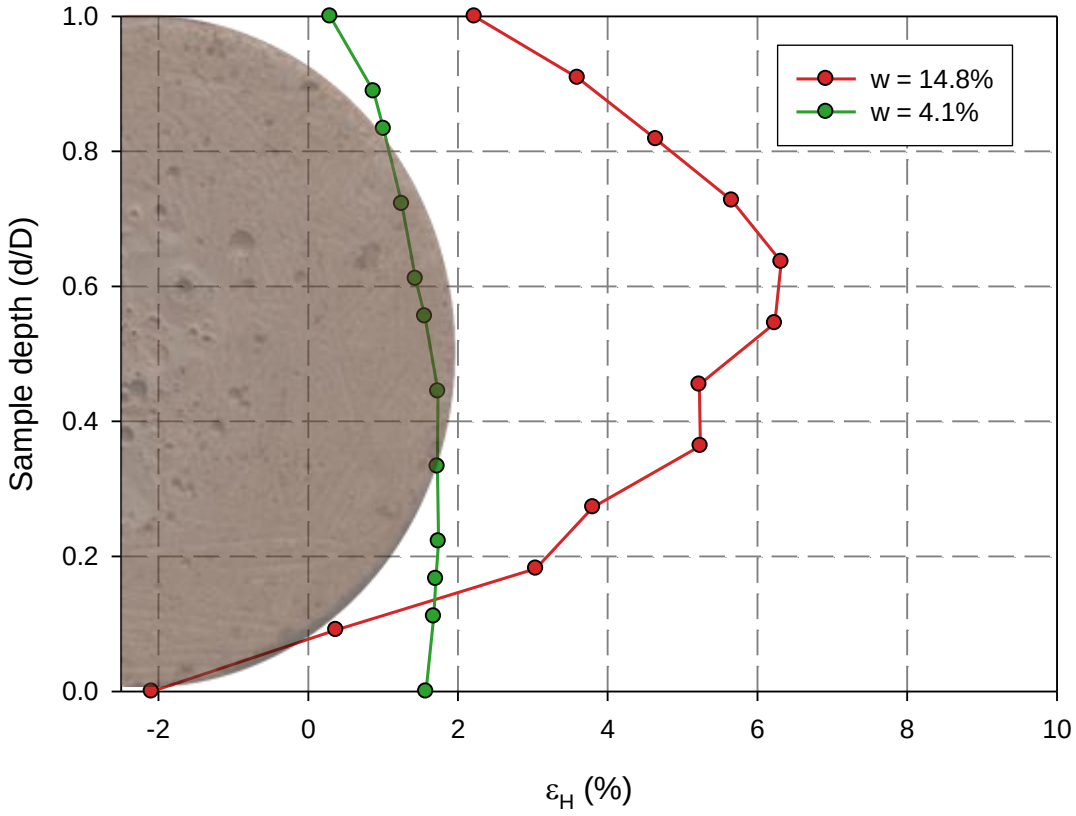

Figure 4-16: Horizontal tensile strain across loaded axis for samples prepared at w = 14.8% and w = 4.1%

The results in Figure 4-14 display a behaviour similar to those of the wetter samples for gold tailings. The stress-compression curve for this sample illustrated a point of inflection (stress at first yield) at Point 1. This stress corresponded closely with the point at which tensile strain began to increase. As described previously, the stress at first yield can satisfactorily provide a conservative estimate of the materials' tensile strength. Similarly, the drier sample presented in Figure 4-15 illustrated a linear stress-compression relationship up until the maximum stress was achieved, at which point a sharp increase in tensile strain was observed (Point b). However, due to the higher tensile strength of the iron tailings at low moisture contents, repeatable results could still be obtained in the drier regimes despite the brittle response of the material. The ability to repeatably measure the tensile strength of brittle iron tailings allowed for a less conservative point of failure to be defined.

The contour plots presented in Figure 4-14 and Figure 4-15 b) qualitatively illustrate the position at which cracking initiated. A comparison of the contour plots for the two samples provide an indication as to the ductility and brittleness of the sample at w = 14.8% and w = 4.1% respectively. At a high moisture content, cracking began in the centre of the sample and propagated outwards, accompanied by a gradual reduction in load. Conversely, for the sample

at w = 4.1%, a crack occurred almost instantaneously across its entire diameter. The distribution of tensile strain along the loaded axis of the samples presented in Figure 4-16 highlights the loss of ductility associated with a reduction in moisture content. From the results presented thus far it can be seen that, for samples in the same regime, the qualitative response of both the gold or iron tailings are similar and can therefore be treated in the same way.

4.2.2 Relationship between tensile strength and moisture content

This section presents the relationship between tensile strength and gravimetric moisture content. An SWRC as determined by Chapman (2016) has also been included to illustrate the variation in matric suction across varying degrees of saturation. Figure 4-17 illustrates the results for both sets of data.

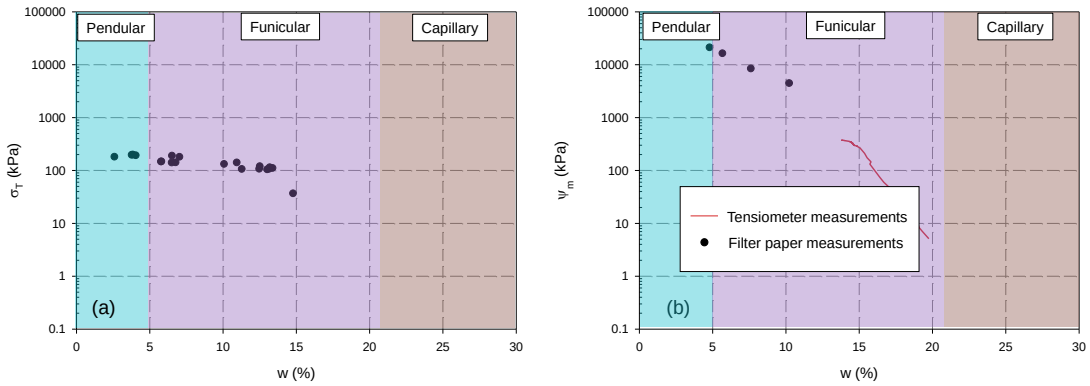

Figure 4-17: a) Relationship between moisture content and tensile strength and b) the SWRC for iron tailings (Chapman, 2016)

From Figure 4-17 b) it is seen that in contrast to what was observed for gold tailings, there is a relatively steep increase in matric suction with decreasing moisture content. This trend is expected due to the wider particle size distribution (and thus pore size distribution) of the iron tailings. Due to the logarithmic scale, the change in tensile strength with reducing moisture content is not clearly visible in Figure 4-17 a). To more closely investigate the relationship, and to illustrate the consistency of the tensile strength results, Figure 4-17 has also been presented on a linear scale in Figure 4-18.

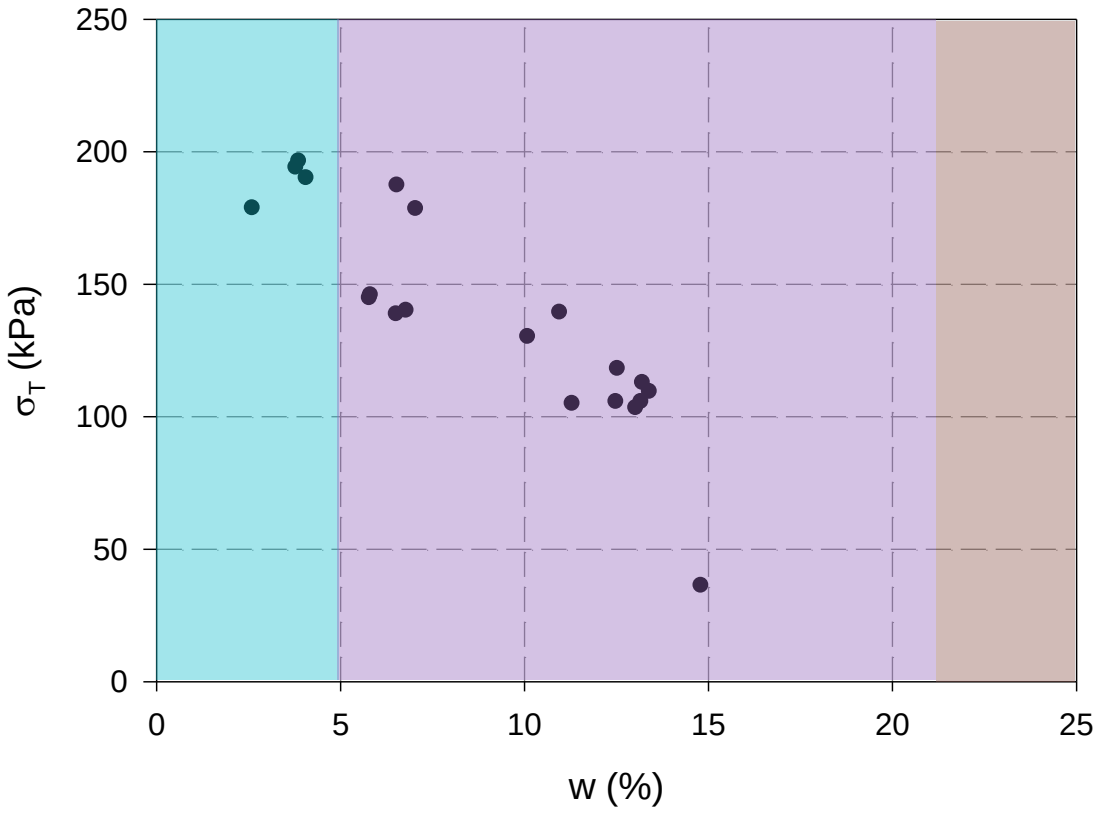

Figure 4-18: Tensile strength vs moisture content (linear scale) for iron tailings

Figure 4-18 illustrates a strong linear correlation (90%) between tensile strength and gravimetric moisture content. As in the case of gold tailings, there are qualitative similarities between the change in tensile strength with moisture content and the SWRC of iron tailings (i.e. both strength and suction increase with a reduction in moisture content). It is however important to note that for a given increase in matric suction, the corresponding increase in tensile strength is not proportional. This is due to the fact that, as was discussed in Section 2.1.4, the contribution of matric suction to the overall strength of the soil diminishes as the degree of saturation is reduced. The results presented in Figure 4-18 illustrate how, for a relatively stronger (finer grained) material, the BDT is capable of producing repeatable results across a wide range of moisture contents (provided a suitable test arrangement is used).

4.3 CENTURION SOIL

The final material tested was a transported soil from Centurion, south of Pretoria. According to the PSDs provided in Figure 3-2, this material contained the smallest clay sized fraction of the soils tested. However, as was revealed by the XRD results in Figure 3-3, such a classification is misleading as the Centurion soil contained 37% kaolinite. Due to the presence of such a high clay content, the Centurion soil was able to develop substantially higher matric suctions than the other materials tested.

As was described for iron tailings, complications were experienced at high moisture contents due to the compressive to tensile strength ratio of the specimen. For the test setup used, these samples underwent excessive compressive deformation (with no cracking occurring at the sample centre), ultimately leading to a 'punching' type failure rather than tensile splitting. In spite of this difficulty, the wettest sample successfully tested was at a gravimetric moisture content of 34% (S_r = 92.6%). Being so close to full saturation, it was decided that a test at this moisture content adequately gave an indication of the behaviour of the Centurion soil in the capillary regime.

Due to the wider pore size distribution of this soil, there was a larger variation in matric suction across the moisture contents considered. For this reason, a greater change in behaviour was observed with variation in moisture content. Figure 4-19 presents the stress vs compression results for five samples tested.

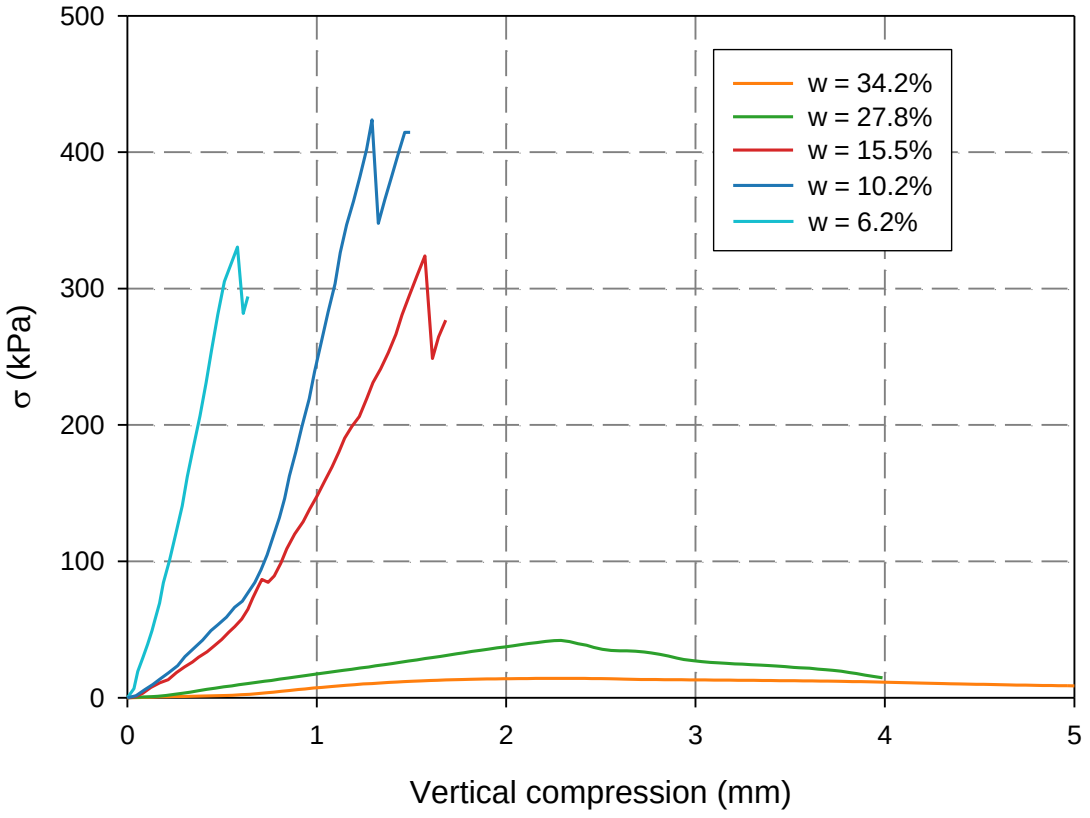

Figure 4-19: Stress vs compression relationship for Centurion soil across different saturation regimes

From Figure 4-19 it is seen that similar to the iron tailings, the Centurion soil illustrated a reduction in ductility with a decrease in moisture content. However, while the tensile strength of the iron tailings tended to increase steadily as it was dried out, the results in Figure 4-19 show that for the Centurion soil, tensile strength began to reduce again at low moisture contents. This decline in tensile strength in the pendular regime is one which has been noted previously by several authors (Vesga & Vallejo, 2006; Kim & Sture 2008; Kim & Hwang, 2003). To further investigate the reduction in ductility with moisture content, the strain analyses performed for the Centurion soil are provided in the following section.

4.3.1 Tensile strain development

As observed for iron tailings, the strain results correlated well with stress vs compression data, showing a distinct reduction in ductility with decreasing moisture content. For the same samples presented in Figure 4-19, Figure 4-20 illustrates the development of tensile strain.

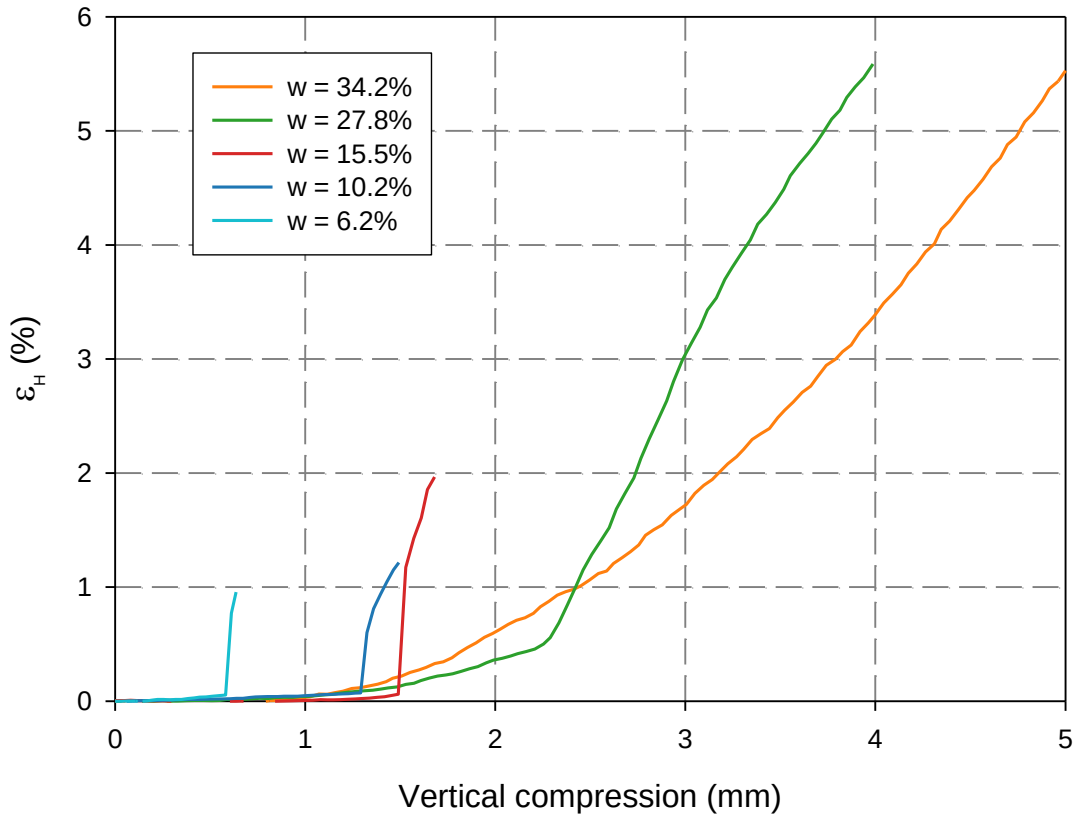

Figure 4-20: Tensile strain development for Centurion soil across varying moisture contents

The strain results presented above illustrate that at lower moisture contents the Centurion soil also displayed two distinct characteristics in the tensile strain vs compression curve. Firstly, there is a point at which horizontal tensile strain across the centre of the sample began to deviate from zero. At a later stage of each test, a sharp increase in the gradient of the curve was observed. Conversely, for the wettest sample tested, the only distinct change in behaviour was the point at which horizontal tensile strain deviated from zero. This finding correlates with tests performed on both gold and iron tailings at high degrees of saturation. Since testing could be successfully performed over such a wide range of moisture contents, the response under loading of the wettest and driest samples varied dramatically.

To illustrate this behaviour, tensile stress and strain vs compression results are combined and presented in Figure 4-21 and Figure 4-22 for moisture contents of 34.2% and 6.2% respectively. As was done for gold tailings, the results include three sub-figures to highlight different aspects of the material behaviour at three stages of the test. Similar to both soils presented thus far, a difference in material behaviour related to its ductility is observed at higher degrees of saturation. As a result, the three stages presented in Figure 4-21 and Figure 4-22 were chosen

to represent different aspects of each test. The justification for choosing each of the three stages has therefore been discussed separately.

Sub-figure a) contains the stress vs compression results together with tensile strain development plotted on a secondary vertical axis. The tensile strain distribution across the diameter of the sample for the three stages is provided in sub-plot b) and finally, contour plots of tensile strain are illustrated in sub-figure c).

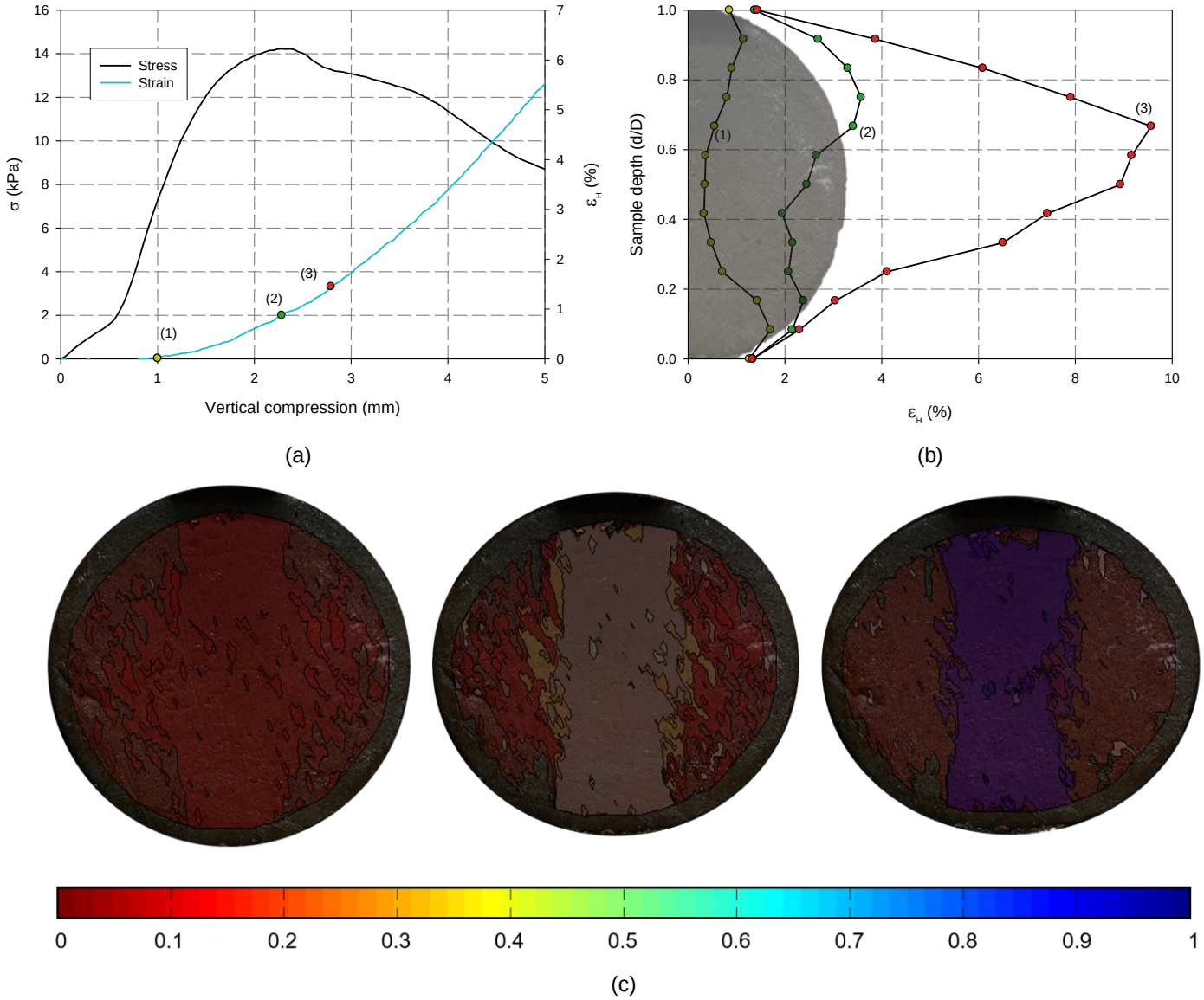

Figure 4-21: Strain analysis for sample at w = 34.2%

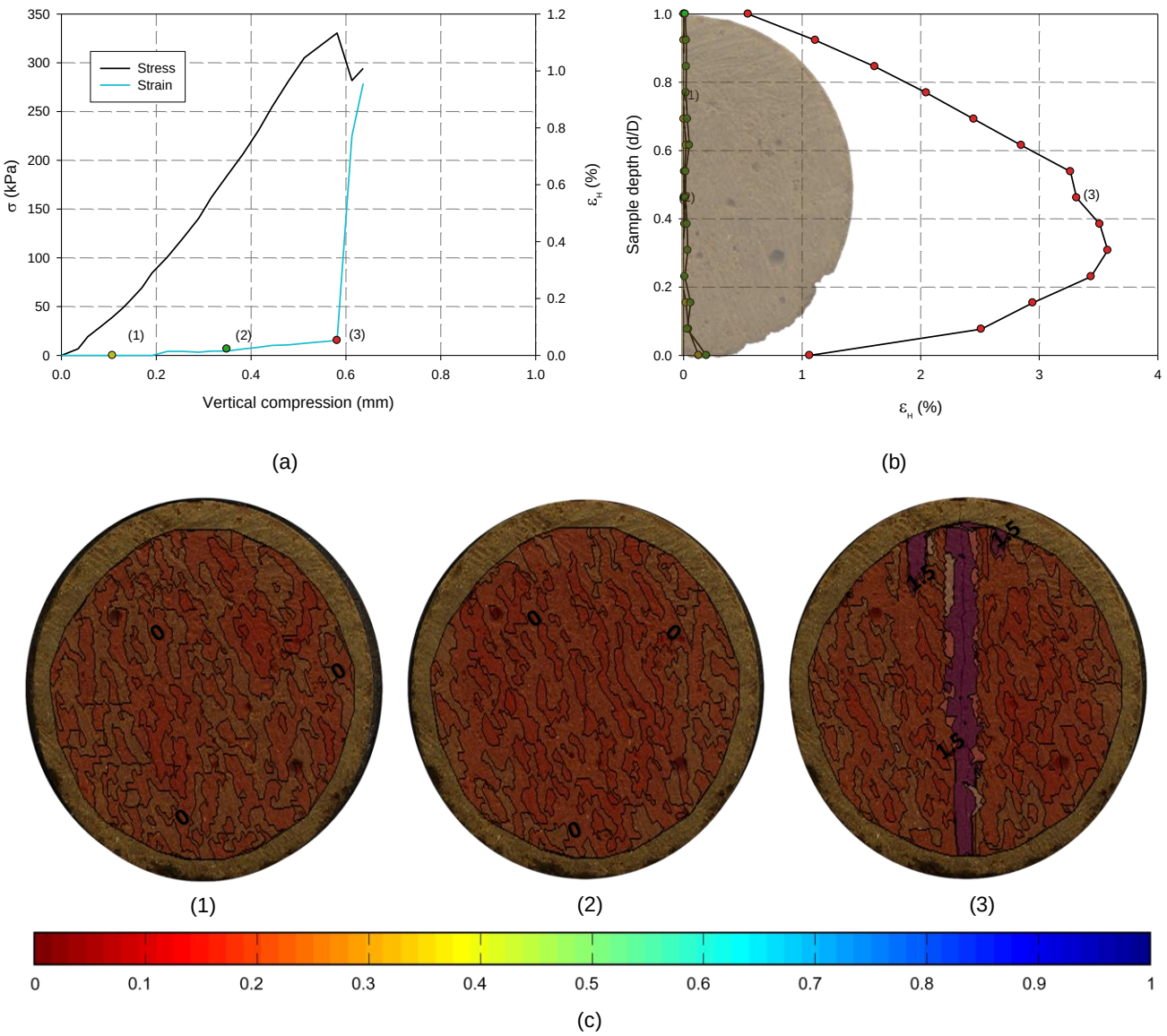

Figure 4-22: Strain analysis for sample at w = 6.2%

For the sample tested at w = 34.2% (Figure 4-21), Point 1 represents the point at which horizontal tensile strain across the centre of the sample began to increase. Point 2 is the stage at which maximum curvature is reached in the tensile strain vs compression curve. This point correlates with the stage of the test at which the maximum load is achieved. Point 3 illustrates the instant at which surface cracking became visible.

A problem which was encountered during sample preparation for the Centurion soil was that of shrinkage. Due to the presence of such a high clay fraction, when samples were dried out from a slurry to the desired moisture content, a significant decrease in volume was observed. This reduction in sample diameter affected the initial strain development within the specimens. For the results presented in Figure 4-21, the radius of the sample at the start of testing was 23.3 mm (3.7 mm less than the radius of the loading strips). For this reason, as the sample was loaded, horizontal tensile strain developed first at the ends of the sample (close to the loading strips). At the point where the sample radius along its vertical axis became equal to the loading strip, tensile strain began to equalise along the diameter of the specimen and eventually resulted in a maximum strain occurring close to the centre of the sample. This trend in strain development is observed in Figure 4-21.

Point 3 in Figure 4-21 illustrates how cracking initiated in the centre of the sample and slowly propagated out towards the loading strips. The growth of the crack in the vertical direction was accompanied by a gradual decrease in load. All of the above-mentioned observations give an indication as to the amount of ductility present in the Centurion soil at high moisture contents.

For the sample tested at w = 6.2%, the results presented in Figure 4-22 show a distinctly different response. The first point presented in Figure 4-22 was chosen to be representative of a relatively unstrained state of the sample. Point 3 highlights a sharp increase in the gradient of the strain vs compression curve, which correlates with both the maximum stress and the instance at which surface cracking became visible. From these results, it can be seen that almost zero strain had occurred between Point 1 and an intermediate stage of the test at Point 2. However, at the maximum achieved load (Point 3), cracking occurred almost instantaneously across the entire diameter of the sample, resulting in a sudden drop in load thereafter.

The trend in material behaviour with a variation in moisture content was seen to be similar to that observed for the previous soils presented. Close to saturation, a sample subjected to diametric loading will experience an increase in tensile stress at an increasing rate, until a point of inflection is reached (previously referred to as the stress at first yield). Following the stress at first yield, the rate at which the sample is able to carry load begins to diminish until a surface crack becomes visible. For these reasons, the tensile strength for samples of Centurion soil

tested at high degrees of saturation was conservatively defined as being equal to the stress at first yield.

4.3.2 Relationship between tensile strength and moisture content

The following section presents the results of tensile strength vs moisture content for the Centurion soil. Similar to the results presented for the previous two materials, an SWRC is provided to give an indication of the variation in matric suction with moisture content. Figure 4-23 illustrates these results.

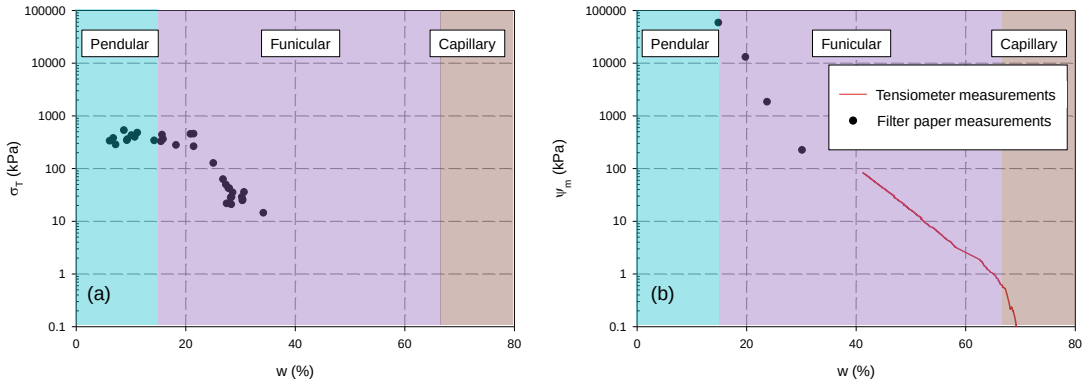

Figure 4-23: a) Relationship between moisture content and tensile strength and b) the SWRC for the Centurion soil

The wider pore size distribution in the coarser fraction of the Centurion soil allowed for a more significant increase in matric suction following the air-entry point. This characteristic allowed for tensile strengths to be measured very close to saturation. The strength vs moisture content plot in Figure 4-23 a) shows an increase in tensile strength, somewhat proportional to the increase in suction in most of the funicular regime. This increase continues until approximately w = 22%, after which the contribution of matric suction to tensile strength begins to diminish and the curve reaches a plateau. To further investigate the repeatability of tensile strength results, Figure 4-23 a) is presented on a linear scale in Figure 4-24.

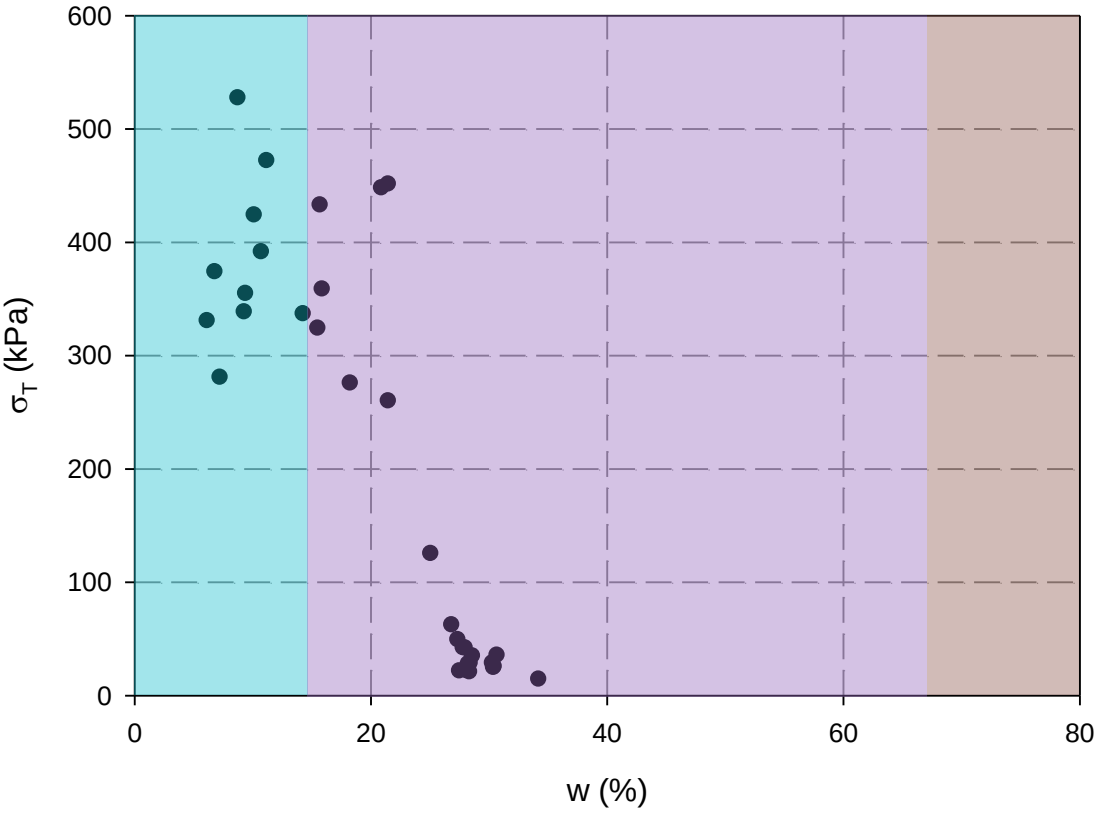

Figure 4-24: Tensile strength vs moisture content (linear scale) for Centurion soil

In Figure 4-24 it is seen that tensile strength increases as moisture content is reduced up until approximately w = 8%, after which a reduction in strength is observed. It was however seen that with a reduction in moisture content, the recorded strengths became more scattered. The increased variability in this region is related to the shrinkage associated with the high clay content of this material. As discussed in Section 3.3.1, samples were prepared by drying out the material from a slurry to the desired moisture content in a mould, which facilitated single drainage from the top of the sample. The consequence of this preparation technique for a material prone to shrinkage is that the sample diameter reduced unevenly along its height. Figure 4-25 presents a cross-sectional view of the sample and mould at the beginning and end of the preparation procedure. From this figure, an exaggerated consequence of this preparation technique is shown.

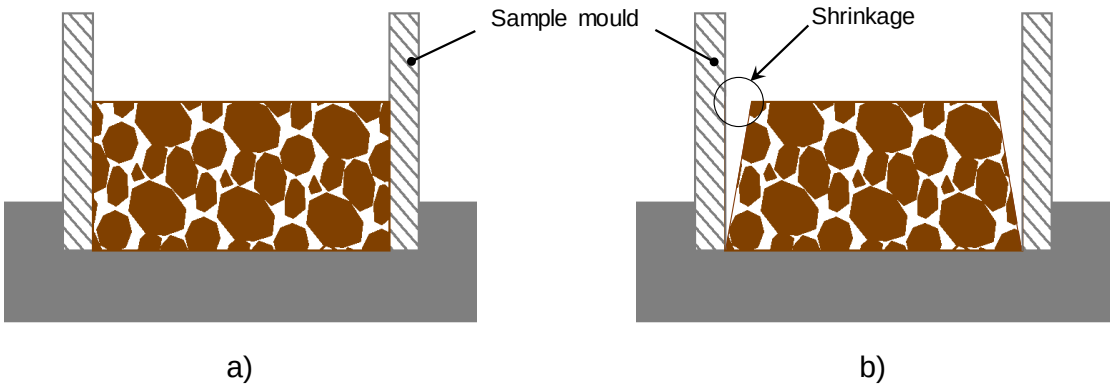

Figure 4-25: a) Cross-sectional view of initial sample geometry in slurry state and b) after uneven shrinkage

The irregular geometry shown in Figure 4-25 b) therefore needed to be corrected by trimming each sample individually to achieve a regular disc-shaped specimen. At high strengths, this process becomes increasingly difficult to perform accurately and as a result, the drier samples presented in this section did not have a perfectly constant diameter across their height. In spite of this variability, it can be seen that tensile strengths could be measured (with a certain degree of consistency) across a wide range of moisture contents. Furthermore, an aspect that is highlighted from the abovementioned results, is that the presence of a high clay content can significantly increase the tensile strength of unsaturated soils. In comparison to the tensile strengths observed for iron tailings, which did not exceed 200 kPa, the tensile strength of the Centurion soil comfortably exceeded this value at lower moisture contents. Furthermore, for the Centurion soil, tensile strength began to decrease at moisture contents less than 10%, while the iron tailings continued to increase in strength for the entire range considered.

4.4 DISCUSSION

The following section presents a general discussion on the behaviour of the three materials tested. The section begins with a discussion on the validity of Equation 2.9 for all soils, across the range of moisture contents considered. Furthermore, an approach to the investigation of the failure mechanisms for BDT results conducted on unsaturated soils is proposed. An explanation as to the decrease in tensile strength with decreasing moisture content observed for the Centurion soil is then provided. Finally, the section is concluded with a general discussion on the implications of the indirect measurement of unsaturated soil properties.

4.4.1 Validity of elastic solution for imposed tensile stress

As described previously, conventional interpretation of the Brazilian Disc Test uses the maximum achieved load to calculate the indirect tensile strength of a material. To do so, the elastic solution given by Equation 2.9 is used. From the results obtained in this study, it was however found that the measured load may not be indicative of the mobilisation of tensile strength for the entire duration of the test.

For all three materials, it was seen that at high values of saturation, samples tended to respond in a ductile manner. A common characteristic that was observed for these samples is that the measured load increased up until a point of inflection was reached. Following this point, the rate at which the sample was able to carry load began to diminish until a surface crack became visible. Prior to the inflection point, referred to as the stress at first tensile yield, the stress-compression curve displayed an approximately linear relationship. It can therefore be stated that for this portion of the test, Equation 2.9 is valid. At this stress, tensile yielding of the sample is initiated as micro cracks begin to grow. This process continues up until a surface crack becomes visible. The increased deviation from linearity following the stress at first yield suggests that the use of the elastic solution becomes increasingly less valid as the soil separates along the sample centreline. At this stage, the conditions of strain compatibility are no longer met and it can therefore be stated that the elastic solution is not valid. For these ductile responses, it was found that the stress at first yield could be repeatably calculated and used to provide a conservative estimate of the soils' tensile strength. Figure 4-26 provides a flow diagram describing the above-mentioned response for ductile materials.

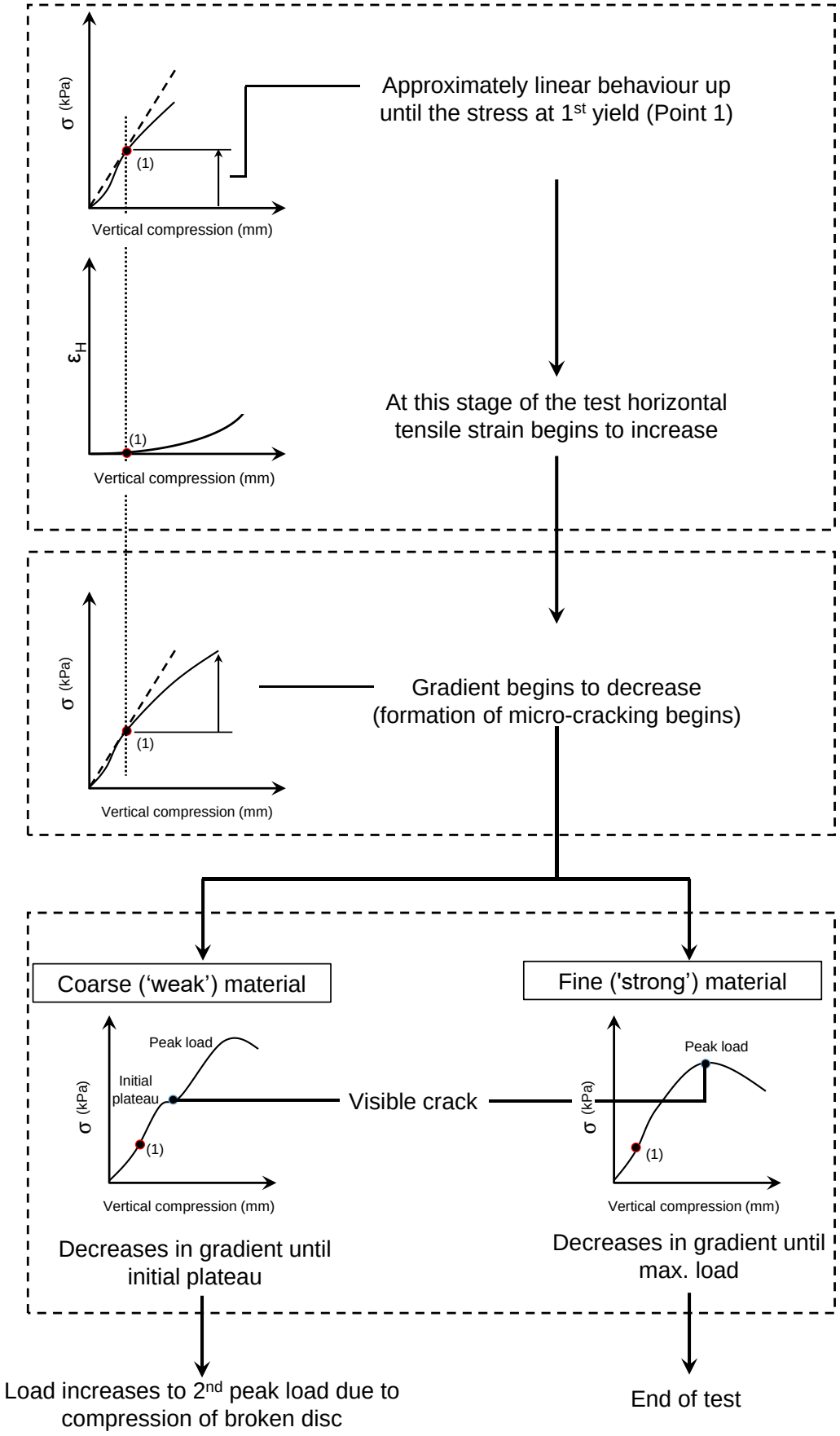

Figure 4-26: Flow diagram illustrating the behaviour of ductile materials subjected to BDTs

Conversely, for brittle materials, it was found that conventional interpretation of the BDT is adequate as the observed behaviour remains approximately linear until the peak load is reached. Simultaneously, at this instant, a sharp increase in horizontal tensile strain is observed and a surface crack becomes visible.

4.4.2 Failure mechanism

Perhaps the most repeatedly emphasised condition for a successful BDT is that cracking should initiate at the centre of the disc. The rationale for this condition is based on the fact that according to the Griffith failure criterion, this is the unique point at which the conditions for tensile failure at a value equal to the uniaxial tensile strength of a specimen are met (Li & Wong, 2013). For materials such as concrete and rock, this condition can easily be verified through the measurements of surface displacements. However, the results presented for gold tailings in the pendular regime indicated that for extremely weak and brittle materials, initial displacements (not representative of sample failure) can initiate close to the loading strips. Such displacements are representative of pieces of material breaking off from the front face of the disc. It was found that such surface displacements are due to the samples' sensitivity to stress concentrations at the points of load application.

Due to the above-mentioned results, it is proposed that for a BDT performed on unsaturated soils, validation of the failure mechanism as occurring due to tensile splitting should be investigated as described below.

- If it is clearly seen that cracking initiates at the centre of the disc, the result can be classified as a tensile failure.
- If initial displacements are observed elsewhere, further investigation of the test data is required before the result can be accepted. In this regard, attention should be paid to tensile strain development along the sample centreline.

4.4.3 Decrease in tensile strength at low moisture contents

One phenomenon revealed by the results of the Centurion soil is the reduction in tensile strength at low moisture contents. This is a characteristic not seen for the other two materials tested. However, if the two components of inter-particle tensile strength (namely surface tension and matric suction) are revisited, this phenomenon can be explained. Consider Figure 4-27 which illustrates the idealised case of two spherical particles bonded by a single liquid bridge.

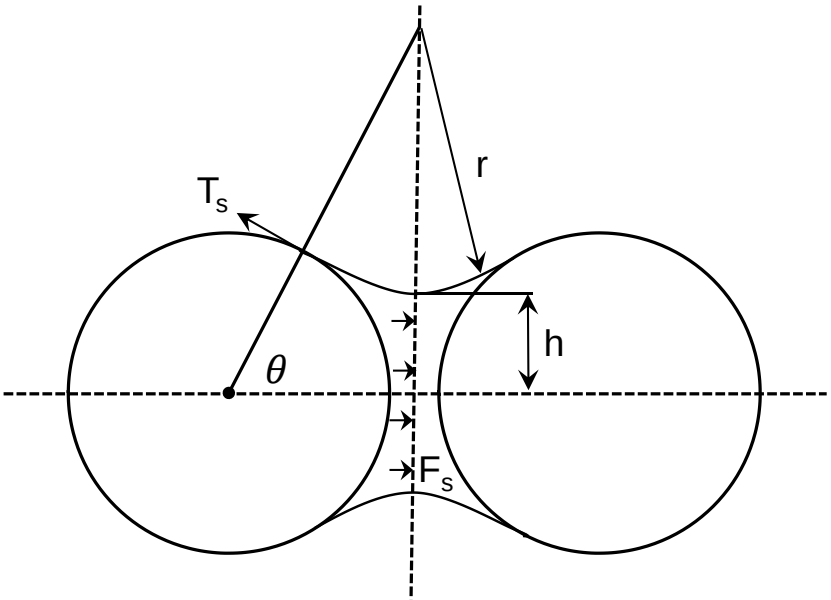

r = Meniscus radius of curvature

θ = Filling angle

h = Height of liquid bridge

F_s = Force due to suction

T_s = Surface tension

Figure 4-27: Interparticle forces acting between two spherical particles (adapted from Kim & Sture (2008))

The contribution of tensile strength, provided by surface tension (T_s) in the pendular regime, is one which increases with moisture content. This is due to the fact that, upon wetting, the length of the contact line between water and solid increases. However, the contribution of matric suction (ψ_m) tends to increase for small filling angles, achieve a maximum value and then decrease with further wetting. This trend was explained by Kim & Sture (2008) as being attributed to the rate at which the two dimensions, *r* and *h* in Figure 4-27, increase with moisture content. As described in Section 2.1.2, the radius of curvature of the meniscus in a liquid bridge is inversely proportional to the magnitude of suction. The dimension *h* in Figure 4-27 is merely indicative of the volume of the liquid bridge.

For low filling angles, Kim & Sture (2008) described how the radius of curvature of the liquid bridge *r* is initially smaller than the dimension *h*. This corresponds to a high magnitude of suction at a very low moisture content. As moisture content is increased, the value of *h* increases at a faster rate than the radius of curvature. This corresponds to a relatively unchanged value of suction acting over a larger area. Since the attractive force between two particles due to suction is the product of ψ_m and the area over which it acts, the interparticle force tends to increase.

However, with continued wetting, *r* begins to increase more rapidly (corresponding to a reduction in suction) and as a result, the inter-particle attractive force due to suction begins to decrease. Figure 4-28 highlights the relative contributions of tensile strength due to surface tension and matric suction for varying filling angles (analogous to moisture content).

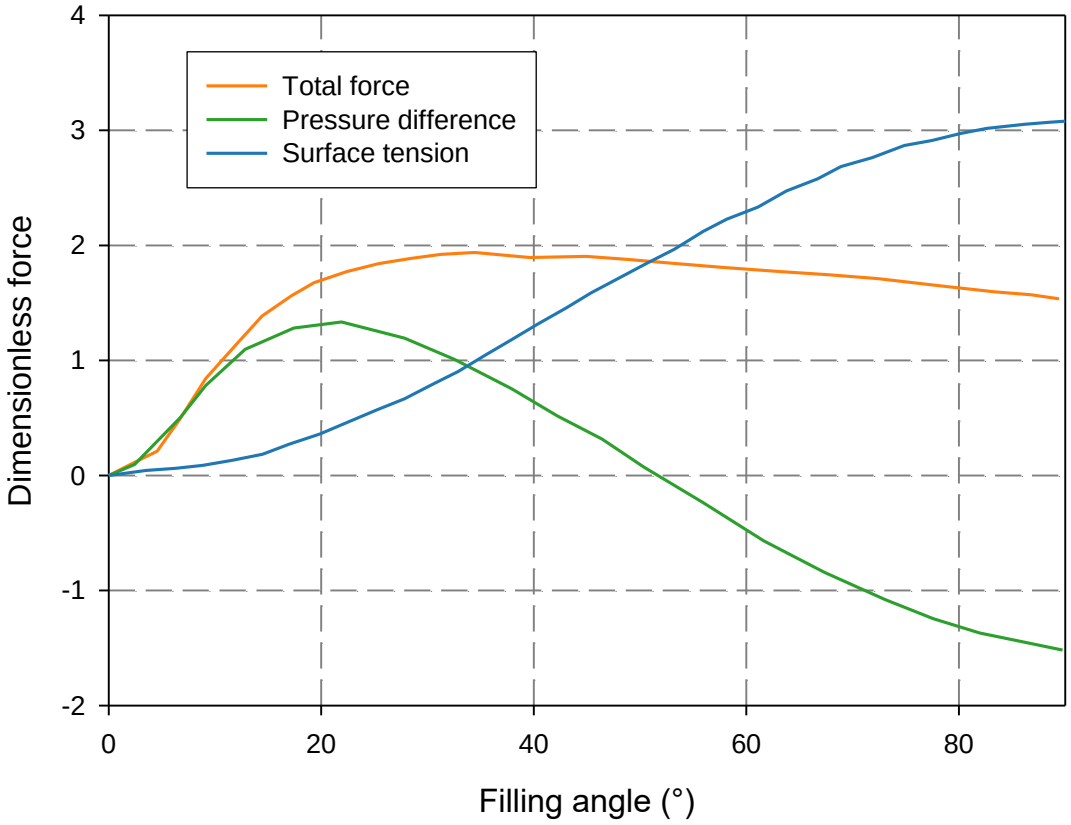

Figure 4-28: Contributions to interparticle tensile strength (adapted from Kim & Sture (2008))

From the above explanations, it is seen that the area over which T_s and ψ_m acts, is a critical parameter governing the tensile strength of an unsaturated soil in the pendular regime. For this reason, it can be stated that particle shape will indirectly have a significant effect on the tensile behaviour of a given soil at such low moisture contents. The difference in particle shape between the iron tailings and Centurion soil could thus explain the different trends observed at low degrees of saturation.

4.4.4 Implications for indirect determination of unsaturated soil properties

A complication in the field of unsaturated soil mechanics is that many important soil properties are difficult and expensive to measure directly. As a result, such soil properties are sometimes estimated through various indirect techniques or correlations.

A method commonly used to estimate hydraulic properties such as SWRCs involve the use of so-called pedotransfer functions. These functions make use of the more easily attainable soil grading properties to estimate unsaturated soil parameters, which are time consuming and difficult to measure. Furthermore, models have been proposed which harness the large amount of information contained in SWRCs to predict soil strength. While these techniques are certainly useful when applied correctly, they should be used cautiously, taking cognisance of any possible sources of error.

If for example, soil grading is estimated from a Particle Size Distribution curve (PSD), one should be aware of the fact that the clay sized fraction of some soils can be difficult to quantify (often due to improper dispersion) and, as a result, can often be underestimated (Stott *et al.*, 2006; Kaur & Fanourakis, 2016). As was observed in the current study, the presence of clay mineralogy can have a significant effect on both the magnitude of tensile strength and the relationship between tensile strength and moisture content. If an SWRC estimated from grading curves is then used to estimate strength properties, the inherent error associated with any empirical model is added to the final prediction. This results in an accumulation of error. Recognising the convenience of indirectly estimating soil properties, one should be aware, especially for the complex behaviour of unsaturated soils, of any sources of error that may influence the final predicted result.

5 CONCLUSIONS AND RECOMMENDATIONS

While engineering practice is largely based on the application of classical saturated soil mechanics, it has become increasingly recognised that such an approach can often be inappropriate. An effort therefore needs to be made to gain a fundamental understanding of unsaturated soil behaviour.

The research presented in this dissertation illustrates how an abundance of useful information can be gained from a relatively inexpensive and simple tensile testing procedure, namely the Brazilian Disc Test. The results of this study provide conclusions on both the implementation of this test to unsaturated soils and the behaviour of different unsaturated soils under tension. This chapter highlights the main conclusions reached in this study and presents recommendations for future research.

5.1 CONCLUSIONS

This section presents the conclusions reached in this dissertation, subdivided to individually address the objectives outlined in Section 1.2. For ease of explanation, some of the sub-sections provide conclusions to more than one of the individual objectives.

5.1.1 The applicability of the Brazilian Disc Test to different unsaturated soils

While the Brazilian Disc Test (BDT) was found to be useful across a range of moisture contents, difficulties were encountered in the capillary regime. For gold tailings (the coarsest material tested), this is due to the relatively low values of matric suction present at high moisture contents. As a result of the low values of suction, samples of gold tailings prepared in the capillary regime collapsed under their own weight.

For the finer grained materials, the upper limit of saturation that could be tested was governed by the compression to tensile strength ratio of the material. Despite being able to prepare stable samples of both iron tailings and Centurion soil in the capillary regime, upon loading these samples underwent excessive deformation (‘barrelling’) without fracture occurring. This ‘barrelling’ response continued up until the loading strips began punching into the soil.

With the exception of the cases mentioned in the above discussion, the use of 30° curved loading strips was shown to consistently produce a centrally located crack for all materials tested, across the range of moisture contents considered. In addition to the experimental results observed, it was analytically shown how the use of curved loading strips substantially reduces compressive stress concentrations close to the points of load application. With an increase in

the contact angle 2α, the magnitude of these compressive stress concentrations was shown to decrease substantially. This finding illustrates that through the use of the appropriate curved loading strips, the tensile strength of a sample can be mobilised at its centre, without premature crushing occurring close to the points of load application.

Strain distributions across the loaded diameter of the sample approximated the theoretical stress distributions of Hondros (1959). This provides an indication that the elastic solutions conventionally used in the interpretation of the BDT are adequate for the initial portion of the test.

While the test was shown to be useful for all soils considered across a range of saturation regimes, it was found that the response of a material can become complex at higher degrees of saturation, particularly for coarse ('weak') materials. It is therefore suggested that the use of significantly sophisticated measurement techniques such as DIC be used to determine:

- The position at which cracking initiates and
- The development of strain across the sample upon loading

5.1.2 Materials' response to loading:

The primary behavioural change observed for all materials tested is that, at higher moisture contents, samples tended to behave in a ductile manner. A progressive loss in ductility (more clearly defined for finer materials) was observed as moisture content was reduced.

The transition from ductile to brittle responses was found to have significant implications on the interpretation of test results. While conventional interpretation of the BDT was found to be adequate for brittle materials, at higher moisture contents samples tended to illustrate a more complex behaviour. For ductile materials, it was found that blindly adopting the maximum achieved load to calculate tensile strength can often result in a gross overestimation. It is therefore proposed that the initial inflection point in the stress-compression curve, i.e. the stress at first yield be used to provide a conservative estimate of a ductile samples' tensile strength.

Prior to the stress at first yield, the stress vs compression curve illustrates an approximately linear behaviour, illustrating that the elastic solution commonly used for interpretation of BDTs is valid up until this point. Following the stress at first yield, micro cracking begins and continues up until a surface crack is visible. This process is accompanied by a progressive reduction in the gradient of the stress vs compression curve. This increased deviation from linearity illustrates how the use of the elastic solution becomes increasingly less valid up until

the soil separates at its centre, after which point the condition of strain compatibility is no longer met and the solution becomes invalid.

5.1.3 Relationship between tensile strength, matric suction and moisture content

For gold and iron tailings, the relationship between tensile strength and moisture content was found to be qualitatively similar to each material's respective SWRC. However, in the pendular regime it was observed that matric suction provided a diminishing contribution to the measured tensile strengths (i.e. for a given increase in matric suction, the corresponding increase in strength was not proportional).

For the Centurion soil, tensile strength was seen to increase with a reduction in moisture content up until approximately w = 8%, after which point a reduction in strength was observed.

5.2 RECOMMENDATIONS

Recommendations for future work include the following:

- Considering the effect of arc-length on the position of crack initiation in a BDT, it is recommended that the use of flat loading strips be abandoned, irrespective of the material being tested. This is due to the high compressive stress concentrations occurring close to the points of load application associated with the use of flat platens Instead, the relationship between arc-length and compression to tensile strength ratio (theoretically illustrated in Figure 3-5) should be investigated experimentally. Verification of the proposed criterion would allow for the calculation of the arc-length required to obtain meaningful results from a BDT for a range of material types.
- The measurement of matric suction should be incorporated for BDTs conducted on unsaturated soils to investigate how matric suction changes with load application.
- With particular reference to unsaturated soils, the effect of specimen size on measured tensile strength as well as on the repeatability of the BDT should be thoroughly investigated. Recognising that the tensile strength of unsaturated soils is relatively low in comparison to materials on which BDTs are commonly performed (e.g. concrete and rock), the measured tensile strength of an unsaturated soil specimen would be more susceptible to sample defects. It is therefore hypothesised that with an increase in sample size, the tendency towards more sample defects would result in lower (and more scattered) results of measured tensile strength.
- Regarding the sample preparation procedure, a technique should be developed to facilitate double drainage of the specimen as it is dried out to a specific moisture

content. This would allow for materials prone to shrinkage to do so evenly across their entire length, thereby increasing the repeatability of the test at lower degrees of saturation.

- The effect of particle shape on the relationship between tensile strength and matric suction at low moisture contents should be investigated.

LIST OF REFERENCES

Aitchison, G.D. 1961. Relationship of Moisture Stress and Effective Stress Functions in Unsaturated Soils. *Pore Pressure and Suction in Soils*. London: Butterworths, pp. 47–52.

Akazawa, T. 1943. New test method for evaluating internal stresses due to compression of concrete: the splitting tension test. *Journal of Japan Society of Civil Engineers*, 29, pp.777–787.

Atkinson, J.H. & Bransby, P.L. 1978. *The mechanics of soils. An introduction to critical state soils mechanics.*

Barbour, S.L. & Fredlund, D.G. 1989. Mechanisms of osmotic flow and volume change in clay soils. *Canadian Geotechnical Journal*, 26(4), pp.551–562.

Beckett, C.T.S., Smith, J.C., Ciancio, D., Augarde, C.E. 2015. Tensile strengths of flocculated compacted unsaturated soils. *Géotechnique Letters*, 5(4), pp.254–260.

Bishop, A.W. 1959. The principle of effective stress. *Teknisk Ukeblad*, pp.859–863.

Blight, G.E. 1994. Keynote lecture: The geotechnical behaviour or arid and semi-arid zone soils Southern African experience. *Proceedings 1st international symposium on engineering behaviour of arid soils*. pp. 221–235.

Burland, J.B. 1965. Some Aspects of the Mechanical Behaviour of Partly Saturated Soils. *Moisture Equilibria and Moisture Changes in Soils Beneath Covered Areas: A Symposium in Print*. Ed. by G. D. Aitchison. London: Butterworths, pp. 270–278.

Carneiro, F. 1943. A new method to determine the tensile strength of concrete. *Proceedings of the 5th meeting of the Brazilian Association for Technical Rules ("Associação Brasileira de Normas Técnicas")*. pp. 126–129.

Chandler, R.J. & Gutierrez, C.I. 1986. The filter-paper method of suction measurement (Technical Note). *Géotechnique*, 36, pp.265–268.

Chapman, G. 2016. *Personal communication*

Clayton, C.R., Matthews, M.C. & Simons, N.E. 1995. *Site investigation.* 2nd ed. Oxford: Wiley-Blackwell.

Consoli, N. C., Caberlon Cruz, R., Consoli, B. S. & Maghous, S. 2012. Failure envelope of artificially cemented sand. *Géotechnique*, 62(6), pp.543–547.

Croney, D., Coleman, J.D. & Black, W.P. 1958. *The Movement and Distribution of Water in Soil in Relation to Highway Design and Performance - Special Report No. 40*, Washington, D.C.

Denneman, E., Kearsley, E.P. & Visser, A.T. 2011. Splitting tensile test for fibre reinforced concrete. *Materials and Structures*, 44(8), pp.1441–1449.

Dexter, A.R. & Kroesbergen, B. 1985. Methodology for determination of tensile strength of soil aggregates. *Journal of Agricultural Engineering Research*, 31(2), pp.139–147.

Erarslan, N., Liang, Z.Z. & Williams, D.J. 2012. Experimental and Numerical Studies on Determination of Indirect Tensile Strength of Rocks. *Rock Mechanics and Rock Engineering*, 45(5), pp.739–751.

Errera, L.A., 1977. *Stress paths and collapsing soils*. MSc Thesis. University of Cape Town.

Fairhurst, C. 1964. On the validity of the "Brazilian" test for brittle materials. *International Journal of Rock Mechanics and Mining Sciences & Geomechanics Abstracts*, 1(4).

Feda, J. 1994. Mechanisms of collapse of soil structure. *Genisis and Properties of Collapsible Soils*. Ed. by E. Derbyshire, T. Dijkstra, & I. J. Smalley. Loughborough: Kluwer Academic Publishers, pp. 149–172.

Fourie, A.B. 1996. Predicting rainfall-induced slope instability. *Proceedings of the Institution of Civil Engineers - Geotechnical Engineering*, 119(4), pp.211–218.

Fredlund, D.G. 2000. The 1999 R.M. Hardy Lecture: The implementation of unsaturated soil mechanics into geotechnical engineering. *Canadian Geotechnical Journal*, 37(5), pp.963–986.

Fredlund, D.G. & Morgenstern, N.R. 1977. Stress State Variables for Saturated and Unsaturated Soils. *Journal of Geotechnical Division*, 103(GT5), pp.447–466.

Fredlund, D.G. & Rahardjo, H. 1993. *Soil Mechanics for Unsaturated Soils*, John Wiley & Sons, Inc.

Fredlund, D.G., Rahardjo, H. & Gan, J.K.M. 1987. Non-linearity of strength envelope for unsaturated soils. *Proceedings, 6th International Conference of Expansive Soils*. New Delhi: Rotterdam: Balkema, pp. 49–54.

Gardner, R. 1937. A method of measuring the capillary tension of soil moisture over a wide moisture range. *Soil Science*, 43(4), pp.227–284.

Gaspar, T.A.V. & Jacobsz, S.W. 2016. Measuring the tensile strength of gold tailings. *Proceedings of the First Southern African Geotechnical Conference*. Ed. by S.W. Jacobsz. Pretoria, South Africa: CRC Press/Balkema, pp. 301–306.

Georgiadis, K. 2003. *Development, implementation and application of partially saturated soil models in finite element analysis*. University of London (Imperial College of Science, Technology and Medicine).

Goulding, R.B. 2006. *TENSILE STRENGTH, SHEAR STRENGTH, AND EFFECTIVE STRESS FOR UNSATURATED SAND*. University of Missouri-Columbia.

Griffith, A.A. 1924. The Theory of Rupture. *Proceedings of the First International Congress for Applied Mechanics*. Farnborough, pp. 55–63.

Hamblin, A.P. 1981. Filter-paper method for routine measurement of field water potential. *Journal of Hydrology*, 53(3), pp.355–360.

Han, Z. & Vanapalli, S.K. 2016. Stiffness and shear strength of unsaturated soils in relation to soil-water characteristic curve. *Géotechnique*, (8), pp.1–21.

Heibrock, G., Zeh, R.M. & Witt, K.J. 2003. Tensile Strength of Compacted Clays. *International conference on unsaturated soils*. pp. 395–412.

Heymann, G. & Clayton, C.R.I. 1999. Block sampling of soil: Some practical considerations. *Geotechnics for Developing Africa*. Ed. By G.R. Wardle, G.E. Blight, & A.Fourie. Durban: A.A Balkema/Rotterdam/Brookfield, pp. 331–339.

Hondros, G. 1959. The evaluation of Poisson's ratio and the modulus of materials of a low tensile resistance by the Brazilian (indirect tensile) test with particular reference to concrete. *Australian Journal of Applied Science*, 10(3), pp.243–268.

Hudson, J.A., Brown, E.T. & Rummel, F, 1972. The controlled failure of rock discs and rings loaded in diametral compression. *International Journal of Rock Mechanics and Mining Sciences & Geomechanics Abstracts*, 9(2).

Institute of Civil Engineers, 2011. *ICE Manual of Geotechnical Engineering* J Ed. by Burland, J., Chapman, T., Skinner, H. & Brown, M. London: ICE Publishing.

Jacobsz, S.W., 2016. Trapdoor experiments studying cavity propagation. *Proceedings of the first Southern African Geotechnical Conference*. Ed. by S.W. Jacobsz. Pretoria: CRC Press/Balkema, pp. 159–165.

Jennings, J.E.B., Brink, A.B.A., Louw, A. &Godwan, G.D. 1965. Sinkholes in the Transvaal. *Proceedings of the Sixth International Conference on Soil Mechanics and Foundation Engineering*. pp. 51–54.

Jennings, J.E.B. 1961. A Revised Effective Stress Law for Use in the Prediction of the Behaviour of Unsaturated Soils. *Pore Pressure and Suction in Soils*. London: Butterworths, pp. 26–30.

Jennings, J.E.B. & Burland, J. 1962. Limitations to the use of effective stresses in partly saturated soils. *Géotechnique*, 12(2), pp.125–144.

Jennings, J.E.B. & Knight, K. 1957. The additional settlement of foundations due to collapse of structure of sandy subsoils on wetting. *Proceedings of the 4th International Conference and Foundation Engineering*. London, pp. 316–319.

Karihaloo, B. 1995. *Fracture mechanics & structural concrete.* Longman Scientific & Technical.

Kaur, A. & Fanourakis, G.C. 2016. Effect of hydrometer type on particle size distribution of fine grained soil. *Proceedings of the first Southern African Geotechnical Conference*. Ed. by S.W. Jacobsz. Pretoria, South Africa, pp. 307–315.

Kim, T.-H. 2001. *Moisture-Induced Tensile Strength and Cohesion in Sand*. PhD thesis. University of Colorado.

Kim, T. & Sture, S. 2008. Capillary-induced tensile strength in unsaturated sands. *Canadian Geotechnical Journal*, 45(5), pp.726–737.

Kim, T.H. & Hwang, C., 2003. Modelling of tensile strength on moist granular earth material at low water content. *Engineering Geology*, 69(3–4), pp.233–244.

Knight, K. 1961. *The collapse structure of sandy sub-soils on wetting*. PhD thesis. University of the Witwatersrand.

Krishnayya, A.V.G. & Eisenstein, Z. 1974. Brazilian Tensile Test for Soils. *Canadian Geotechnical Journal*, 11(4), pp.632–642.

Lambe, T.W. 1960. A Mechanistic Picture of Shear Strength in Clay. *Proceedings of the ASCE Research Conference on Shear Strength of Cohesive Soils*. Colorado, Boulder, pp. 555–580.

Le Roux, P.F. 2016. *Personal communication.*

Li, D. & Wong, L.N.Y. 2013. The brazilian disc test for rock mechanics applications: Review and new insights. *Rock Mechanics and Rock Engineering*, 46(2), pp.269–287.

Lu, N, Kim, T-H., Sture, S. & Likos, W.J. 2009. Tensile Strength of Unsaturated Sand. *Journal of Engineering Mechanics*, 135(12), pp.1410–1419.

Lu, N. & Likos, W. 2004. *Unsaturated Soil Mechanics*, Hoboken, New Jersey: John Wiley & Sons, Inc.

Lu, N., Wu, B. & Tan, C.P. 2005. A tensile strength apparatus for cohesionless soils. *Advanced Experimental Unsaturated Soil Mechanics: Proceedings of the International Symposium on Advanced Experimental Unsaturated Soil Mechanics*. Ed by A. Tarantino, E. Romero, & Y. J. Cui. Trento, Italy: CRC Press/Balkema, pp. 105–110.

Mitchell, J.K. 1976. The properties of cement stabilized soils. Residential Workshop on Materials and Methods for Low Cost Road, Rail and Reclamation Works.

Murrell, S.A.F. 1958. The Strength of Coal under Triaxial Compression. *Mechanical properties of non-metallic brittle materials : proceedings of a Conference on Non-Metallic Brittle Materials*. Ed. by W.H. Walton. London: Butterworths, pp. 123–146.

Narasimhan, T.N. 2005. Buckingham, 1907: An appreciation. *Vadose Zone Journal*, 4(2), p.434.

Perkins, S.W. 1991. *Modelling of regolith structure interaction in extraterrestrial constructed facilities.* PhD thesis. University of Colorado, Boulder.

Pham, H.Q., Fredlund, D.G. & Barbour, S.L. 2005. A study of hysteresis models for soil-water characteristic curves. *Canadian Geotechnical Journal*, 42(6), pp.1548–1568.

Radcliffe, D. & Šimůnek, J. 2010. *Soil Physics with HYDRUS: Modelling and Applications*, Taylor & Francis.

Richards, B.G. 1966. The Significance of Moisture Flow and Equilibria in Unsaturated Soils in Relation to the Design of Engineering Structures Built on Shallow Foundations in Australia. *Symposium on Permeability and Capillarity*. Atlantic City, N.J.: American Society for Testing Materials.

Richards, L.A. & Gardner, W. 1936. Tensiometers for measuring the capillary tension of soil water. *Journal of the American Society of Agronomy*, 28(5), pp.352–358.

Richardson, S. 2013. *Sinkhole and subsidence record in the chuniespoort group dolomite,*

Gauteng, South Africa. MSc thesis. University of Pretoria

Ridley, A.M. & Burland, J.B. 1993. A new instrument for the measurement of soil moisture suction. *Géotechnique*, 43(2), pp.321–324.

Rogers, C.D. 1994. Types and distribution of collapsible soils. *Genisis and Properties of Collapsible Soils*. Ed.by E. Derbyshire, T. Dijkstra, & I. J. Smalley. Loughborough: Kluwer Academic Publishers, pp. 1–17.

Rust, E., Heymann, G. & Jones, G. 2005. Collapse potential of partly saturated sandy soils from Mozal, Mozambique. *Journal of the South African Institution of Civil Engineering*, 47(1), pp.8–14.

Schwartz, K. 1985. Collapsible soils: problem soils in South Africa. *The Civil Engineer in South Africa*, 27(7).

Schwartz, K. & Yates, J.R.C. 1980. Engineering properties of aeolian Kalahari sands. *Proceedings of the 7th Regional Conference for Africa Soil Mechanics and Foundation Engineering*. Accra: AA Balkema.

Sophocleous, M. 2010. Understanding and explaining surface tension and capillarity: an introduction to fundamental physics for water professionals. *Hydrogeology Journal*, 18(4), pp.811–821.

Stott, P.R., Monye, P.K. & Theron, E. 2006. Assessment of reliability of the hydrometer by examination of sediment. *Proceedings of the first Southern African Geotechnical Conference*. Ed. by S.W. Jacobsz. Pretoria, South Africa: CRC Press/Balkema, pp. 281–286.

Terzaghi, K., 1936. The shearing resistance of saturated soil and the angle between the planes of shear. *Proceedings of the First International Conference for Soil Mechanics and Foundation Engineering*. Harvard, Massachusetts, pp. 54–56.

Tiab, D. & Donaldson, E.C., 2004. Capillary pressure. In *Petrophysics: Theory and Practice of Measuring Reservoir Rock and Fluid Transport Properties*. Elsevier, Inc, pp. 313–359.

Tien, H., 1996. *A Literature Study of the Arching Effect*. MSc thesis. Massachusetts Institute Of Technology.

Timoshenko, S. 1934. *Theory of Elasticity*. California: McGraw-Hill book company, inc.

Toker, N.K., Germaine, J.T., Sjoblom, K.J. & Culligan, P.J. 2004. A new technique for rapid

measurement of continuous soil moisture characteristic curves. *Géotechnique*, 54(3), pp.179–186.

Toll, D.G. 2012. The behaviour of unsaturated soils. *Handbook of Tropical Residual Soils Engineering*. Ed. by B.B K. Huat, D.G. Toll & A. Prasad. London: Taylor & Francis.

Toll, D.G. 2016. Unsaturated Soils. *Unsaturated and Tropical Soils Course*. Sun City, South Africa, pp. 1–27.

Vesga, L.F. & Vallejo, L.E. 2006. Direct and Indirect Tensile Tests for Measuring the Equivalent Effective Stress in a Kaolinite Clay. *Fourth International Conference on Unsaturated Soils*. Carefree, Arizona, United States: American Society of Civil Engineers, pp. 1290–1301.

Wagener, F.V.M. 1985. Dolomites: problem soils in South Africa. *The Civil Engineer in South Africa*, 27(7).

Warren, A. 1994. Proceedings of the 1st international symposium on engineering characteristics of arid soils. *General report: Arid environments and description of arid soils*.Ed. by P.G. Fookes & R.H. Parry. London: A.A. Balkema, pp. 3–4.

Warren, J. 2000. Dolomite: Occurrence, evolution and economically important associations. *Earth Science Reviews*, 52(1–3), pp.1–81.

White, D.J., Take, W.A. & Bolton, M.D. 2003. Soil deformation measurement using particle image velocimetry (PIV) and photogrammetry. *Géotechnique*, 53(7), pp.619–631.

Wulfsohn, D., Adams, B.A. & Fredlund, D.G. 1998. Triaxial testing of unsaturated agricultural soils. *Journal of Agricultural Engineering Research*, 69(4), pp.317–330.

Yang, H., Rahardjo, H., Leong, E-C & Fredlund, D.G. 2004. Factors affecting drying and wetting soil-water characteristic curves of sandy soils. *Canadian Geotechnical Journal*, 41(5), pp.908–920.

APPENDIX A: MATERIAL DETAILS

Table A-1: Gold tailings sample details (G_s = 2.69)

Sample number	Sample dimensions (mm)								Mass (g)	Density (kg/m^3)	Unit weight (kN/m^3)	W_{ave} (%)	S_r (%)
	h_1	h_2	h_3	h_4	h_{ave}	d_1	d_2	d_{ave}					
12/07/15-S1	26.42	26.22	25.18	25.91	25.93	49.16	49.41	49.29	82.52	1668.00	16.36	13.0	56.9
23/11/15-S1	23.36	23.51	23.17	23.22	23.32	48.84	48.46	48.65	68.70	1585.13	15.55	12.5	48.3
23/11/15-S2	23.09	22.80	23.63	23.47	23.25	49.01	49.29	49.15	73.90	1675.45	16.44	14.0	61.9
23/11/15-S3	24.05	23.30	23.29	23.64	23.57	49.39	49.36	49.38	73.10	1619.77	15.89	11.8	48.1
23/11/15-S4	24.28	23.70	23.72	24.31	24.00	49.59	49.33	49.46	77.30	1676.20	16.44	18.8	83.5
24/11/15-S1	24.04	24.43	24.45	24.61	24.38	49.64	49.39	49.52	72.80	1550.56	15.21	12.6	46.0
24/11/15-S2	25.14	25.85	25.38	24.97	25.34	49.60	49.57	49.59	82.90	1694.51	16.62	19.7	90.2
25/11/15-S1	19.93	19.38	49.45	19.38	27.04	49.87	49.80	49.84	61.10	1158.66	11.37	13.8	28.1
29/12/15-S2	25.29	25.68	25.18	24.54	25.17	49.98	49.93	49.96	77.10	1562.72	15.33	5.0	18.5
30/12/15-S2	23.33	23.25	22.78	22.59	22.99	49.80	49.31	49.56	64.70	1459.31	14.32	0.8	2.7
30/12/15-S3	22.24	22.81	22.30	22.30	22.41	50.42	50.01	50.22	67.70	1525.25	14.96	4.3	15.1
04/01/16-S1	23.00	23.98	23.33	23.35	23.42	49.47	49.62	49.55	68.30	1512.99	14.84	4.6	15.8
04/01/16-S2	19.94	19.35	20.74	21.08	20.28	49.65	49.86	49.76	59.70	1514.25	14.85	7.7	26.6
05/01/16-S1	24.23	25.02	24.55	23.98	24.45	49.50	49.11	49.31	72.80	1559.80	15.30	7.3	26.9
05/01/16-S2	26.31	26.56	25.74	25.52	26.03	49.78	49.50	49.64	79.40	1575.98	15.46	6.9	26.2
06/01/16-S1	19.42	18.37	19.13	19.08	19.00	49.68	49.62	49.65	58.40	1587.56	15.57	7.3	28.2
06/01/16-S2	24.68	25.84	25.24	24.84	25.15	49.17	49.53	49.35	74.70	1552.81	15.23	8.5	31.2
04/04/16-S1	25.29	25.81	24.82	24.99	25.23	49.92	49.99	49.96	84.49	1708.77	16.76	8.4	32.2
04/04/16-S3	26.09	25.78	25.15	25.35	25.59	49.68	49.95	49.82	86.63	1736.78	17.04	8.7	34.2
04/04/16-S4	25.33	26.38	25.77	25.50	25.75	49.90	50.37	50.14	88.66	1744.47	17.11	13.3	48.5
04/04/16-S5	24.94	25.62	26.21	25.27	25.51	49.85	50.08	49.97	91.75	1834.32	17.99	12.8	52.1
07/06/16-S1	25.50	25.06	26.00	25.72	25.57	50.02	49.86	49.94	86.76	1732.22	16.99	13.4	47.1
07/06/16-S2	23.85	24.70	25.18	24.62	24.59	50.04	49.80	49.92	82.15	1707.08	16.75	14.4	48.9
07/06/16-S3	25.78	25.77	26.86	26.39	26.20	49.95	49.95	49.95	87.59	1706.05	16.74	12.7	44.0
07/06/16-S4	25.24	26.32	25.04	25.10	25.43	49.98	49.78	49.88	84.74	1705.63	16.73	13.1	45.8
07/06/16-S5	26.44	24.81	24.69	24.86	25.20	49.75	49.83	49.79	82.87	1688.97	16.57	12.3	41.7
20/06/16-S1	24.16	23.66	24.94	29.93	25.67	49.70	49.48	49.59	80.91	1631.76	16.01	12.0	38.2

20/06/16-S2	24.87	25.99	26.44	25.45	25.69	49.85	50.31	50.08	87.89	1737.00	17.04	11.7	43.3
20/06/16-S3	25.60	25.80	25.93	25.08	25.60	49.88	49.87	49.88	85.44	1708.14	16.76	9.1	34.1
20/06/16-S5	23.59	23.48	24.08	23.07	23.56	50.36	49.78	50.07	80.00	1724.89	16.92	11.3	42.2
27/06/16-S1	25.14	26.30	26.30	25.41	25.79	49.69	49.75	49.72	89.47	1786.97	17.53	18.5	62.8
27/06/16-S2	22.69	22.21	22.68	23.22	22.70	49.93	50.02	49.98	80.58	1809.70	17.75	18.0	65.3
27/06/16-S3	22.58	22.68	22.89	23.15	22.83	50.02	49.52	49.77	84.00	1891.66	18.56	20.2	78.0
27/06/16-S4	23.49	22.72	24.21	24.09	23.63	49.98	50.42	50.20	85.64	1831.31	17.97	20.0	70.0
27/06/16-S5	25.43	24.92	25.41	25.60	25.34	49.66	49.83	49.75	90.39	1835.38	18.01	20.5	71.8
27/06/16-S6	25.28	25.83	26.12	26.01	25.81	49.63	49.75	49.69	88.00	1758.19	17.25	14.2	51.4
27/06/16-S7	25.47	25.14	24.59	24.85	25.01	49.87	50.31	50.09	83.88	1701.80	16.69	14.2	46.1
27/06/16-S8	25.76	25.64	25.36	24.99	25.44	50.14	50.16	50.15	88.29	1757.14	17.24	15.7	55.1
27/06/16-S10	24.90	25.99	27.19	26.14	26.06	50.09	49.96	50.03	90.39	1765.08	17.32	15.6	55.0
11/08/16-S1	23.11	23.51	23.71	23.60	23.48	49.62	49.76	49.69	80.75	1773.25	17.40	16.1	56.7
11/08/16-S2	24.69	24.69	25.64	24.51	24.88	49.78	49.87	49.83	87.06	1794.49	17.60	17.3	61.3
11/08/16-S3	24.41	24.60	24.86	23.54	24.35	49.53	49.48	49.51	86.96	1855.19	18.20	18.8	70.6
11/08/16-S4	24.19	23.86	24.17	24.45	24.17	49.46	49.68	49.57	84.14	1804.03	17.70	18.4	64.9
11/08/16-S5	24.68	24.34	24.29	24.50	24.45	49.49	49.88	49.69	86.32	1820.74	17.86	17.9	65.4
10/08/16-S1	22.94	23.44	23.37	23.06	23.20	49.76	49.69	49.73	82.03	1820.53	17.86	19.3	67.6
10/08/16-S2	21.28	22.51	22.52	21.69	22.00	49.34	49.80	49.57	78.02	1837.62	18.03	20.5	72.1
10/08/16-S3	24.84	24.60	24.79	25.06	24.82	49.49	49.81	49.65	87.68	1824.43	17.90	20.0	69.6
10/08/16-S4	26.48	25.74	25.41	25.71	25.84	49.80	49.90	49.85	93.12	1846.78	18.12	19.6	70.5
10/08/16-S5	25.53	25.23	26.07	25.85	25.67	50.27	50.00	50.14	95.27	1880.00	18.44	21.4	77.9
29/08/16-S1	26.06	24.97	25.22	24.74	25.25	49.76	49.73	49.75	78.73	1604.48	15.74	4.1	14.7
29/08/16-S2	25.67	25.57	25.47	25.22	25.48	49.69	49.72	49.71	81.40	1646.24	16.15	6.8	24.3
29/08/16-S3	24.90	24.74	23.67	23.30	24.15	49.98	49.99	49.99	78.61	1658.62	16.27	6.9	25.4
29/08/16-S5	25.50	25.34	25.37	25.31	25.38	49.68	49.83	49.76	80.06	1622.41	15.92	6.2	21.9
16/11/16-S1	24.13	25.00	24.20	23.32	24.16	49.45	49.61	49.53	68.69	1475.45	14.47	0.2	0.7
16/11/16-S2	26.66	27.48	26.27	25.47	26.47	49.21	49.07	49.14	70.38	1401.96	13.75	0.3	0.9
16/11/16-S3	27.25	26.47	25.92	26.23	26.47	49.68	48.82	49.25	74.16	1470.80	14.43	0.2	0.6
16/11/16-S4	26.12	25.91	26.97	26.58	26.40	48.84	48.59	48.72	73.02	1484.24	14.56	0.1	0.5

Table A-2: Iron tailings sample details (G_s = 3.89)

Sample number	Sample dimensions (mm)								Mass (g)	Density (kg/m^3)	Unit weight (kN/m^3)	W_{ave} (%)	S_r (%)
	h_1	h_2	h_3	h_4	h_{ave}	d_1	d_2	d_{ave}					
19/09/2016-S1	23.02	23.14	24.58	22.96	23.43	45.19	45.77	45.48	86.58	2275.14	22.32	23.7	82.9
19/09/2016-S2	26.11	23.25	24.68	24.45	24.62	45.56	45.94	45.75	94.82	2342.59	22.98	15.2	65.0
19/09/2016-S4	24.21	24.63	24.31	24.21	24.34	46.04	45.25	45.65	95.05	2386.47	23.41	15.6	68.8
19/09/2016-S5	24.47	26.47	26.52	25.61	25.77	45.21	44.35	44.78	96.18	2370.03	23.25	14.8	65.2
21/09/2016-S1	24.22	24.96	24.78	24.53	24.62	45.43	45.26	45.35	89.15	2242.03	21.99	11.3	47.3
21/09/2016-S2	25.57	24.45	24.52	25.64	25.05	45.59	45.92	45.76	93.61	2273.18	22.30	12.5	52.7
21/09/2016-S3	24.85	25.05	25.13	25.58	25.15	46.53	46.46	46.50	94.21	2206.04	21.64	12.5	49.6
21/09/2016-S4	25.01	25.14	25.26	25.41	25.21	46.17	45.96	46.07	95.36	2270.11	22.27	13.0	54.2
21/09/2016-S5	25.57	25.59	25.28	25.55	25.50	45.51	45.76	45.64	96.56	2315.33	22.71	13.2	56.8
22/09/2016-S1	24.46	24.42	24.94	24.78	24.65	44.14	44.16	44.15	90.92	2409.30	23.64	7.1	37.7
22/09/2016-S2	26.11	26.14	26.54	25.72	26.13	44.52	44.44	44.48	99.98	2462.61	24.16	13.2	65.3
22/09/2016-S3	25.50	25.33	25.06	25.29	25.30	44.20	44.25	44.23	96.47	2482.74	24.36	13.4	67.2
22/09/2016-S4	25.50	24.99	24.81	24.80	25.03	44.51	44.44	44.48	93.05	2393.43	23.48	11.0	52.8
22/09/2016-S5	24.00	23.31	23.89	22.88	23.52	44.23	44.07	44.15	87.76	2437.29	23.91	10.1	51.8
29/09/2016-S1	21.93	22.56	21.96	21.21	21.92	43.36	43.55	43.46	81.29	2501.07	24.54	6.5	38.7
29/09/2016-S2	22.48	22.72	23.75	23.06	23.00	44.05	43.37	43.71	85.46	2475.92	24.29	6.8	39.0
29/09/2016-S3	24.41	23.70	24.39	24.47	24.24	44.17	43.50	43.84	89.70	2451.79	24.05	6.5	36.9
29/09/2016-S4	24.50	22.99	23.26	24.06	23.70	44.22	42.91	43.57	86.65	2452.50	24.06	5.8	33.5
29/09/2016-S5	24.48	24.91	24.21	23.91	24.38	44.44	43.23	43.84	89.98	2445.82	23.99	5.8	33.1
07/10/2016-S1	20.57	20.10	20.46	20.79	20.48	44.67	43.79	44.23	77.12	2450.83	24.04	3.8	22.8
07/10/2016-S2	22.86	23.60	23.54	23.20	23.30	43.26	44.78	44.02	83.23	2347.11	23.03	2.6	14.5
07/10/2016-S3	23.19	22.75	22.01	22.14	22.52	44.18	44.98	44.58	84.23	2395.96	23.50	4.1	22.9
07/10/2016-S4	23.64	23.58	23.75	23.18	23.54	43.53	44.34	43.94	86.45	2422.67	23.77	3.9	22.6

Table A-3: Centurion soil sample details (G_s = 2.75)

Sample number	Sample dimensions (mm)								Mass (g)	Density (kg/m^3)	Unit weight (kN/m^3)	W_{ave} (%)	S_r (%)
	h_1	h_2	h_3	h_4	h_{ave}	d_1	d_2	d_{ave}					
05/09/2016-S1	23.59	25.46	25.37	24.11	24.63	47.59	47.68	47.64	79.14	1802.79	17.69	40.4	97.6
05/09/2016-S2	24.12	24.86	25.19	23.87	24.51	47.32	46.89	47.11	75.84	1775.54	17.42	30.3	81.9
05/09/2016-S4	26.97	26.78	26.35	26.30	26.60	46.82	47.01	46.92	85.51	1859.61	18.24	30.7	90.4
05/09/2016-S5	23.34	26.26	25.22	24.79	24.90	46.55	46.67	46.61	77.77	1830.29	17.96	34.2	92.8
10/09/2016-S1	23.17	23.95	23.88	22.77	23.44	46.91	46.65	46.78	67.54	1676.28	16.44	28.3	70.2
10/09/2016-S2	22.27	22.14	23.33	22.70	22.61	46.69	46.35	46.52	63.70	1657.56	16.26	28.1	68.5
10/09/2016-S3	23.17	23.80	24.55	23.76	23.82	46.45	46.47	46.46	67.08	1661.13	16.30	28.4	69.5
10/09/2016-S4	26.05	25.49	26.73	26.46	26.18	46.25	46.28	46.27	75.73	1720.53	16.88	28.4	74.7
10/09/2016-S5	25.92	26.09	26.38	25.73	26.03	47.62	47.28	47.45	76.54	1662.85	16.31	27.5	67.9
12/09/2016-S2	25.62	26.38	26.43	24.89	25.83	45.83	45.45	45.64	67.08	1587.40	15.57	18.3	47.9
12/09/2016-S3	25.67	25.53	25.43	25.90	25.63	45.33	44.58	44.96	67.08	1648.76	16.17	21.5	57.5
12/09/2016-S4	24.04	23.47	25.57	24.33	24.35	44.84	44.62	44.73	67.08	1752.92	17.20	21.5	65.4
12/09/2016-S5	25.69	25.45	25.79	25.62	25.64	45.11	45.03	45.07	76.54	1871.32	18.36	20.9	74.3
13/09/2016-S1	21.82	22.90	23.65	22.51	22.72	46.64	47.41	47.03	68.00	1723.27	16.91	38.4	87.5
13/09/2016-S2	23.58	23.43	24.77	24.48	24.07	46.61	46.51	46.56	70.49	1720.39	16.88	27.8	73.1
13/09/2016-S3	23.14	23.24	23.18	23.41	23.24	45.59	45.80	45.70	65.40	1715.80	16.83	30.5	77.1
13/09/2016-S4	24.50	25.36	24.73	23.79	24.60	45.57	45.79	45.68	71.21	1766.66	17.33	30.4	81.2
13/09/2016-S5	26.09	25.60	26.33	24.85	25.72	45.46	45.42	45.44	72.84	1746.52	17.13	28.6	76.8
16/09/2016-S1	23.92	25.13	26.19	26.46	25.43	47.82	46.44	47.13	75.63	1705.09	16.73	42.3	89.8
16/09/2016-S2	25.75	25.60	26.63	26.10	26.02	45.97	45.57	45.77	78.59	1835.73	18.01	41.1	101.2
16/09/2016-S3	25.31	24.39	23.61	23.89	24.30	46.24	46.32	46.28	71.23	1742.53	17.09	40.6	91.5
16/09/2016-S4	24.55	25.97	26.16	25.84	25.63	46.50	46.71	46.61	76.33	1745.79	17.13	40.0	91.2
16/09/2016-S5	25.85	29.12	26.70	24.92	26.65	46.18	47.23	46.71	79.51	1741.60	17.09	40.6	91.6
19/09/2016-S1	24.76	26.02	25.55	24.09	25.11	43.59	43.67	43.63	65.27	1738.97	17.06	15.7	52.0

19/09/2016-S2	25.00	25.29	25.39	24.56	25.06	43.36	44.50	43.93	64.15	1688.90	16.57	15.9	49.4
19/09/2016-S4	22.25	24.53	24.82	24.41	24.00	43.22	43.27	43.25	63.32	1796.07	17.62	14.3	52.7
19/09/2016-S5	23.33	23.84	24.51	23.27	23.74	44.32	43.27	43.80	59.79	1672.07	16.40	15.5	47.5
03/10/2016-S1	26.43	26.36	27.09	26.95	26.71	43.51	45.33	44.42	66.61	1609.38	15.79	10.7	33.0
03/10/2016-S2	26.66	26.20	26.82	25.85	26.38	43.69	43.73	43.71	64.14	1620.17	15.89	10.2	32.1
03/10/2016-S4	25.08	25.59	26.86	26.35	25.97	44.34	43.16	43.75	63.67	1630.86	16.00	9.3	30.4
04/10/2016-S1	25.62	26.21	26.51	25.17	25.88	42.79	43.90	43.35	65.04	1703.30	16.71	11.2	39.1
04/10/2016-S2	26.72	27.52	26.81	25.53	26.65	42.87	43.07	42.97	66.35	1717.14	16.85	8.8	32.5
04/10/2016-S4	26.41	27.60	27.45	25.95	26.85	42.90	44.05	43.48	67.40	1690.85	16.59	9.4	33.2
05/10/2016-S1	26.22	26.19	27.10	26.80	26.58	46.91	46.19	46.55	75.22	1662.99	16.31	27.4	67.8
05/10/2016-S2	25.68	25.85	26.93	26.71	26.29	46.01	45.21	45.61	72.87	1696.32	16.64	26.9	69.9
05/10/2016-S3	25.41	26.04	26.19	26.39	26.01	45.96	45.15	45.56	72.65	1713.86	16.81	28.0	73.0
05/10/2016-S4	25.04	25.80	25.76	25.05	25.41	45.48	44.86	45.17	72.33	1776.16	17.42	25.1	73.6
20/10/2016-S1	26.30	26.98	26.40	25.67	26.34	42.96	43.49	43.23	64.15	1659.82	16.28	6.8	24.4
20/10/2016-S2	24.64	24.97	25.10	25.02	24.93	42.95	43.19	43.07	59.54	1639.09	16.08	7.3	25.0
20/10/2016-S3	22.84	23.37	22.98	22.36	22.89	42.78	42.64	42.71	52.42	1598.64	15.68	6.2	20.6

APPENDIX B: CONFERENCE PUBLICATION

from

Proceedings of the First Southern African Geotechnical Engineering Conference

Measuring the tensile strength of gold tailings

T.A.V. Gaspar & S.W. Jacobsz
University of Pretoria, Pretoria, South Africa

ABSTRACT: This paper discusses the modification of the Brazilian disk test so that it can be applied to measure the tensile strength of unsaturated soils. The study involved testing the tensile strength of unsaturated gold tailings prepared across a range of moisture contents. In order to monitor the initiation and propagation of cracking within each sample, Particle Image Velocimetry (PIV) was utilised. The study revealed that across the range of moisture contents considered the Brazilian disk test, performed with curved loading strips, consistently resulted in cracking initiating in the centre of the sample, thereby validating the measured failure load as the result of a tensile failure. An investigation of load-displacement relationships for all samples tested showed that in the pendular regime, the behaviour of the material was particularly erratic. However, at higher saturation levels, material behaviour was found to be significantly more stable.

1 INTRODUCTION

1.1 *Background*

Soils can possess a certain amount of tensile strength provided by cementation, particle interlock, pore water suction under partially saturated conditions, or a combination of these factors. Although the tensile strength is normally small, it is significant when studying problems such as soils arching across cavities in the formation of sinkholes, slope stability problems, the design of retaining structures, bearing capacity analyses and other stability problems.

The Brazilian disk test is a method commonly used to indirectly determine the tensile strength of brittle materials such as rocks, concrete and in more recent years, weakly cemented soils (Consoli et al. 2012). Despite its frequent use in the abovementioned fields, the test has rarely been performed on soils and, as a result, little development has been made regarding the applicability thereof. This deficit in research can possibly be attributed to the fact that in practice, soils are generally regarded as having very little to no tensile strength. Over the past few decades however, a greater amount of emphasis has been placed on the research of unsaturated soils. It has become commonly understood that as a soil becomes unsaturated, it develops some additional strength from pore water suction, the extent of which is related to the degree of saturation of the soil in relation to its particle size distribution (Lu et al. 2009). This additional strength can be described as being a result of two separate components, both of which have been highlighted in Figure 1: (1) the surface tension which acts along the air-water interface and (2) the pressure difference acting across the air-water interface which is termed matric suction (u_a-u_w) (Kim & Changsoo 2003).

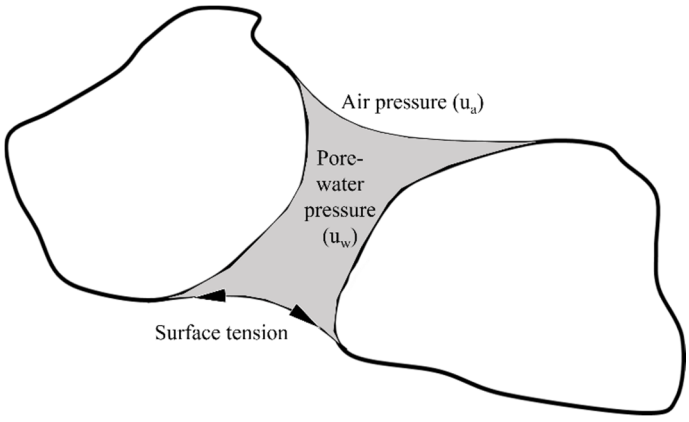

Figure 1. Components contributing to additional strength of unsaturated soil.

When a given soil is subject to negative pore water pressure, three distinct regimes can be identified. At low moisture contents, the water phase is discontinuous and exists only as thin layers surrounding isolated soil particles. This soil state is referred to as the pendular regime (Kim & Changsoo 2003). As the soil reaches higher levels of saturation, the water phase becomes more continuous and the soil transitions into the funicular regime. Finally, the capillary regime is

a term used to describe the portion of soil above the phreatic surface which is kept saturated due to the presence of a negative pore water pressure (commonly referred to as the capillary fringe) (Lu & Likos 2004).

Although the transition between each of the phases described above is not distinct, each state will result in a different soil behaviour, all of which have been investigated in the current study. The additional strength present in unsaturated soils arising from matric suctions results in a non-zero value of tensile strength. Depending on the particle size, the strength magnitudes are generally small and difficult to measure accurately. The contribution of a certain amount of tensile soil strength may, however, be significant in several classes of problems. Examples could include slope stability and bearing capacity problems, as well as heterogenous soil masses arching over cavities, i.e. the sinkhole problem.

A modification of the Brazilian disk test, which is relatively simple in comparison to direct tension tests, to measure the tensile strength of soil samples was therefore undertaken in the present study to determine the tensile strength of unsaturated soil samples accurately and repeatably. The study will examine a range of material types, but commenced with the testing of silts. Gold tailings was selected as the first silty material tested and selected results are reported in this paper.

1.2 *The Brazilian disk test*

Perhaps the most extensive development of the Brazilian disk test has been in the field of rock mechanics and it is from this viewpoint that the present study departed (Li et al. 2013). The test involves diametrically loading a disk specimen, resulting in the development of tensile stress perpendicular to the direction of load application. It is obvious that at the portions of the sample where the load is applied and in the immediately adjacent zones close to the loading strips, the sample experiences compressive stresses. If the applied load resulted in tensile failure, cracking would initiate in the centre of the disk sample and propagate outwards towards the loading strips. If this failure mechanism is observed, and if it is seen that the sample is not crushed appreciably at the points of load application, it provides confidence that the sample is indeed failing in tension (Li et al. 2013). In this case the indirect tensile strength of the specimen can be determined using Equation 1:

$$\sigma_t = \frac{2P}{\pi DL} \quad (1)$$

where P is the measured failure load and D and L are the diameter and length of the cylindrical specimen respectively. A study performed by Erarslan & Liang (2012) highlighted the profound effect of loading conditions on the resulting failure of the disk specimen. The study revealed that by loading samples of Brisbane tuff with the use of standard Brazilian jaws, a compressive failure was observed. In contrast, it was found that through the use of 30° loading arcs, a centrally located crack and thus a tensile failure could be achieved. One of the aims of this study was therefore to investigate whether the conclusions obtained by Erarslan & Liang (2012) are applicable to the testing of unsaturated soil samples across a range of moisture contents.

2 EXPERIMENTAL PROCEDURE

2.1 *Sample preparation procedure*

The Brazilian disk tests carried out for the current study were performed on a number of disk samples of gold tailings. The particle size distribution is included in Figure 2. In order to avoid unwanted stress concentrations within the samples as they were loaded, care was taken to ensure that the samples prepared were free of defects. Due to the low tensile strength of the soil tested, any defects present in a sample would likely have resulted in the failure mode being affected, possibly initiating at one of the sample defects rather than in the centre of the sample where the soil would be in tension.

Disk specimens, with a diameter and thickness of 50 mm and 25 mm respectively, were prepared to achieve gravimetric moisture contents of 5, 8, 12 and 17%. Due to the amount of moisture loss that would take place as each sample was being placed onto the testing equipment, final (more representative) measurements of moisture contents were taken immediately after each sample was tested. The samples were prepared from a uniform reconstituted slurry with a moisture content of approximately 30% (based on workability considerations). The slurry was used to fill up several cylindrical split moulds in five separate lifts, lightly tamping the mould after each lift to allow the slurry to distribute itself evenly and to allow air bubbles to escape. The slurry mixtures were subsequently placed in an oven at 65°C and allowed to lose some moisture. In order to monitor the amount of moisture lost throughout the drying process, periodic mass readings were taken until such point that the desired moisture content of each sample had been reached.

Once a sample achieved its desired moisture content, a final mass reading together with a series of height and diameter measurements were taken to determine the unit weight of each sample. Finally, before being stored, samples were wrapped with a combination of both clingfilm and aluminium foil, as suggested by Heymann & Clayton (1999), to minimize the amount of moisture loss prior to testing.

2.2 *Test setup & procedure*

The test setup, illustrated in Figure 3 consisted of the following equipment:

- two curved loading strips with 30° arcs as suggested by Erarslan & Liang (2012). The strips were manufactured to have a 27 mm radius (2 mm greater than the sample radius) to cater for initial deformation of the soil without the edges of the loading strips cutting into the sample;
- a Linear Variable Differential Transformer (LVDT) to measure the vertical displacement of the sample throughout loading;
- a sensitive load cell with a maximum capacity of 200N;
- triaxial loading rig, allowing the diametric load to be applied at a constant rate of deformation;
- a high resolution digital camera (not visible in Figure 3) was mounted in front of the specimen so that strains within the sample could be monitored. The camera was set such that a photograph of the sample would be taken every five seconds.

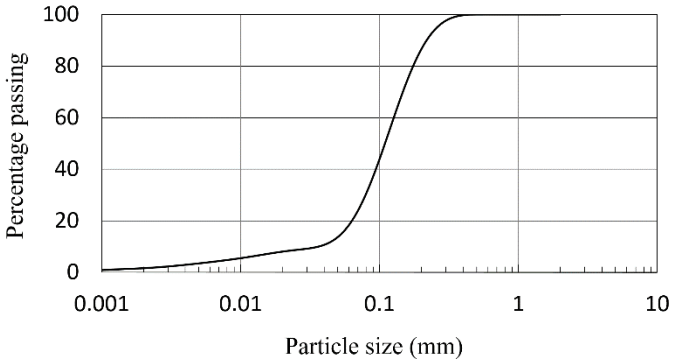

Figure 2. Particle size distribution.

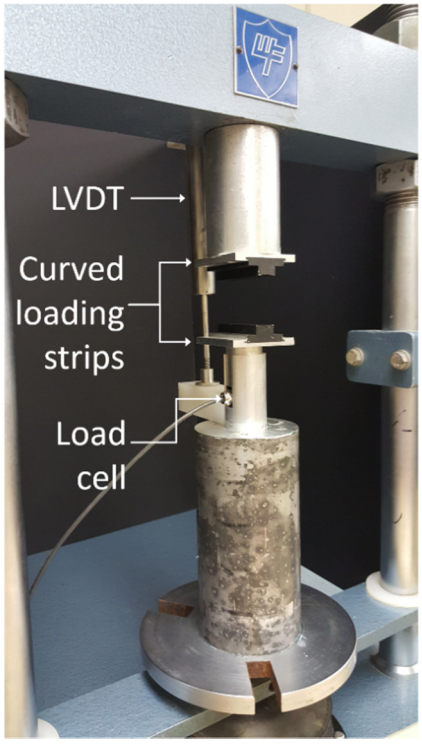

Figure 3. Test setup.

3 RESULTS

The results of the testing performed were sorted into four separate groups according to water content. This was done to characterise the behaviour of the soil across varying degrees of saturation. The data for all tests performed have been included in Table 1. From both Table 1 and Figure 6 it can be seen that at lower moisture contents a higher degree of scatter is observed owing to the extremely brittle nature of the material in that state. As the saturation levels of the samples increased, it was however observed that the material behaviour became less erratic, as is evident by the corresponding lower standard deviations in Table 1.

The variation in the consistency of the results with moisture content is further illustrated when considering the load-displacement curves presented in Figure 4 & 5. Figure 4 illustrates the load-displacement curves for an average water content of 5.18%. The load-displacement curves initially rise steeply, then yield, after which the load increases more slowly to a peak. From this figure it can be seen that there is relatively poor consistency in the results for the samples tested.

In contrast, the results presented in Figure 5 illustrate considerably less variation. In general, the load-displacement curves rise more gradually, then plateau, exhibiting a more ductile response than the dryer, more brittle material. The consistency of results within this moisture regime is highlighted when considering the amount of displacement that took place before the yield point was reached, as well as the maximum tensile strength that was achieved for each sample.

One trend that is present across all samples tested is related to the double stress peak seen in both Figure 4 and 5. This is attributed to two failure mechanisms which mobilised. Initially, as the diametric load was applied, the soil experienced tensile stresses perpendicular to the direction of load application, resulting in the soil failing in tension at the first stress peak. Thereafter, the sample was able to sustain higher compressive loads as the soil was gradually crushed. This behaviour was confirmed when examining the photographic records. Minimal sample deformation occurred as tensile stress mobilised. Then, at the first peak, a crack rapidly started to grow and then, with further deformation, crushing became evident at the points of load application.

Figure 6 plots the results of yield stress vs moisture content. Also displayed is a trend line connecting the average yield stress within each water content group. These results point towards a similar trend as observed by Lu et al. (2009) where the tensile strength of unsaturated sands was noted to increase in the pendular regime, achieve a maximum value in the funicular regime, and decrease again in the capillary regime.

Table 1. Brazilian disk test results.

Sample number	Water content (%)	Average water content (%)	Max. recorded stress (kPa)	Standard deviation of max. stress (kPa)	Yield stress (kPa)	Standard deviation of yield stress (kPa)
1	4.29	5.18	3.34	0.97	3.31	1.31
2	4.58		2.51		1.78	
3	4.98		1.19		0.62	
4	6.89		3.15		0.51	
5	7.26	7.69	1.73	1.06	0.83	1.39
6	7.29		3.59		3.41	
7	7.69		2.69		2.53	
8	8.51		4.15		4.05	
9	11.85	12.49	4.97	0.52	4.15	0.81
10	12.54		4.15		3.97	
11	12.58		4.18		3.03	
12	12.99		3.71		2.44	
13	13.82	16.59	2.86	0.44	2.17	0.90
14	13.97		3.87		1.29	
15	18.83		3.68		3.33	
16	19.74		3.45		2.93	

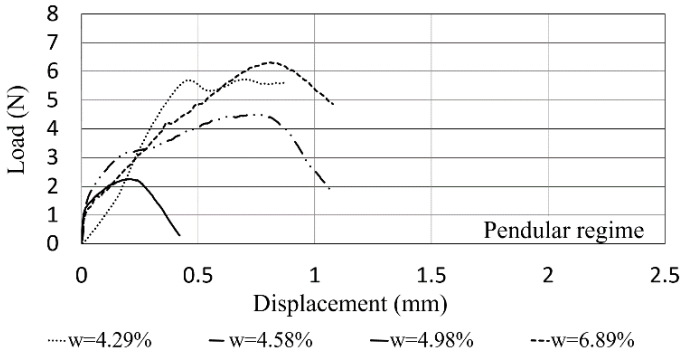

Figure 4. Load-displacement (w=5.18%).

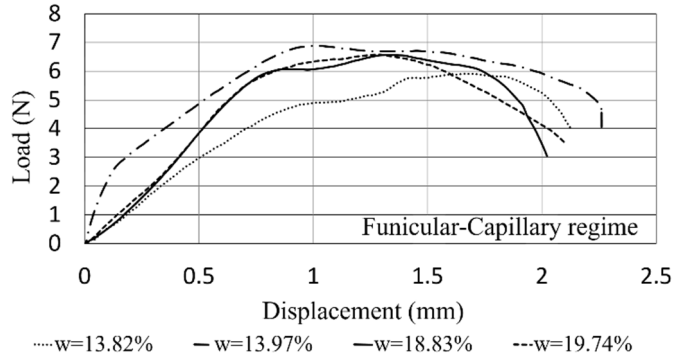

Figure 5. Load displacement (w=16.59%).

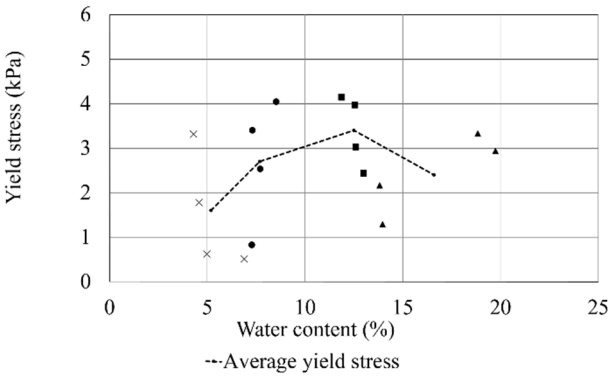

Figure 6. Yield stress vs water content.

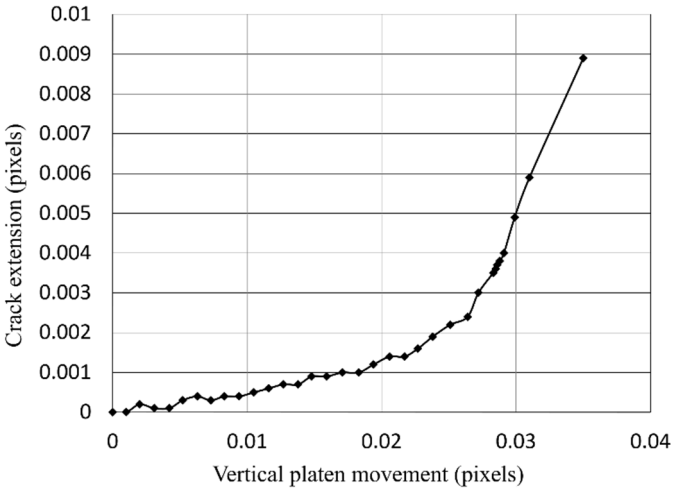

Figure 7. Crack extension vs vertical platen movement.

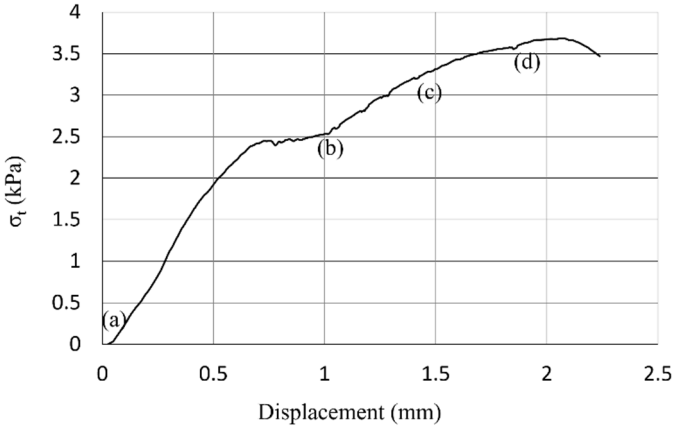

Figure 8. Load vs displacement (w=12.99%).

In order to more closely monitor the opening of the crack, the coordinates of two, vertically centred patches on the extreme left and right of the sample were analysed. Using these coordinates, the distance between the two patches in successive photographs

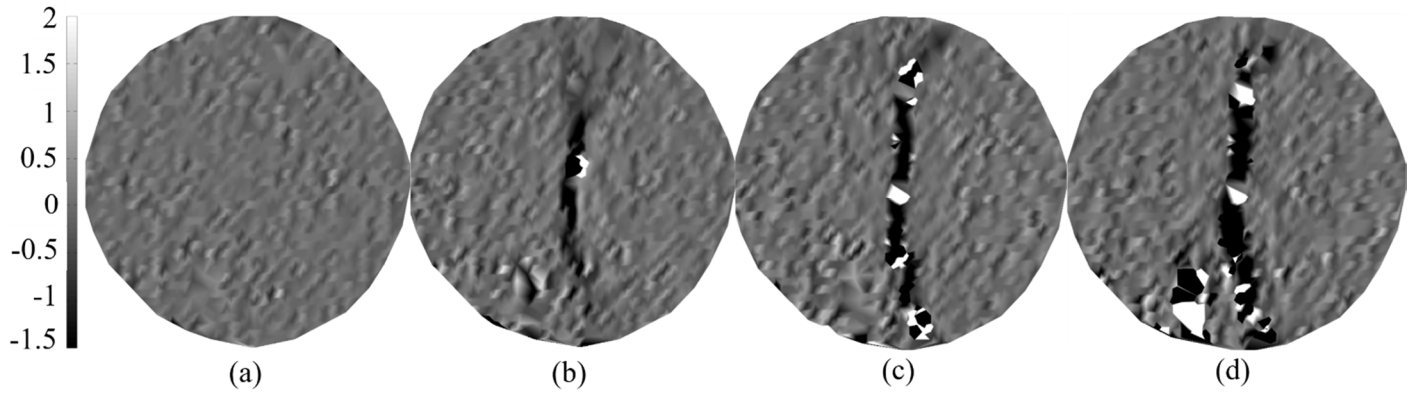

Figure 9. Horizontal strain development.

was tracked photogrammetrically using Particle Image Velocimetry (White et al. 2003). The value of horizontal crack extension for Sample 12 is plotted as a function of vertical displacement in Figure 7. From this figure it can be seen that at a vertical displacement of 0.0264 pixels, behaviour of the soil became linear and it is at this point that the crack in the centre of the sample became visible. At this point it can be stated that the maximum tensile strength of the soil had been mobilized and that any increase in load recorded after this point, was as a result of compression of the sample.

Figure 8 illustrates the load-displacement behaviour of Sample 12 with Figure 9 presenting the corresponding development of horizontal strain in the sample during load application. From Figure 9 the initiation and propagation of cracking with an increase in diametric load can be seen.

Upon first load application, no visible straining of the sample was detected. In fact, it can be seen that the first peak (Figure 8) was mobilised before measureable strains were detected. As is required for a valid Brazilian disk test result, the crack initiated in the centre of the sample and propagated outwards towards the loading strips until failure of the sample occurred.

Of the 16 samples tested, 14 were observed to have an initial crack positioned in the centre of the sample. This result highlights the effectiveness of the use of curved loading strips in achieving a tensile failure as was observed by Erarslan & Liang (2012) on samples of Brisbane tuff. In contrast, Hudson et al. (1972) found that the use of flat loading platens consistently resulted in failure originating directly below the loading points.

4 CONCLUSIONS

For the range of moisture contents considered, it was observed that the use of 30° curved loading strips consistently resulted in cracking initiating in the centre of the sample which is essential for carrying out a valid tensile test. In contrast, compressive failures originating directly below the point of load application were observed when flat loading strips were used (Hudson et al. 1972).

The load-displacement behaviour and measured tensile strength of the gold tailings was found to be highly erratic and very brittle in the pendular regime. However, with an increase in moisture content, results were seen to be significantly more consistent and repeatable and a more ductile behaviour was observed.

For all moisture contents considered, the behaviour of unsaturated gold tailings repeatedly resulted in the following trend: the load displacement curve rose to yield point corresponding to the mobilisation of tensile strength, then plateaued before rising somewhat further as the crack opened and the sample was crushed.

In terms of the recorded tensile strengths, it was found that, similar to the results of Lu et al. (2009), strengths tended to increase in the pendular regime, achieve maximum strength in the funnicular regime and decrease in the capillary regime.

The present study is ongoing and will need to examine the tensile strength behaviour of other unsaturated fine grained materials and the factors influencing it.

REFERENCES

Consoli, N.C., Cruz, R.C., Consoli, B.S. & Maghous, S. 2012. Failure envelope of artificially cemented sand. *Géotechnique*, 62(6): 543-47.

Erarslan, N. & Liang, Z.Z. 2012. Experimental and Numerical Studies on Determination of Indirect Tensile Strength of Rocks. *Rock Mechanics and Rock Engineering*,45(5): 739-51.

Heymann, G. & Clayton, C.R.I. 1999. Block sampling of soil: Some practical considerations. In Wardle, G.R., Blight, G.E. & Fourie, A.B., eds. *Geotechnics for Developing Africa*. Rotterdam, 1999. A.A. Balkema.

Hudson, J.A., Brown, E.T. & Rummel, F. 1972. The controlled failure of rock disks and rings loaded in diametral compression. *International Journal of Rock Mechanics and Mining Sciences & Geomechanics* Abstracts, 9(2): 241-48.

Kim, T.-H.K. & Changsoo, H. 2003. Modeling of tensile strength on moist granular earth material at low water content. *Engineering Geology*, 69(3): 233-244.

Li, D., Ngai, L. & Wong, N. 2013. The Brazilian Disk Test for Rock Mechanics Applications: *Review and New Insights. Rock Mechanics and Rock Engineering*, 46(62): 269-287.

Lu, N., Kim, T.-H., Sture, S. & Likos, J. 2009. Tensile Strength of Unsaturated Sand, *Journal of Engineering Mechanics*: 1410-1419.

Lu, N. & Likos, W.J. 2004. *Unsaturated Soil Mechanics*. New Jersey: John Wiley & Sons.

White. D.J., Take, W.A. & Bolton, M.D. 2003. Soil deformation measurement using particle image velocimetry (PIV) and photogrammetry, *Géotechnique* 53(7): 619-631.